Dynamics of Cellular Rigidity Sensing on the Micron and Sub-micron Scale

Saba Ghassemi

Submitted in partial fulfillment of the
requirements for the degree
of Doctor of Philosophy
in the Graduate School of Arts and Sciences

COLUMBIA UNIVERSITY

2011

ABSTRACT

Dynamics of Cellular Rigidity Sensing on the Micron and Sub-micron Scale

Saba Ghassemi

This thesis describes a study of the effect of environmental cues including physical attribute of the cellular environment on cellular force and force transduction. Different mechanical parameters such as geometry and rigidity of the substrate are controlled independently and forces exerted by cells were measured. The experimental system for this study is based on fabrication of micron and submicron pillar substrates and their surface functionalization and finally measurement of forces that cells exert to these substrates.

In chapter 2, the interplay between the rigidity of the substrate and the cell's force response was studied. Arrays of flexible PDMS pillars used to measure the pattern of traction force generation on matrices. Using three different pillar diameters (2, 1 and 0.5 micrometers), and three different pillar stiffnesses for each diameter, we showed that cells treat larger, fibronectin-coated pillars fundamentally differently than sub-micron pillars during initial contact formation. In the case of larger pillars, mouse embryo fibroblasts generated a constant force per unit area of about 1 nN/μm^2 on pillars of different stiffness by causing different displacements; whereas, the sub-micrometer pillars were displaced by about 60 nm irrespective of stiffness. In addition, micron-scale pillars are all pulled toward the center of the cell, whereas sub-micron pillars were also pulled toward each other locally. Further, the focal adhesion protein, paxillin, was concentrated at the edges of large pillars but it was focused on the tops of small pillars in a pattern analogous to the pattern on continuous substrates. Thus, we suggested that initial rigidity sensing involves measuring the force needed to produce displacements of about 60 nm in local regions ($\sim 1\mu$m) of the substrate. In addition, these results suggested that, to examine the effects of substrate rigidity on cellular behavior, sub-micron pillars more closely approximate continuous substrates than

do micron-scale pillars.

In chapter 3, a technique was described for fabricating substrates whose rigidity can be controlled locally without altering the contact area for cell spreading. The substrates consist of elastomeric pillar arrays in which the top surface is uniform but the pillar height is changed across a sharp step. Results demonstrated the effects on cell migration and morphology at the step boundary.

In chapter 4, a technique was described for the fabrication of arrays of elastomeric pillars whose top surfaces are treated with selective chemical functionalization to promote cellular adhesion in cellular force transduction experiments. The technique involves the creation of a rigid mold consisting of arrays of circular holes into which a thin layer of Au is deposited, while the top surface of the mold and the sidewalls of the holes are protected by a sacrificial layer of Cr. When an elastomer is formed in the mold, Au adheres to the tops of the molded pillars. This can then be selectively functionalized with a protein that induces cell adhesion, while the rest of the surface is treated with a repellent substance. An additional benefit is that the tops of the pillars can be fluorescently labeled for improved accuracy in force transduction measurements. The same fabrication process was used for fabrication of magnetically actuated pillars in order to be able to exert external force to cells and study the effect of localized mechanostimulation.

Table of Contents

List of Figures

List of Tables

Acknowledgments

In writing this acknowledgment it was hard for me to decide where to start, but I have no doubt in my heart that my thesis advisor Dr. James Hone is the one to thank first and foremost!

So, to him, Im indebted and grateful for providing the opportunity to learn and participate in my favorite research topic in a fascinating environment. I am thankful to him for helping me better develop my methods of scientific thinking. His professionalism, as well as his brilliant ideas taught me the etiquettes of the trade and his dedication and eternal enthusiasm instilled courage in me. He provided full support and an extremely enjoyable atmosphere which has been a great pleasure to work in. I have enjoyed his guidance and helpfulness in full measure. To him and to his patience, I am indebted and forever thankful.

I would like to express my sincere respect and deepest gratitude to Dr. Michael Sheetz, whose professional expertise was essential for my research projects. He taught me how to look at cells and learn to observe them almost as individual beings. He has always provided great insight and given valuable suggestions that greatly helped me carry out a multidisciplinary research. I felt lucky to have worked with him and learned (at least a little bit of) biology too!

Many thanks go to Dr. Shalom Wind, who educated me in many ways during these past years. I benefited tremendously form his professional expertise and learned a lot from our collaboration. His contribution has been invaluable, both in academic and personal level. To him, I am extremely grateful.

No less is my appreciation for my colleagues and fellows from nanomedicine center for mechanobiology and nanobiofabrication group at Columbia, from whom I learned a lot in my interactions with them. They have always extended their help and support during those years of studying. I would particularly like to thank Dr. Changgu Lee for his continuous

help in the field of nanofabrication, accompanied with his great patience and his excellent teaching skills. I also would like to thank Dr. Pere Roca-Cusachs, Dr. Nicolas Baias and Dr. Nils Gauthier for their assistance in developing my research projects and their useful advice, tips, interesting conversations and always being present when I needed help.

To all the lab personnel and members of Dr. Sheetz, Dr. Hone and Dr. Wind I owe many thanks for helping me with innumerable questions/problems.

All the nanofabrication work has been done in the facilities of the CEPSR clean room at Columbia University and The Cornell NanoScale Science Technology Facility (CNF). I would like to thank all the facilitys staffs for their support. A special thanks goes to Dr. Rob Ilic and Meredith Metzler for helping me with their professional expertise and always available hand, in my experience at in the CNF clean room. Without their presence, I would have lost my only source of positivity or entertainment, during those hard times of staying at Cornell.

I would like to thank Dr. Kysar, Sandra and others in the department of mechanical engineering for all their help and presence.

My warmest of emotions are reserved for my parents. Their love is as everlasting as are never-ending their encouragements and staunch support. My father always reminded me to live life and not sacrifice the moment for the end point, which helped me make this rough road a path full of memories. And to my mother, who shared with me all those moments by her continual presence in them. The same goes for my two brothers, Hooman and Sina, who give me strength and fill my life with their presence. To them all, I owe ineffably.

Finally, no small credit goes to my closest friends whose friendships made enjoyable an otherwise entirely mechanical endeavor. Arezu, Shaadi, Nasim, Narges, Saeid, Sheida, Liz, Sebastian, Azra, Ronin, Sameer, Prerena, Gabriella, Matei, Nicola, Negar (2), Hessam, Siavash, Hoda, Maria, Amparvin, Soolmaz, Mariam, Pegah, Zohre, Samira, Hamid and Shahriar, I can not imagine doing all this without you, my best friends, around me and always there for me. And to all those friends and colleagues whose names are not mentioned here, I wish to say thank you. You know who you are!

And thank you New York for being New York; always awake, beautiful and inspiring. And for helping me be the king of the hill....

For mom and dad

زندگی صحنه یکتای هنرمندی ماست

هر کسی نغمه خود خواند و از صحنه رود

صحنه پیوسته به جاست

خرم ان نغمه که مردم بسپارند به یاد . . .

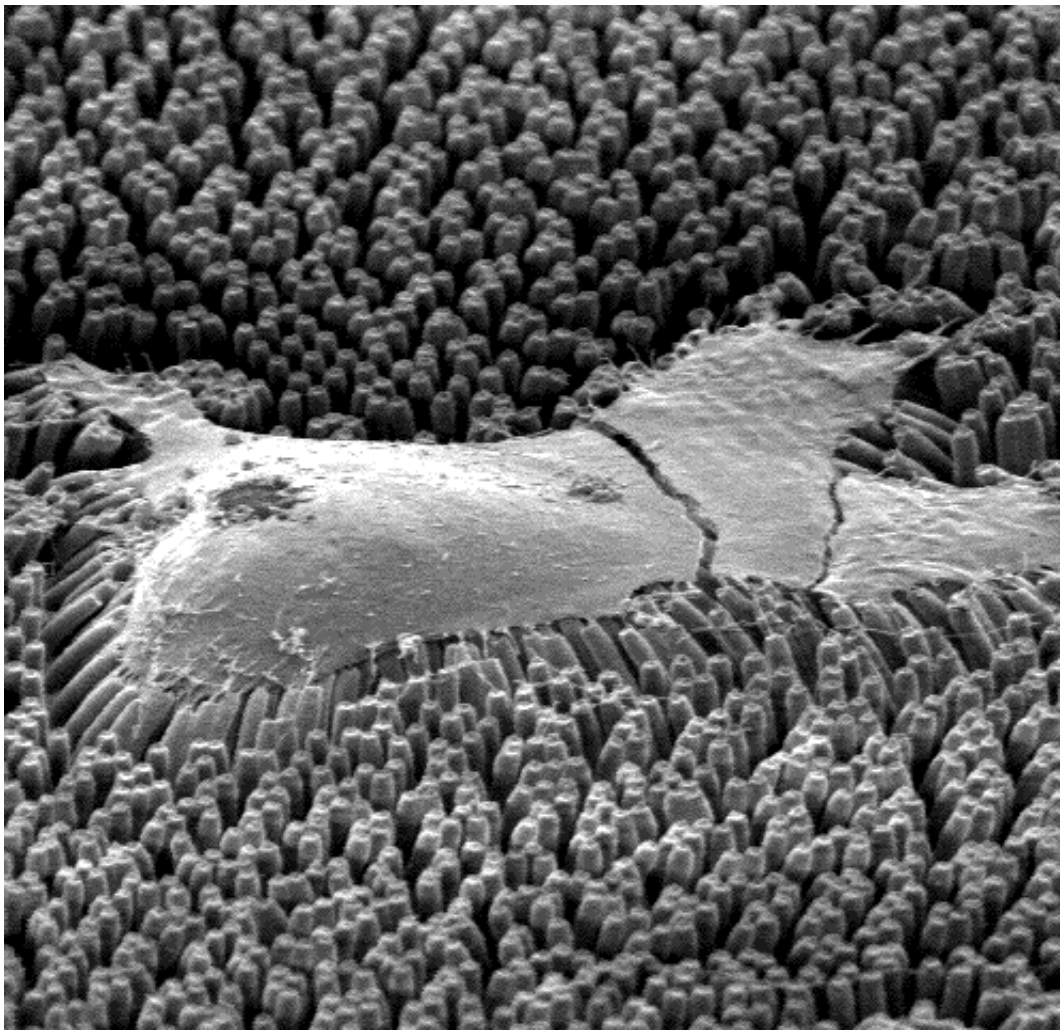

Part I

Introduction

Chapter 1

Background and motivation

1.1 The importance of rigidity in living systems

Many cellular processes such as adhesion and migration are governed not only by chemical cues but also by mechanical interactions. Cells interact with their environment by generating traction forces in the nN range and respond to many environmental cues and physical attributes such as geometry, density and rigidity of their environment [1; 2; 3; 4; 5]. Numerous cellular processes, ranging from migration to adhesion and cell differentiation depend on the rigidity of their environment. Therefore it is important to understand the processes by which the rigidity is sensed. In fact, this bidirectional communication is crucial for survival of humans and other multicellular organisms and its misregulation is associated with many diseases. For example, the signal for wound healing is often the loss of tissue integrity and the loss of mechanical interaction with the environment. Contraction of wounds by fibroblast depends on its rigidity sensing ability [6]. Likewise, a characteristic difference between normal and cancerous cells is their different cellular response to rigidity. Cancerous cells, unlike normal cells, grow in soft agar or liquid media while not sensing any difference between soft and hard agar [7; 8; 9]. Other examples are tumor cells, which are less adhesive compared to normal cells and deposit less extracellular matrix, which is a rigidity dependent function in cells [10].

1.2 Rigidity

Rigidity is a measure of relationship between applied forces and the resulting displacement of a material. In biology, the material could refer to the cell or its extra cellular matrix (ECM) components. ECM is the extracellular part of the cell which provide the structural support to the cells.

The rigidities of biological tissues vary over a wide range from brain tissue (0.1-10), which is softer than muscle (10-100 kPa), which is softer than connective tissue (100-1000 kPa) and softer than bone (1000-30,000,000 kPa) [11]. The rigidity of tissues is not static. For instance, the stiffness of brain tissue decreases with age. The rigidity of tissues is heterogeneous. Tissues are consist of different local rigidities [12].

Cells also have rigidity preferences, which generally reflect their native environments. Neurons can become more branched and can extend faster on soft substrates compared to stiffer substrates [13; 14]. Fibroblasts and endothelial cells, originating from tissues of midrange stiffness, do not spread or display actin stress fibers on soft surfaces [15; 16] and from the stiff environment of cartilage and bone, chondrocytes do not spread well on substrates with midrange stiffness [7]. Cells can also be guided by differences in rigidity. This phenomenon is called durotaxis. The migration of fibroblasts may be directed toward rigid substrates [1; 17]. Engler *et al.* showed that the rigidity of the extracellular matrix plays a role in stem cell differentiation [18]. Naive mesenchymal stem cells (MSCs) were cultured on soft matrices that mimic brain, medium matrices that mimic muscle and rigid matrices that mimic collagenous bone. After several weeks, cells were committed to the lineage specified by matrix elasticity. Soft matrices were neurogenic, medium matrices were myogenic, and rigid matrices prove osteogenic.

The complex interplay between the rigidity of the substrate and the cellular force response is not yet well understood. In order to explore how cells can sense the rigidity of their environment and study the effect of it on cellular behavior, a system is needed that can mimic biological stiffness.

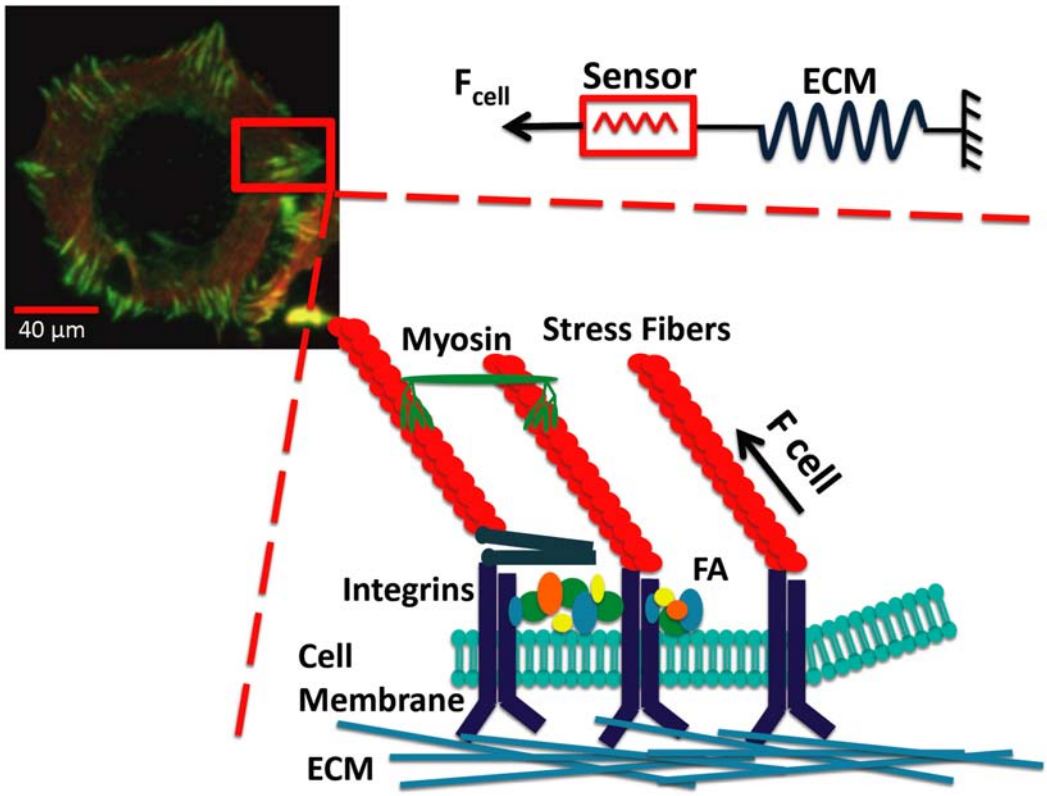

Figure 1.1: Schematic of the major components of the cell mechanotransduction system. The stress generated at components depends on cell generated force and the stiffness of ECM.

1.3 Mechanotransduction and rigidity response pathway

Cells probe the mechanical features of their environments by pulling on them. To do so, they must adhere to their ECM [19]. Once this link to the ECM is established, a pulling force is generated by the cell through the activation of small G proteins such as Rho. Forces induce the maturation of cell-ECM contacts into focal complexes and tehn into focal adhesions (FA), and formation of stress fibers. The stress fibers are linked on one side to focal adhesions and on the other side, they are linked to myosins and exert traction forces on ECM through their association with myosin.

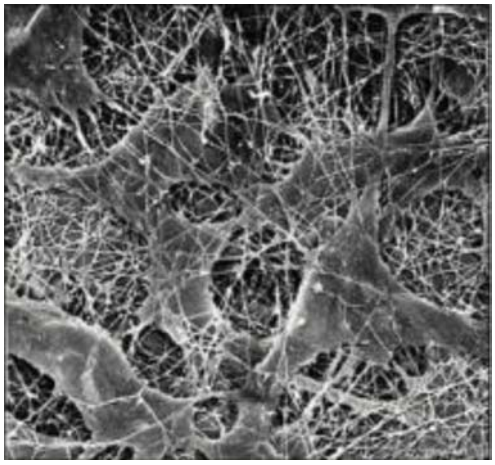

Figure 1.2: SEM image of cells embedded in a fibrous ECM (from [20]).

From the extracellular environment to the cell interior, the force bearing elements are in this order: the ECM, the adhesion molecules that bind to the ECM and cross the membrane of the cell, and molecules that interact directly or indirectly to the cell machinery that generates force. This chain of molecular complexes is then responsible for the transduction of the force to the cell's environment, which appears to be controlled by a series of mechanical steps. The major components of this mechanotransduction system are depicted in figure 1.1. and described below.

The extra cellular matrix

Extracellular matrix provides structural support to the cells from the outside. In vivo, ECM is composed of different proteins assembled in a complex fibrous meshwork (Fig. 1.2). This meshwork is mainly composed of structural proteins, such as collagen and elastin, and adhesive proteins such as fibronectin, vitronectin, and laminin [20]. In this work, our main focus is on fibronectin.

Fibronectin plays a major role in cell adhesion. It is secreted by cells and deposited in ECM in a form of highly insoluble filaments and then cross-links. It is a pervasive component of ECM during development and healing wounds. Fibronectin is composed of

three types of modules (Fn1, Fn2 and Fn3), which contain a large number of molecular recognition and cryptic sites that are exposed when forces applied to the protein and unfold certain protein domains [21]. One such site is the Arg-Gly-Asp (RGD) motif in Fn3 that binds to integrin receptors of cells [22]. The RGD sequence is known to be the minimal peptide sequence required for cell adhesion [23].

Adhesion molecules: the integrins

Cells adhere and interact with ECM through integrins. The integrin-ECM linkage is responsible for cell-ECM adhesion and is crucial for tissue repair. Integrins are transmembrane heterodimer proteins composed of two distinct chains, the α and β subunits. In mammals, 18 α and 8 β subunits have been characterized [24]. Integrins play a role in cell signaling. They are outside-in and inside-out receptors, *i.e.*, they transfer information from ECM to the cell as well as transmitting signals to the ECM. The signals transmitted from integrins into the cell provide information of the physical properties of the surrounding matrix and adhesive state [25]. These two types of behaviors are combined for rapid response of the cell to the changes in its environment [26].

The mechanosensing process begins with integrin binding to the ECM and integrin clustering. This binding and clustering affect the assembly of focal adhesion [27]. This linkage to ECM and focal adhesions, followed by change in conformation of integrins is needed for force to transduce across integrins.

The interface between the integrins and the force generating machinery: from focal complexes to focal adhesions

The binding of integrins to the ECM results in clustering and recruitment of scaffolding proteins in formation called focal complexes. Focal complexes, which are small structures located at the edges of lamellipodia [28], grow in size in a linear proportion to the forces exerted upon them [29]. These forces induce maturation of focal complexes to focal adhesions, which physically connect integrins to the actin cytoskeleton31 [30]. Focal adhesions (FA) are large molecular assemblies that can contain over 100 proteins. They can be up to a few microns in length. Proteins inside these complexes are in constant remodeling and

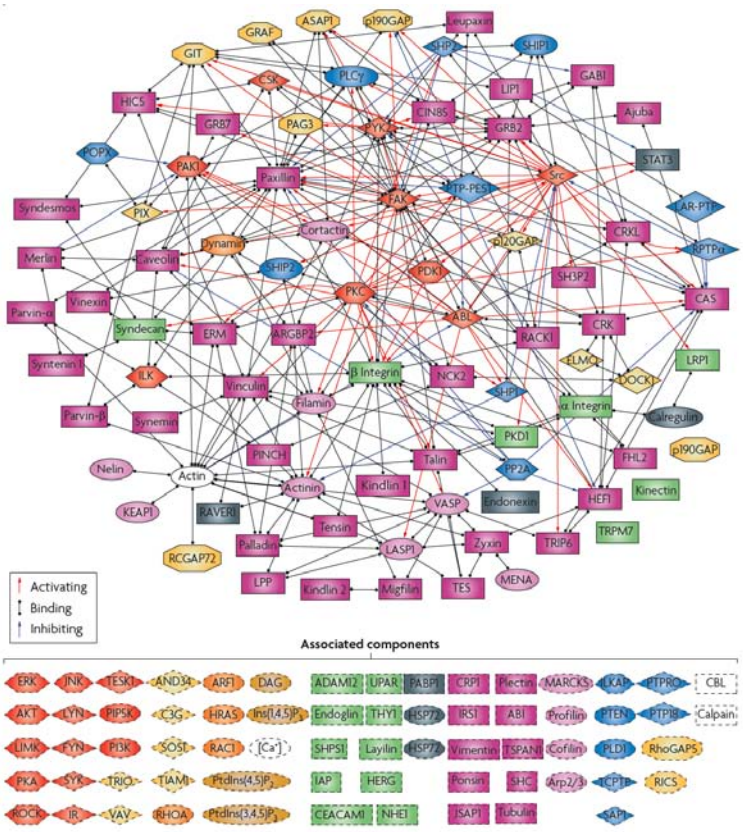

Figure 1.3: The integrin adhesome network; it includes 156 components which are linked via 690 interactions (from [31]).

dynamically change in order to transmit the condition of ECM to the cell. Cells respond to the new condition and thus, new FA proteins are recruited. Geiger *et al.* recently described a network of 156 components which are linked via 690 interactions in the integrin adhesome network (Fig. 1.3) [31].However, the hierarchy of interaction of specific FA proteins and cytoskeletal and ECM molecules is not yet fully determined. Among all those proteins, some have been clearly identified as the main players of FA formation. One of these proteins is talin that represents the major link between integrins and the acto-myosin cytoskeleton, as depicted in figure 1.1. Talin binds to the cytoplasmic tail of β-integrins and connect them to actin filaments either directly or by interacting with vinculin and α-actinin. Talin

and vinculin are involved in mechanotransduction. In fact, application of forces causes the stretching of a single talin rod that exposes cryptic binding sites for recruitment of vinculin. Vinculin activity regulates signaling for assembly and reorganization of actin cytoskeleton.

There are some other proteins that observed to be involved in binding integrins to actin filamentssuch as focal adhesion kinase (FAK). They are important in adhesion and activation of integrins [32]. Paxillin, which is recruited in early adhesion is another important molecule. It binds to FAK and is essential in integrin signaling [33].

Myosins, particularly myosin II, which are linked to the actin fibers, exert a pulling force on them.

The force generating machinery: the actomyosin cytoskeleton

The acto-myosin cytoskeleton, as its name shows, is composed of two major organizations: actin and myosin. Actin monomer is a globular protein. Myosin is a large family of motor proteins. Actin is the scaffold scaffold on which myosin proteins generate force. In order to work as part of the force generating machinery, it is first polymerized to make filaments that are subsequently bundled into fibers. These fibers are linked on one side to the focal adhesion molecules (*e.g.* talin). On the other side, they are linked to myosin. Individual fibers are further oriented in a parallel meshwork to form acto-myosin cytoskeleton. The myosins, also organized as multi protein complexes, pull on different actin fibers, and in opposite directions. Since myosin works only in one direction on actin fibers, this anti-parallel nature of the meshwork is required to create actin bundles called stress fibers. Those stress fibers can link different FA proteins to one another inside the cell and form a cohesive cytoskeleton. The generated force is then transmitted via actin fibers to the FA proteins, then to integrins and finally to ECM.

1.4 Conversion of force into biochemical signals

Cells are constantly interacting with their environment via components explained above. This interaction responds to biophysical changes in the environment. The generation of the force by myosin II is a response to this interaction (Fig. 1.4). Every component has dynam-

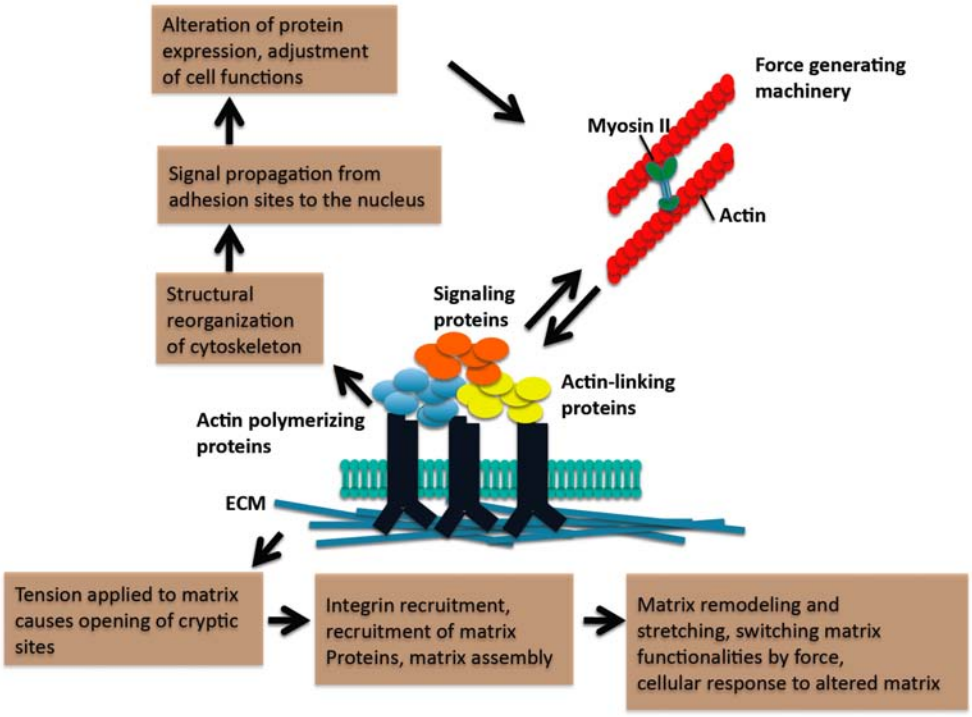

Figure 1.4: A schematic of the feedback loops that connects the actin-myosin force generating machinery and integrin-mediated adhesions. Cells sense the mechanical features of the environment and modify the ECM and the protein content. Intracellular signals will also alter the protein expression and therefore cell function (after [19]).

ics and as the cell generates forces on them, their response to the force and the mechanical properties of the environment will cause a secondary response. Thus, cells are continually encountering new ligands and the structural and signaling functions of ECM-integrin-cytosleton molecular complexes are constantly modified depending on the magnitude of the forces they tranduce. Forces can accelerate activation of molecules, both by extra and intracellular rearrangements. It induces protein recruitment through protein stretching, and accelerates the clustering of protein. At each step described previously, there is a potential mechanosensor that can dynamically respond to mechanical changes. There are three basic mechanisms of force sensing: 1) protein unfolding, 2) formation of catch bonds and 3)

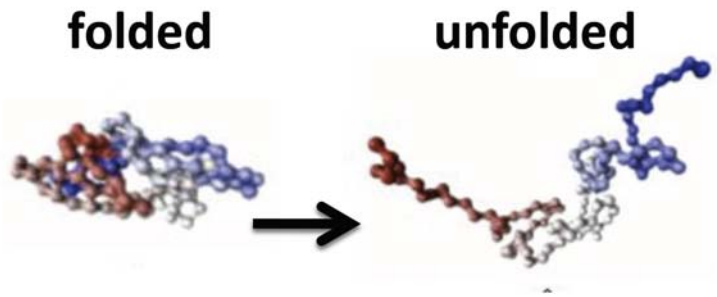

Figure 1.5: Conversion of force into biosignals by protein unfolding.

channel opening.

Protein unfolding

Forces within the cell can cause conformational modifications in proteins that can serve in the mechanosensensory mechanism. Most ECM proteins such as fibronectin, as well as proteins that link the integrins to cytoskeleton such as talin, can be unraveled by force, which results in exposure of protein-protein binding sites [34; 35] (Fig. 1.5). Application of force can unfold fibronectin and expose protein interaction sites, including RGD, which is a cell-binding site [21]. Cellular contraction can expose cryptic sites in fibronectin that are important in its assembly into a matrix [36]. In the talin-vinculin system, a force that stretches talin results in exposure of cryptic binding sites and can cause recruitment of additional actin binding proteins that is essential in reinforcement of early adhesion.

Catch bonds

Two interacting proteins can be described as having a bond. The interaction and therefore the lifetime of a bond generally decreases with the application of force. This type of behavior, common to most protein interactions, is called a slip bond. However, there is another set of protein interaction, which increases in lifetime with increasing force, called catch

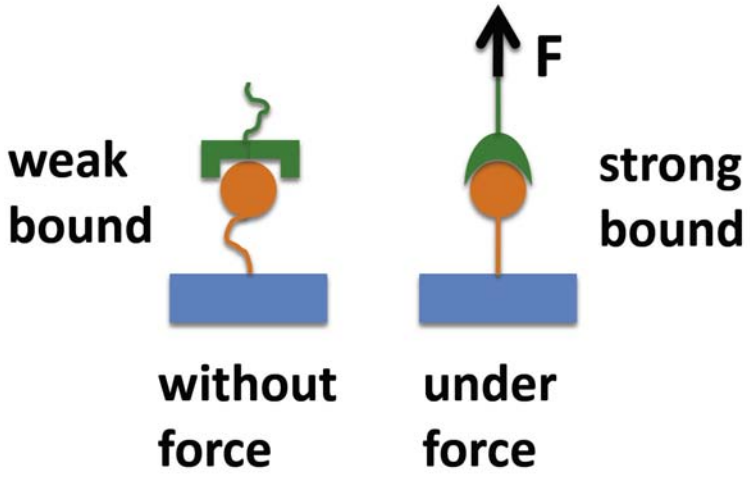

Figure 1.6: Conversion of force into biosignals by formation of catch bonds. The life-time of protein-protein bonds increases under application of force.

bonds (Fig. 1.6). In the mechanical cycle of force transduction, integrins are reported to be involved in the mechanosensing process by forming a catch bond with ECM. Several reports have shown that extracellular rigidity causes strengthening of the integrin linkage [29; 30; 37; 38].

Ion channels

Force can also open ion channels, which convert mechanical force into electrical and chemical signals [39]. In hair cells, force that is perpendicular to the membrane opens the channel. Similarly, cytoskeletal forces can open channels associated with early adhesions complex through integrins. Force activated ion channels have reported to be important in mechanotransduction [40].

The continual feedback between cell sensing of force and rigidity, and the conversion of these parameter to biochemical signals can regulate cell functions. Substrates with different patterns, topographies and rigidities can be engineered in order to learn more about the

contribution of each element and also study their various physical properties involved in the regulation of cell function. In fact, nanofabrication and nanotechnology will enable us to test molecular mechanism of mechanosensing and force transduction by fabricating substrates at micro- and nano-scale, the size scale of cells and their organelles. The molecular base of cellular response can be studied by using cells with modified protein expression levels and therefore different behaviors.

1.5 Force mapping during cell migration

The existence of cellular force was reported by Harris *et al.* in 1980. It was demonstrated by the ability of adherent cells to wrinkle thin film of silicone elastomers [41] (Fig. 1.7) and has since been quantified using a variety of approaches. Cells can probe the elasticity of their environment by deforming it. They exert traction forces in range nN range [38]. Early works on studying force at the cell to substrate interface used deformation within elastic materials such as thin polymer films or thick polymer gels, where the crosslinking chemistry used to control the mechanical properties of the substrate [1; 15; 30; 42; 43]. To be more quantitative, the displacement of the fluorescently tagged micro beads [44] (Fig. 1.8a) or micro-patterned motifs [29] (Fig. 1.8b), which were embedded randomly inside the polymer gels, are correlated to deformation generated by cells. In these methods, the substrate is deformable but not soft enough for cells to wrinkle. These methods have provided important quantitative information of force distribution and have led to significant improvement in understanding of traction response in cells [29; 44; 45; 46]. Dembo and Wang (1999) produced maps of the tractions exerted by 3T3 fibroblasts during steady locomotion using Fluorescent latex marker beads embedded randomly throughout polyacrylamide sheets [46]. Balaban *et al.* (2001) studied the traction force in cells using micro patterned motifs combined with fluorescence imaging of focal adhesions [29]. It was suggested that force applied by the cell on its substrate is closely linked to the assembly of the adhesion sites and scaled with adhesive area [43]. A constant force per unit area of about 5 nN/mm^2 was measured [29; 46].

Although these methods allowed us to track the deformation and measure the forces

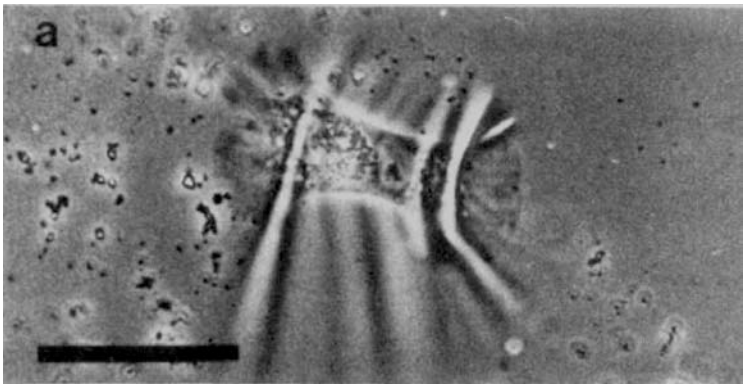

Figure 1.7: Formation of wrinkles on thin film of silicone elastomers by a cell (from [41]).

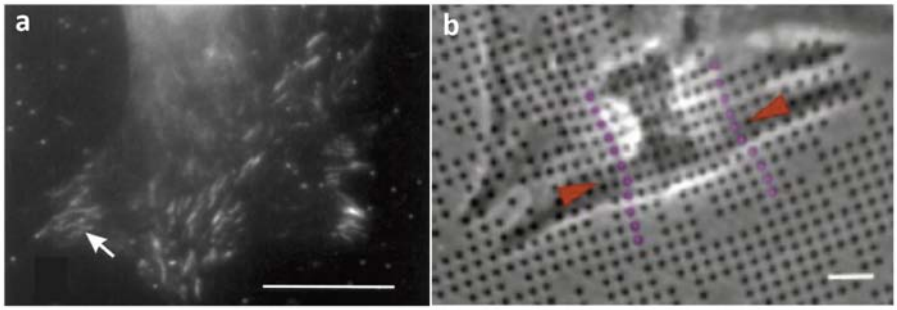

Figure 1.8: (a) Fluorescently tagged micro beads and (b) micro-patterned motifs for cellular force measurement (from [44; 29]).

exerted by cells [29; 46; 47] but fundamental limitations remained. In all these techniques, deformation occurs on continuous surfaces, which makes it difficult to measure relation between the force and displacement. Also, beads form a discrete network and force between them cannot be measured [48; 49] and therefore cellular force map of the cell cannot be obtained. More over, changing the stiffness of the substrate by altering the chemistry of it, may effect on the chemical properties of the material such as adhesiveness and therefore cell behavior.

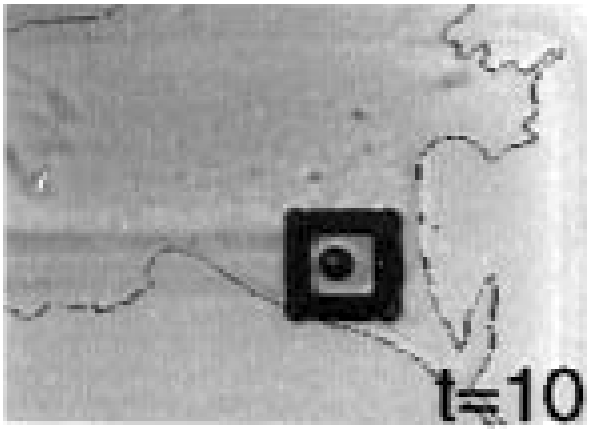

Figure 1.9: Micro fabricated cantilever for cellular force measurement (from [50]).

An alternate strategy to continuous substrate, was using a micro fabricated cantilever (Fig. 1.9). This cantilever was placed horizontally on the cell substrate and was deflected as individual cells migrate across it. In this method force could be measured by detecting the deflection of the cantilever but was limited to the number of the sensors on the surface and could not provide cellular force map. Galbreith and Sheetz (1997) reexamined the stresses produced by fibroblast using silicone cantilever [50] and found the stress magnitude.

All of these methods, in which a deformable soft material used, provided us significant information about cellular behavior. For example, with using a soft material with a well-defined stiffness, the rigidity sensing preference of the cell has been characterized. It has been shown that most cells such as fibroblast can actively sense the stiffness of their environment [11]. In fact, rigidity of the substrate plays a major role in direction of migration [1; 51; 52], cell spreading [53; 54], the traction and forces that they exert on a substrate [1]. Also, mechanical interactions between cells and their substrates clearly direct how cells organize their cytoskeleton and focal adhesion and function in their environment [15; 16; 50; 55; 56]. It has been shown that on rigid substrates, stress fibers and strong focal adhesions predominate. In contrast, adhesive contacts on soft substrates are less organized.

A new method was developed in 2003 by Tan *et al.* using microfabricated pillar array which represent a significant improvement to force measurement techniques [3]. In this

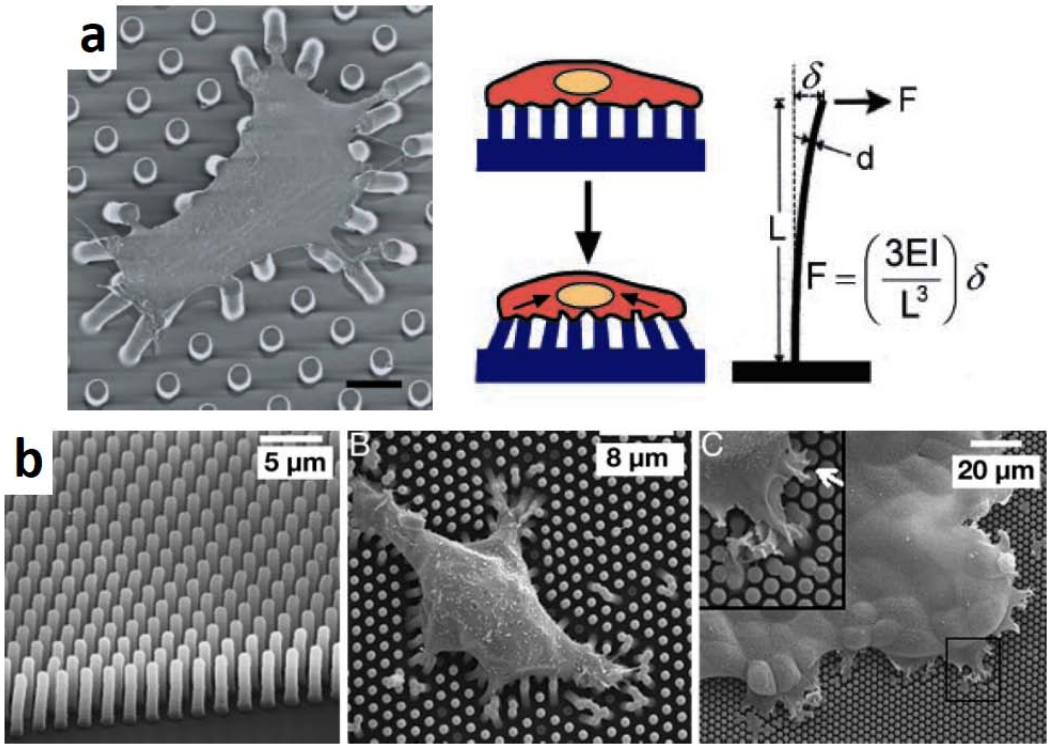

Figure 1.10: (a) Elastomeric microfabricated pillar arrays for cellular force measurements. cells spread on pillars and deflect the pillars depending the geometry of the elastomeric pillars. (b) SEM image of cells lying on the top of PDMS pillar arrays (from [3; 2]).

approach, an array of elastomeric pillars used as cantilevers on which cells attach and exert forces. When cells are cultured on these arrays, they adhere to the top of the pillars. As cells exert force on them, they could bend the pillars depending the stiffness of the pillars (Fig. 1.10a). Stiffness of the pillars depends on the dimension of the pillars and the Young's modulus of its material. In the reported study, pillars were 3 μm in diameter, 11 μm in height and 9 μm center-to-center distance. By detecting the deflection of the pillars, force can be measured at each pillar independently and therefore cellular force map can be obtained. Another advantage of these substrates is that force can be measured in real time. For small deflection, the pillars behave like a springs such that the deflection

is directly proportional to the force. Linear elastic theory of a bending beam gives the force-displacement relationship as:

$$F = \left(\frac{3}{4}\pi E \frac{r^4}{L^3}\right)\delta \tag{1.1}$$

where E, r, L, δ are the Young's modulus, radius, length and the deflection of the pillars respectively [57]. Since pillars are made with known physical and chemical properties, the stiffness of the pillars can be altered by changing the dimension of the pillars without altering bulk mechanical properties of the substrate or surface properties of the material.

The microfabricated pillar technique overcame some of the limitation of force measurement techniques explained before. However, in the previous experiments, because of the limitation of fabrication process because, the density of micropillars under the cells was low leading to a spatial resolution limited to center-to-center distance of 9 μm. Along the same line, high-density of microfabricated pillar arrays were used to measure traction forces exerted by different cell lines [2; 4; 45; 51; 58; 59; 60]. The dimension of pillars were about 1-3 μm in diameter and 5-10 μm in height with 2-10 μm spacing (Fig. 1.10b). The high density of the pillars made the substrate seems to affect less on cell adhesion and cell locomotion compared with a flat and continuous surface.

The pillar technique makes it possible to observe the complete spatial pattern of actin-myosin driven traction forces applied to the substrate. Large pillar density of these substrates improves the spatial force resolution and can resemble continuous surfaces so as not to interfere with cell spreading and locomotion. However the resolution is limited to the lateral movement of the pillars. If too closed, pillars will adhere to each other.

This method along with other tools enables ways to determine how the linkage between the ECM and the cytoskeleton is stabilized by mechanical force and the mechanism by which these forces are transduced. However, detailed mechanism of cell-ECM interaction during adhesion, migration or other cellular processes such as differentiation is yet to be identified.

1.6 Goals of this study

The main goal of this research work is to perform a comprehensive study of the effect of environmental cues including physical attribute of the cellular environment on cellular force and force transduction. Different mechanical parameters such as geometry and rigidity of the substrate are controlled independently and forces exerted by cells were measured. The experimental system for this study is based on fabrication of micron and submicron pillar substrates and their surface functionalization and finally measurement of forces that cells exert to these substrates.

Chapter 2 describes the fabrication process of pillar substrates with different diameters and heights, in order to study the effect of adhesive area and rigidity on cellular traction force. The force is measured and finally, existence of a characteristic intracellular length and time in mechanism of cellular rigidity sensing is examined.

Chapter 3 describes a novel method for fabrication double height pillar substrates to control the rigidity of the substrate and study the cellular response.

Chapter 4 describes a novel method for fabrication of gold-tipped pillars and their biofunctionalization, in order to selectively functionalize the top of pillars. It also describes the fabrication process of magnetically actuated pillars in order to be able to exert external force to cells and study the effect of localized mechanostimulation.

Part II

Pillar Substrates

Chapter 2

Cell rigidity sensing by local displacements

2.1 Abstract

If cells are to sense rigidity of a matrix, they must measure both matrix displacements and forces. Two fundamental aspects of rigidity sensing are 1) what is the minimum area of matrix sensed and 2) do cells sense the force required for a given displacement or the displacement for a given force? To test both of these issues, we measured the time course of displacement of elastomer pillars of three different diameters and three different stiffness. In the case of micron-scale pillars, mouse embryo fibroblasts generated a constant force per unit area of about 1 nN/μm^2 irrespective of stiffness; in contrast, on sub-micron pillars, cells displaced pillars by about 60 nm irrespective of stiffness. In addition, micron-scale pillars are all pulled toward the center of the cell, whereas sub-micron pillars were also pulled toward each other locally. The focal adhesion protein paxillin localized at the edges of micron-scale pillars, but on the on the tops of sub-micron pillars in a pattern analogous to that seen on continuous substrates. Thus, we suggest that initial rigidity sensing involves measuring the force needed to produce displacements of about 60 nm in local regions ($\sim 1\mu$m) of the substrate. This constrains possible models for the rigidity sensing system, and provides a new method to identify the proteins involved. In addition, these results suggest that, to examine the effects of substrate rigidity on cellular behavior, sub-micron pillars more closely

approximate continuous substrates than do micron-scale pillars.

2.2 Introduction

Cell growth and differentiation is critically dependent upon matrix rigidity [11; 16; 21; 61]. How the cellular motility machinery can sense matrix rigidity is unknown but the mechanism(s) of rigidity sensing must be constrained by the basic characteristics of cell motility, including the size of the rigidity sensing machinery and the physical quantity 'measured' by the cell [12]. Studies using beads point to a critical dimension of $\sim 1\mu$m for rigidity sensing. Galbraith *et al.* determined that the area of contact with Fn-coated surface could influence the formation of adhesive complexes. They added different sizes of Fn-coated beads to the lamella of fibroblast and examined the pattern of accumulation of vinculin around the beads. It was found that that cells would assemble adhesion contacts at the edges of large beads with contact areas of more than about 1 micrometer squared [62] (Fig. 2.1) whereas with sub-micron beads force from a rigid laser tweezers was needed to cause adhesion contact assembly [53] (Fig. 2.2). Studies also suggest that cells measure the force required to produce local displacements of $\sim$ 100 nm in order to deduce rigidity. The amount of matrix displacement needed to sense a rigid surface was estimated to be on the order of 100 nm from studies of bead displacement in laser tweezers [62].

By using arrays of 1 and 2 μm diameter elastomeric pillars of different stiffness, Saez *et al.*, showed that force exerted by cells increased linearly with rigidity of the pillars [60]. Thus, the cells generated average pillar displacements on the order of 130 nm independent over the range 2-130 nN/μm (Fig. 2.3)

Because the bead studies suggest a change in behavior below $\sim 1\mu$m, in this study we extend the micropillar force measurement technique3 to the sub-micron regime, in order to explicitly examine force dynamics as a function of length scale, contact area, and contact rigidity. In addition, because the measurement of rigidity must be transient due to the plasticity of normal cells [12], we examine the dynamics of pillar displacement and force generation. Finally, because cells rapidly measure the rigidity of the substrate in the initial contact period, we concentrate on force dynamics in the initial spreading phase, which has

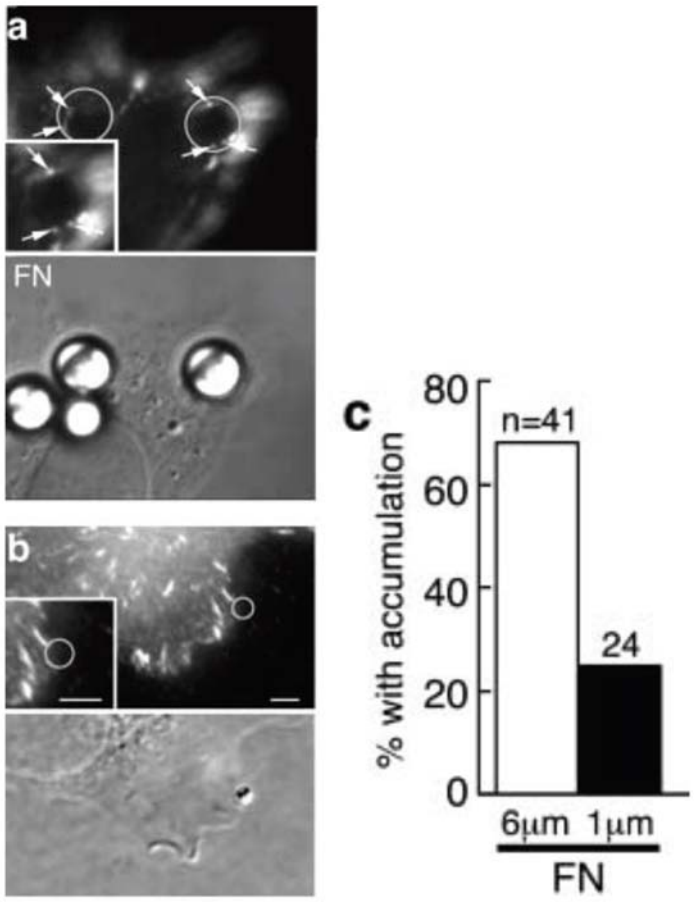

Figure 2.1: (a) Vinculin accumulates as punctate focal complexes around 6 μm fibronectin-coated beads. (b) Focal complexes do not form around 1 μm beads. (c) Only 6 μm fibronectin-coated beads induce focal complexes. Numbers indicate number of beads (from [62]).

not previously been examined.

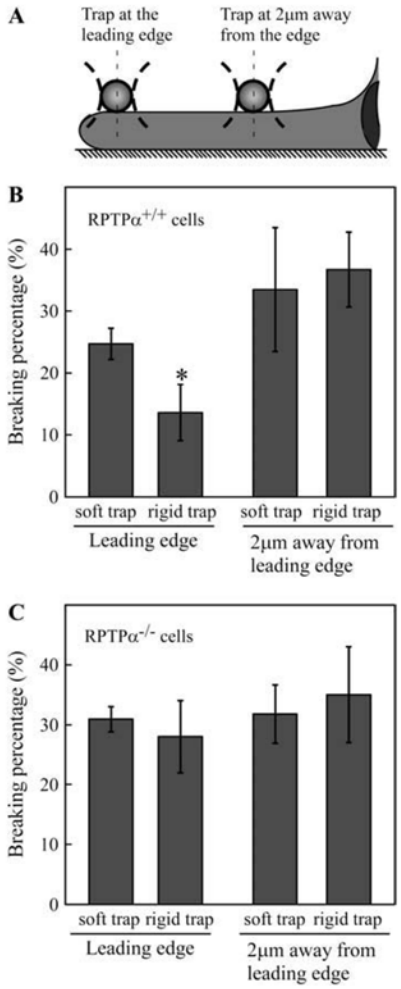

Figure 2.2: (a) Schematic graph showing the position of rigid or soft trap on the lamellipodia of a spreading cell. (b-c) Force from a rigid laser tweezers is needed to cause adhesion contact assembly (from [53]).

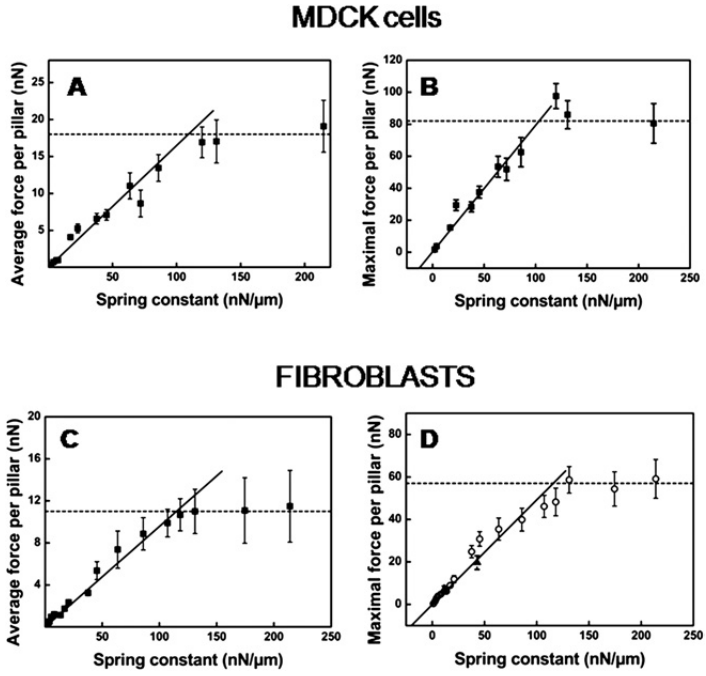

Figure 2.3: Traction forces exerted by islands of epithelial cells (a-b) and fibroblast (c-d) as a function of substrate rigidity. Force exerted by cells increased linearly with rigidity of the pillars (from [60]).

2.3 Experimental

2.3.1 Fabrication process of molds

2.3.1.1 Micron-scale pillar arrays

The central part of the work described below involves fabrication of a Si structure, which is then used as a mold for fabrication of the elastomer posts. The mold is made by etching a uniform array of holes in a hexagonal pattern into a Si wafer. Molding silicone elastomer into the structure yields the reverse structure, namely an array of hexagonal pillars. The molds were fabricated using photolithography.

Photolithography

The fabrication process is illustrated in figure 2.4. Si wafers are RCA-cleaned. The RCA clean is the industry standard for removing contaminants from wafers which present on the surface of silicon wafers at the start of processing, or accumulated during processing, have to be removed at specific processing steps in order to obtain high performance and high reliability semiconductor devices, and to prevent contamination of process equipment, especially the high temperature oxidation, diffusion, and deposition tubes. The RCA cleaning procedure has three major steps used sequentially:

I. Organic Clean: Removal of insoluble organic contaminants with a $5:1:1$ $H_2O:H_2O_2:NH_4OH$ solution.

II. Oxide Strip: Removal of a thin silicon dioxide layer where metallic contaminants may accumulate as a result of (I), using a diluted $50:1$ $H_2O:HF$ solution.

III. Ionic Clean: Removal of ionic and heavy metal atomic contaminants using a solution of $6:1:1$ $H_2O:H_2O_2:HCl$.

The RCA cleaning technique does not attack silicon, and only a very thin layer of silicon dioxide is removed (in II) in the process. The procedure was also designed to prevent replating of metal contaminants from solution back to the wafer's surface. When finished, the polished side should be specular with no residue.

RCA-cleaned Si wafers were oxidized at 1100 °C for 2 h. to form a 950 nm-thick SiO_2 film. Adhesion promoters are used to enhance the bonding of photoresist to a silicon dioxide surface. Here HMDS was applied as an adhesion promoter from the gas phase on heated substrates. The wafers were coated with 1.2 μm-thick photoresist (Shipley SPR 7000). The resist was then soft-baked on a hot plate at 90 °C for 60 s, followed by another bake at 115 °C for 60 s to remove residual solvent and mechanical stress in the film.

The wafers were patterned by conventional UV photolithography (Fig. 2.4b). A photomask, with hexagonal arrays of holes, was fabricated using a Heidelberg DWL 66 laser pattern generator. After exposing the photoresist in a GCA Autostep 200 system, the wafer was post exposure baked at 90 °C for 60 s on the hotplate and developed with AZ 300 MIF

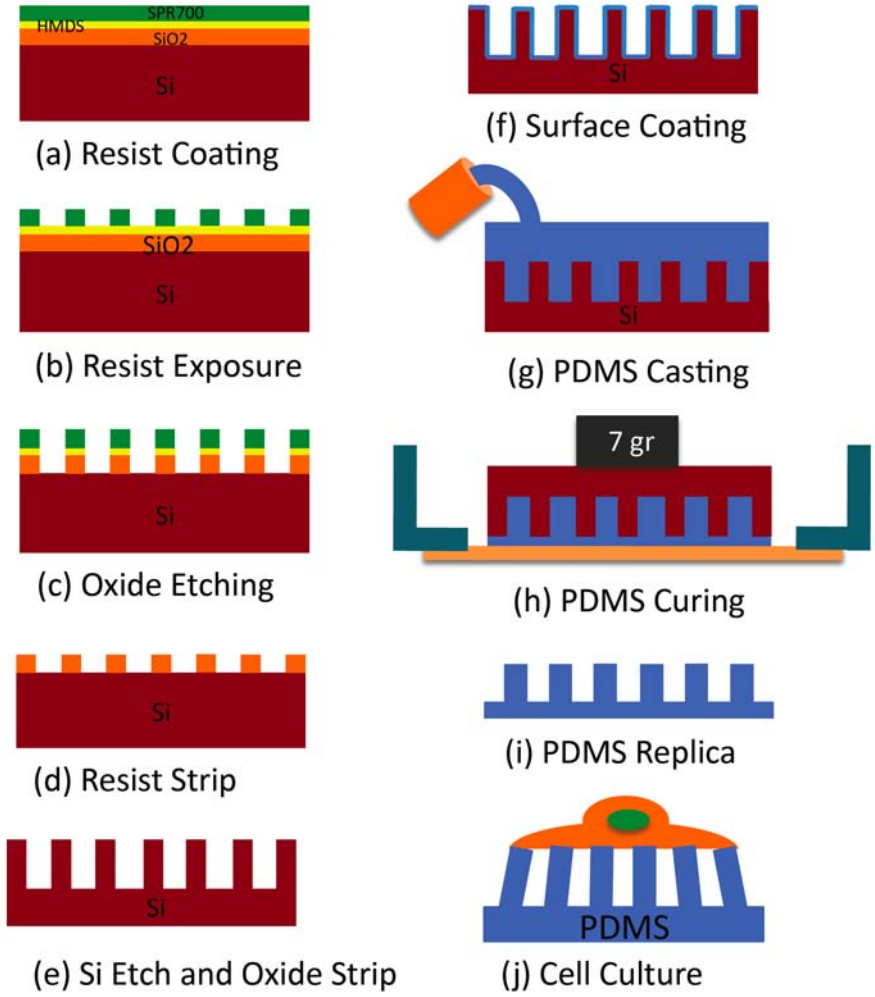

Figure 2.4: Schematic process flow for drawing fabrication of arrays of PDMS pillars

developer. The patterned resist was then treated with a long post-development bake at 90 °C for one hour in order to smooth the sidewalls, followed by O_2 plasma descum for one minute (Fig. 2.5).

Using the patterned resist as a mask, the SiO_2 was etched by RIE (Oxford PlasmaLab 80+) (Fig. 2.4c). Using gas flow rates of 2 sccm O_2, 50 sccm CHF_3, 40 mTorr pressure and 200 W RF power, the etch rate of the silicon dioxide was measured to be about 29 nm/min.

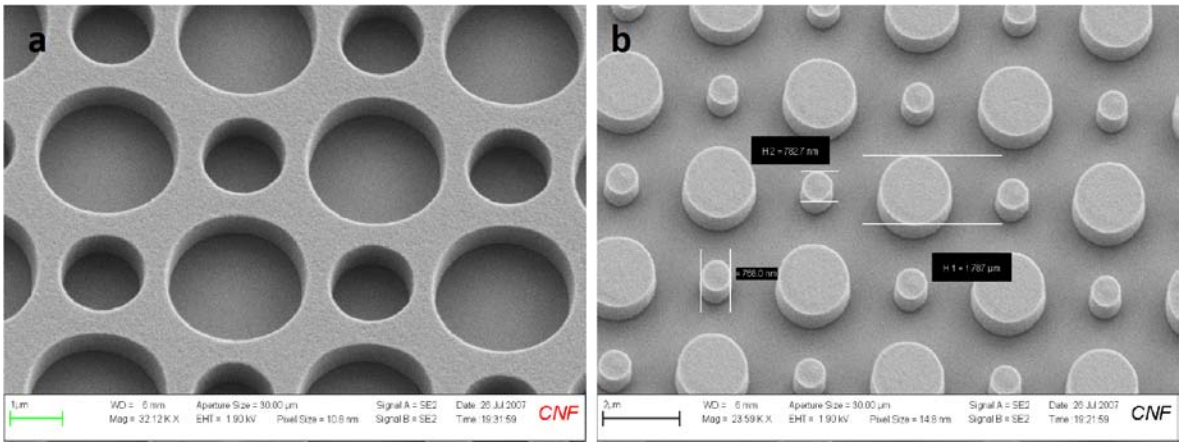

Figure 2.5: SEM image of patterned resist by photolithography in (a) holes and (b) posts.

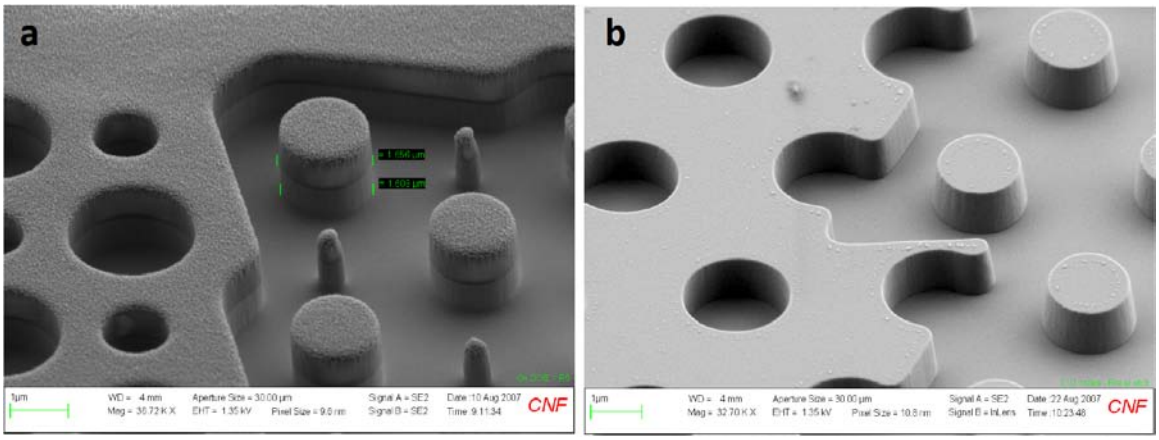

Figure 2.6: (a) SEM image of etched holes and posts with different diameters in oxide. The resist mask is still on the top. (b) SEM image of oxide while resist masks are removed.

A 20% overetch was applied in order to ensure a clean sidewall. Figure 2.6 is an SEM image of etched oxide with the resist mask on the top. The oxide etch has an important impact on the final result since the etch profile of the underlying Si depends critically upon the profile of the oxide hard mask. An underexposed resist masking will result in a non-vertical oxide

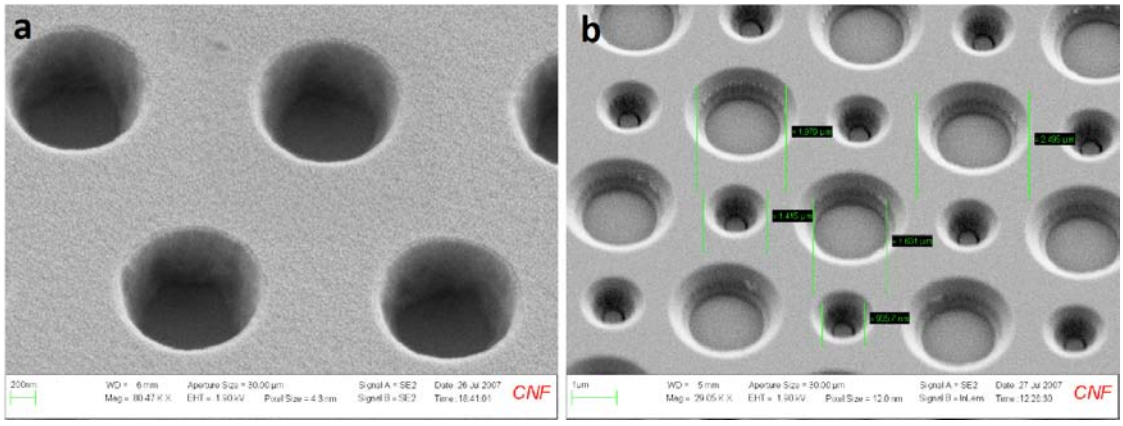

Figure 2.7: (a) SEM image of underexposed resist in oxide substrate. (b) SEM image of etched oxide with underexposed resist mask. The side walls are not vertical.

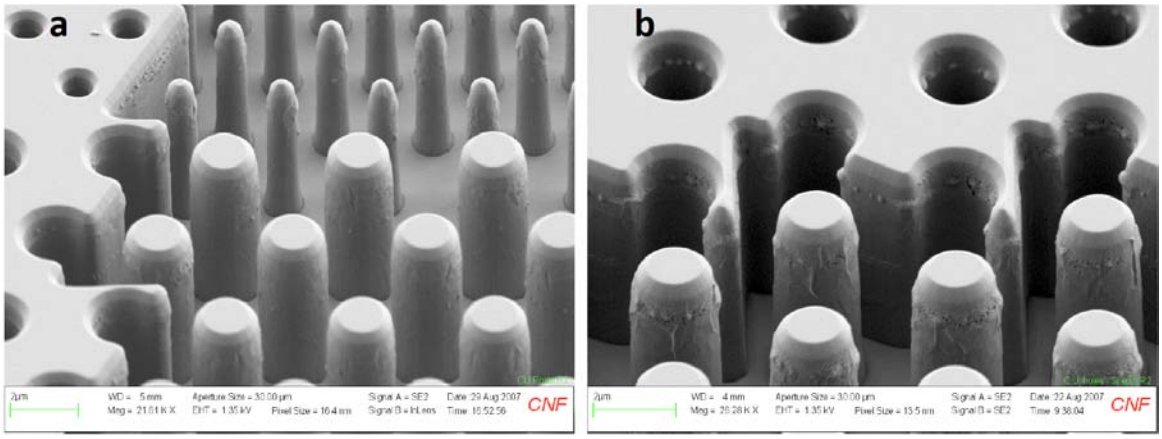

Figure 2.8: SEM image of etched holes and posts in silicon substrate with different diameter. The oxide mask is still on the top of silicon.

etch (Fig. 2.7). A non-vertical or rough oxide masking will result in non-vertical wells.

The next fabrication step involved etching Si using the SiO_2 as a hard mask (Fig. 2.4d-e). First, the resist was removed in a PlasmaTherm 770 ICP-RIE system. The Si holes were then etched to the desired depth in a Chlorine based ICP-RIE system under the following

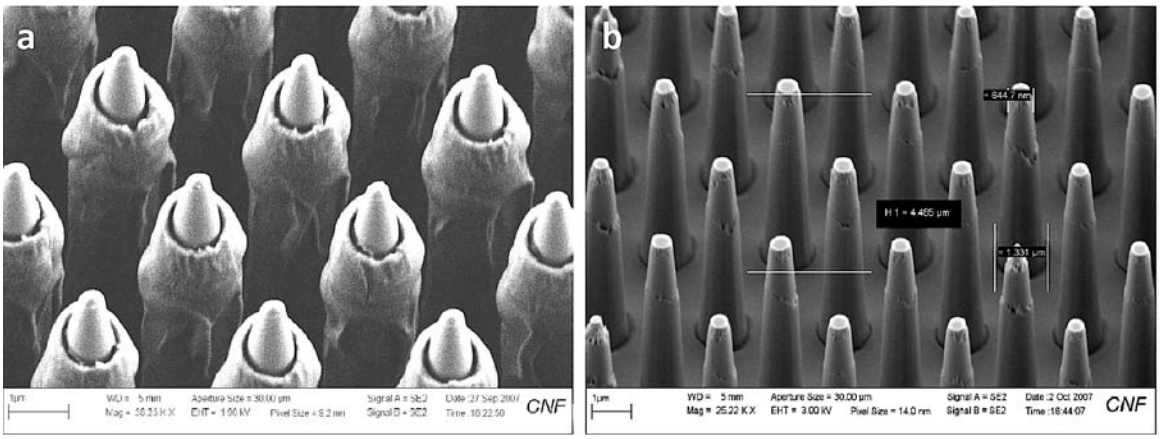

Figure 2.9: (a) SEM image of etched posts in silicon substrate with thin oxide masks. (b) SEM image of etched posts in silicon after removing of the oxide. The profile of etched posts are tapered.

condition: 70 sccm Cl_2, 2 sccm BCl_3, 2 sccm H_2; 20 mTorr pressure; 85 W RF power and 800 W ICP power. The etch rate of the silicon was about 300 nm/min. Figure 2.8 shows the SEM image of etched silicon in holes and posts with different sizes. The holes and posts have vertical and smooth sidewalls. If the thickness of the oxide mask is not thick enough, the final etch profile of the etched Si will be tapered (Fig. 2.9). The resulting wafer was then immersed in BOE to remove the oxide mask.

Bosch process

Bosch process is an etch process consisting of a series of sequential etching (using SF_6) and passivation (using C_4F_8) steps in order to achieve vertical structure. The pattern goes through an etch step, afterward, the etched part get passivated. The passivation layer protects the entire substrate from further chemical attack. In next step, the directional ions etch the passivation layer at the bottom of the holes (and not sidewalls) and expose substrate to further etching step. These steps repeat until the desired depth.

The fabrication process is illustrated in figure 2.10. RCA-cleaned Si wafers were treated

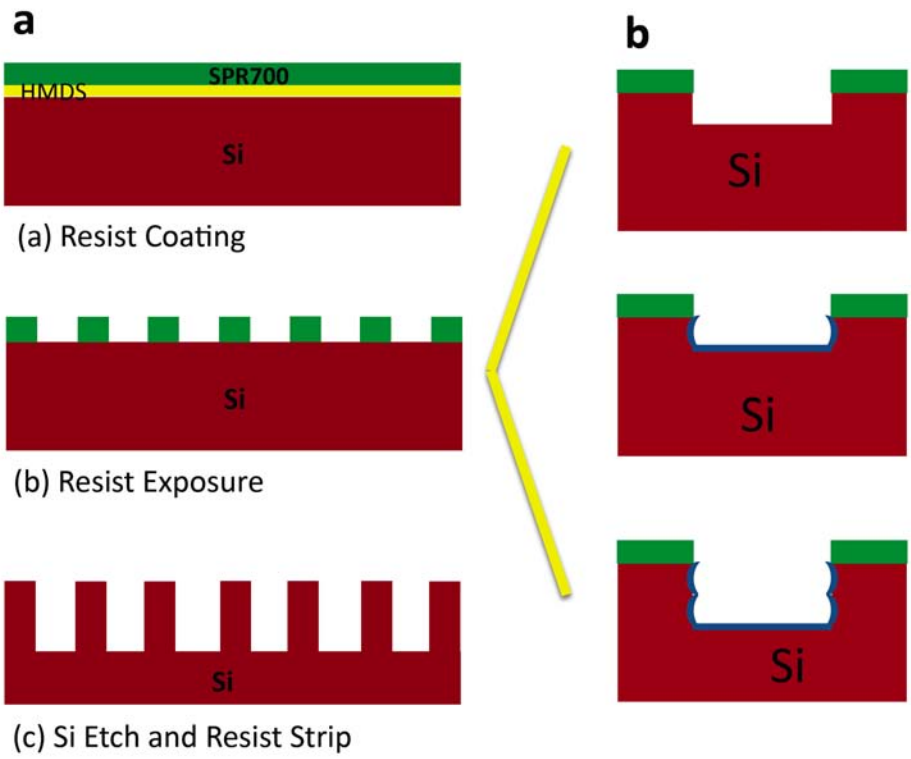

Figure 2.10: Schematic process flow for drawing fabrication of arrays of holes using Bocsh process.

with HMDS and coated with 1.2 μm-thick photoresist (Shipley SPR 7000). The resist was then soft-baked on a hot plate at 90 °C for 60 s, followed by another bake at 115 °C for 60 s to remove residual solvent and mechanical stress in the film.

The wafers were patterned by conventional UV photolithography (Fig. 2.10a). A photomask, with hexagonal arrays of holes, was fabricated using a Heidelberg DWL 66 laser pattern generator. After exposing the photoresist in a GCA Autostep 200 system, the wafer was post exposure baked at 90 °C for 60 s on the hotplate and developed with AZ 300 MIF developer. The patterned resist was treated with O_2 plasma descum for one minute.

Using the patterned resist as a mask, the Si was etched by Bosch Process in a Unaxis 770 ICP-RIE system (Fig. 2.10b). Using gas flow rates of 60 sccm C_4F_8, 30 sccm SF_6,

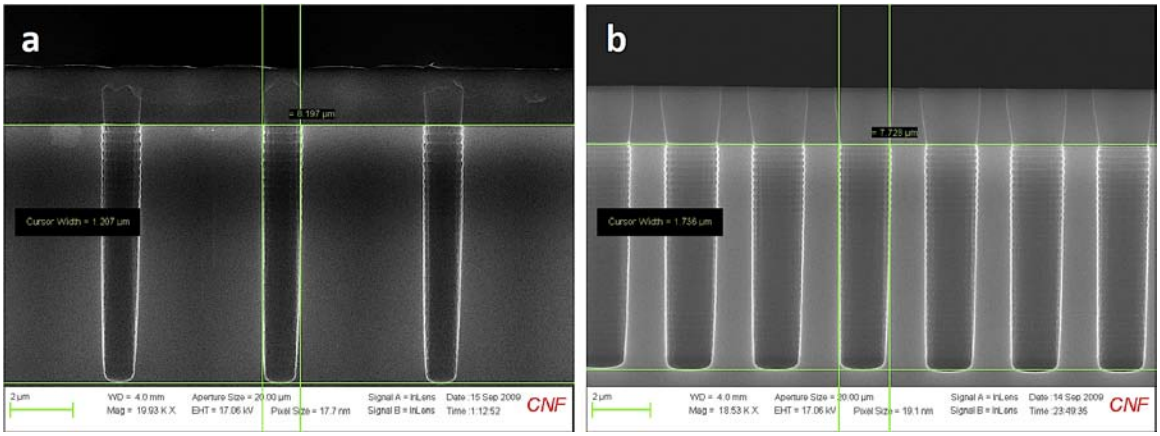

Figure 2.11: SEM images of (a) 1 μm diameter hole and (b) 1.7 μm diameter hole in silicon substrate using Bosch process. The height of holes are about 8 μm .

40 sccm Ar, 10 sccm O_2, 8 mTorr pressure and 10 W RF_1 and 700 RF_2 power, the etch rate of the silicon dioxide was measured to be about 360 nm/min. The resist was then removed in an acid-etching tank. Figure 2.11 is the SEM image of high aspect ratio holes in silicon using Bosch process technique. The default Bosch process recipe in Uniaxis has about 100nm scallops, which will be problematic in release of elastomer from the holes after curing. In order to reduce the scallops, the Si structures were thermally oxidized (1000 °C, 30 min) and dipped in HF. This process was repeated twice. This reduces the scalloping to less than 50nm (Fig. 2.12).

2.3.1.2 Sub-micron scale pillar arrays

The fabrication process of submicron holes is very similar to the micron holes described in Bosch process section. Briefly, RCA-cleaned Si wafers were treated with HMDS and coated with 1.2 μm-thick photoresist (Shipley 700). The resist was then soft-baked on a hot plate at 90 °C for 60. The wafers were patterned by conventional UV photolithography. After exposing the photoresist in a GCA Autostep 200 system, the wafer was post exposure baked at 90 °C for 60 s on the hotplate and developed with AZ 300 MIF developer. The patterned

Figure 2.12: (a) SEM image of etched holes in silicon substrate using Bosch process. The scallops are more more than 100 nm. (b) Holes are further thermal oxidized and dipped in HF. The scallops are less than 50 nm.

resist was treated with O_2 plasma descum for one minute.

Using the patterned resist as a mask, the Si was etched by Bosch Process in a Unaxis 770 ICP-RIE system. Using gas flow rates of 60 sccm C_4F_8, 30 sccm SF_6, 40 sccm Ar, 10 sccm O_2, 8 mTorr pressure and 10 W RF_1 and 700 RF_2 power, the etch rate of the silicon dioxide was measured to be about 237 nm/min. The resist was then removed in an acid-etching tank. Figure 2.13 is the SEM image of submicron hole in silicon using this technique.

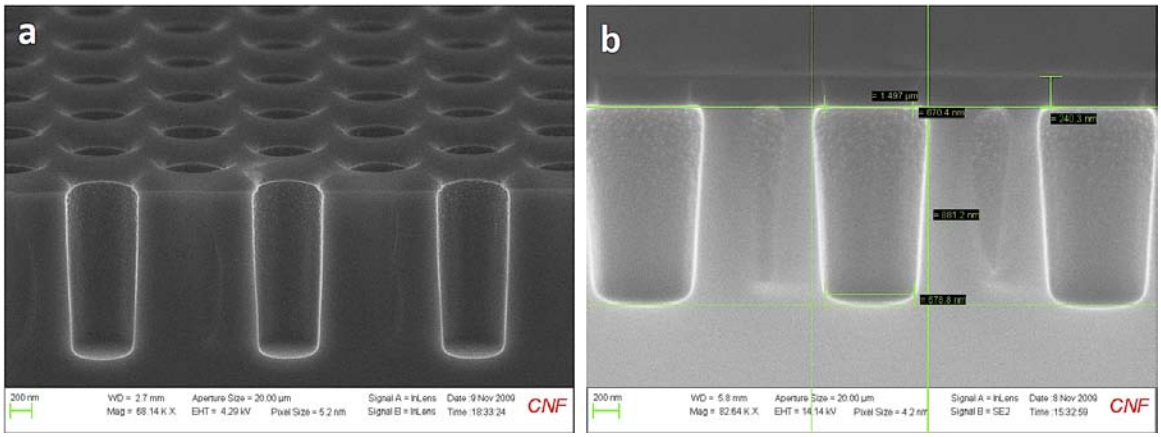

Figure 2.13: SEM image of sub-micron holes in Silicon substrate. The diameter of holes are 500 nm and the pitch is 1 μm. The height of the holes is 1.5 μm.

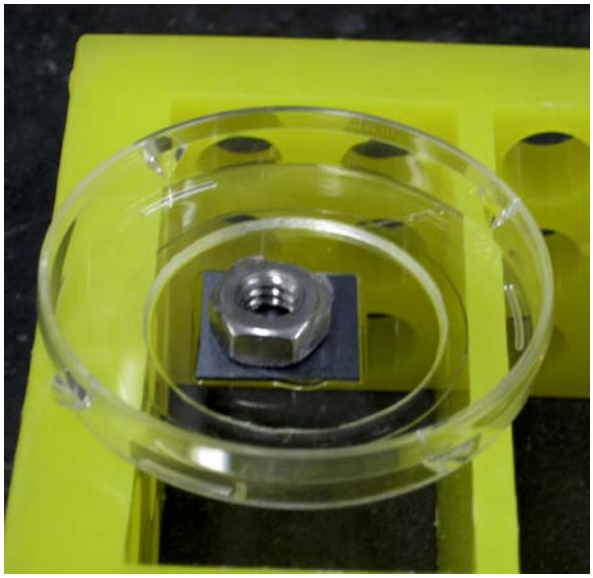

Figure 2.14: The silicon mold with PDMS is flipped and placed in the glass bottom petri dish. The weight on the top of mold ensures the substrate to be thin enough for microscopy.

2.3.2 Elastomer pillars, surface chemistry

The Si structures were used as molds for fabrication of post arrays using Polydimethylsiloxane (PDMS). Prior to PDMS molding, the patterned wafers were piranha cleaned for 6 h at room temperature, followed by a one minute O_2 plasma clean and overnight silanization in vapor phase tridecafluoro-trichlorosilane in vacuum (100 μL in a glass vial inside the vacuum jar). This facilitates the subsequent release of elastomer from the wafer after curing. The PDMS (Sylgard 184, Dow Corning) was mixed thoroughly with its curing agent (10:1) for no less than 5 minutes, centrifuged (2000 RPM, 3 min) and degassed in a vacuum for about 10 minutes or until cleared. For micron-scale pillar array, PDMS was poured over the silicon mold and cured at 70 °C for 12 h, in order to achieve a Young's modulus of 2 $\pm$ 0.1 MPa. The PDMS was then peeled off of the mold while immersed in ethanol (Fig. 2.4i). Use of ethanol is critical to this step considering the high aspect ratio of the posts. If the pillars are allowed to dry, they tend to irreversibly adhere to one another.

To observe sub-micron pillar array, a high magnification objective, 100X (NA = 1.4, working distance = 0.13 mm), is needed. Since the objective working distance decreases as the magnification and numerical aperture both increase, the PDMS base of the pillar substrate needs to be thin so that the tip of pillars could be observed. To this end, the glass bottom petri dish was treated with O_2 plasma for $1 \sim 2$ minutes. This helps PDMS substrate to stick to the glass after curing. Having the glass bottom petri dish ready, a drop of PDMS was placed on the top of the mold and was degassed again in a vacuum for a few minutes. This helps PDMS to completely enter the holes and the air trapped at the bottom of holes comes out. Bubbles appeared in the PDMS ensuring the removing of trapped air. The mold with PDMS was then flipped and placed in the glass bottom petri dish. A 1 gr weight was placed on the top of mold to make the substrate even thinner (Fig. 2.4h and 2.14). PDMS was then cured at 70 °C for 12 h. The mold was removed off of the PDMS while immersed in ethanol (Fig. 2.4i).

Figure 2.15 shows a scanning electron micrograph of a uniform array of micron and sub-micron PDMS pillars.

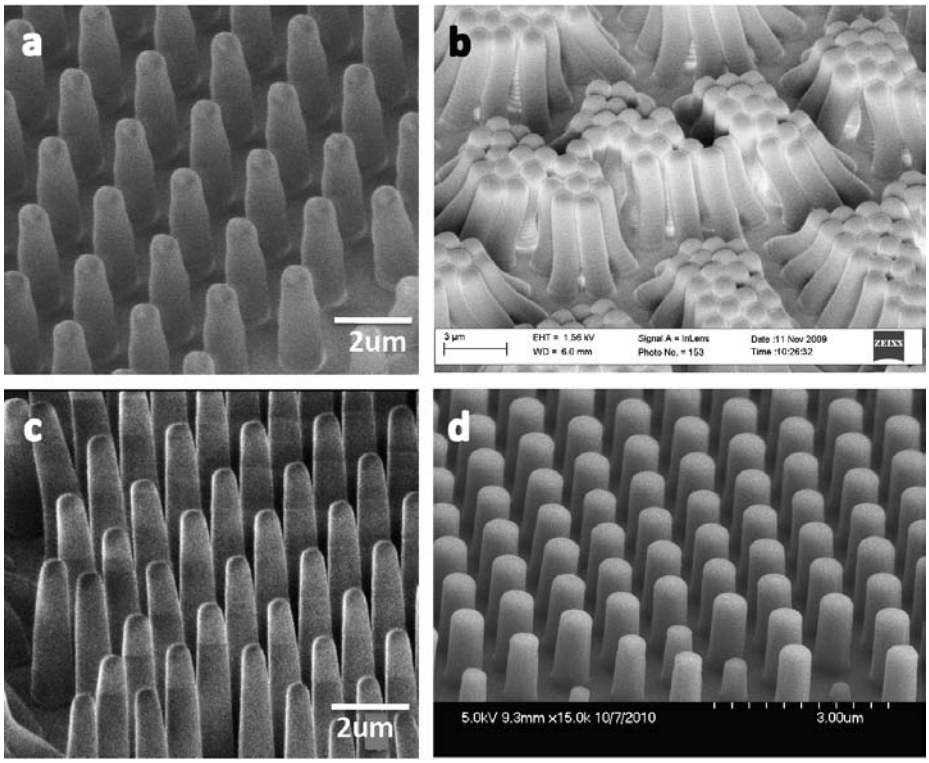

Figure 2.15: SEM image of uniform arrays of micron and sub-micron PDMS pillars with different diameters and heights. (a-c) Micron-scale hexagonal array of PDMS pillars using different etch techniques. (d) Sub-micron scale hexagonal array of PDMS pillars.

2.3.3 Cell culturing and preparation

Mouse embryonic Fibroblast cells (MEF) were cultured in DMEM supplemented with 10 % fetal bovine serum (FBS), 1% L-glutamine and 100 IU/mg penicillin-streptomycin (Invitrogen) at 37°C and 5% CO_2 (all from Gibco). Before measurements, PDMS pillar substrates were coated with human plasma fibronectin (50 μg/ml; Roche) and incubated at 37 °C and 5% CO_2 for 1 hour. Cells were then trypsinized, resuspended in DMEM for 30 minutes at 37 °C for recovery, and plated on the substrate. In all the processes, pillar substrate has to stay under media (in wet atmosphere) in order to avoid pillars to adhere each other.

For immunostaining, cells were cultured on PDMS pillar substrates for 30 minutes, fixed

in 4% paraformaldehyde in PBS (Phosphate Buffered Saline) for 15 minutes, quenched with 50 mM ammonium chloride in PBS for 15 minutes, and permeabilized with 0.1% Triton X-100 in PBS. Cells were then rinsed with 0.2% fish gelatin in PBS, incubated with a primary antibody to paxillin (BD transduction labs, clone 349) for one hour and then with fluorophore-conjugated secondary antibodies to IgG (Invitrogen).

2.3.4 Video microscopy and data analysis

Time-lapse imaging of pillars was performed with bright field microscopy using a CoolSNAP HQ (Photometrics) attached to an inverted microscope (Olympus IX-70) maintained at 37 °C. Images were recorded at 1 Hz using a 100X (1.4 NA, oil immersion; Olympus) objective for sub-micron pillars and a 40X (0.6 NA, air; Olympus) for micron-scale pillars. Temporal variation of the position of pillars was collected in a period of time. The position of each pillar in each frame was determined using the particle tracking plug-in for ImageJ software [National Institutes of Health (NIH)], which employs an autocorrelation algorithm. In all cases, pillars were tracked before the cell spread over them, in order to establish an equilibrium (zero force) position. The time-dependent displacement of a given pillar was then calculated by subtracting its initial position (corresponding to zero force) from the position in a given frame. To remove stage drift the average displacement of a set of pillars far from any cells was subtracted from the data. Finally, the position vs. time data for each pillar was low-pass filtered with a cutoff frequency of 0.1 Hz. Figure 2.16a shows an example of a pillar highlighted in red at its initial position until the cell has passed by. Figure 2.16b represents the deflection magnitude for the highlighted pillar plotted versus time. For a given pillar, the displacement was zero ($\pm$ 5 nm noise) outside the cell and then would rise to a maximum value after initial contact, followed by a gradual decrease as the spreading edge moved away from the pillar. Additional displacement oscillations also appeared on top of this broad pattern. The black trace represents the noise, which is about 5 nm, measured and averaged on pillars that are not associated with any cells. This collected data was analyzed from the point when the cell was associated with the selected pillar. A custom code in MATLAB was written to find sequential maxima and minima in the displacement traces. The threshold for the peak finder was set to 15% of the average

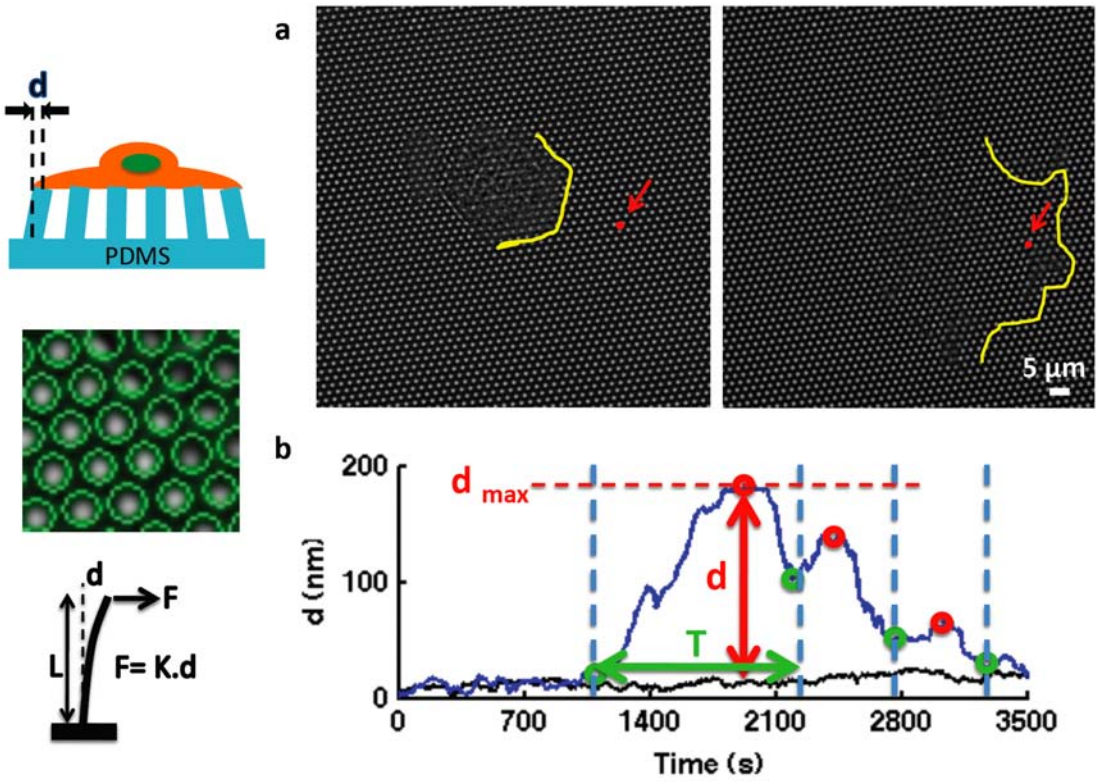

Figure 2.16: Illustration of the method of calculation of forces exerted by cell to pillar substrate. (a) shows the position of cell toward the selected pillar at initial and after cell passes the pillar over a period of time. (b) The temporal variation of the magnitude of deflection of the selected pillar as a function of time is shown in blue. The black trace represents the noise that is the deflection of a pillars that were not associated with the cell. The maxima and minima of the trace are shown in red and green, respectively. For each peak, the displacement (d), the period (T), and the corresponding force (F) is calculated

maximum point of tracked data for a set of same size pillars. The maxima and minima are shown in red and green circles on the trace respectively. For each individual peaks, the displacement and period of the peaks and the corresponding force is calculated as shown in figure 2.16b. With the existing resolution of the pillar deflection, we are able to obtain

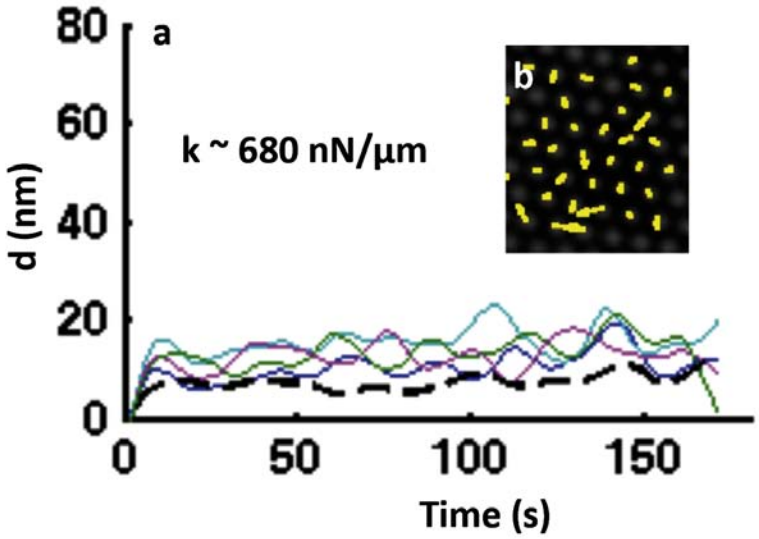

Figure 2.17: Deflection of single pillars with diameter 0.5 μm and height 0.3 μm, and stiffness 680 nN/μm. (a) The colored traces represent pillars under the cell, while the black trace represents the average measured deflection of pillars outside the cell. (b) Spatial distribution of the force field (yellow arrows) of representive pillars

force resolution from 0.12 up to 3.5 nN over the range of pillar stiffness.

Epifluorescent imaging was completed on an Olympus IX-81 microscope with 100X (1.4 NA, oil immersion; Olympus) objective and a Cascade II camera (Photometrics). Imaging software was SimplePCI (C-Imaging).

2.3.5 Lensing effect

To establish the accuracy of the detection technique, cells were seeded on high stiffness, non-deformable pillars ($D = 500$ nm, $H = 300$ nm, $k = 680$ nN/μm). These pillars showed an apparent displacement of only ~ 15 nm (Fig. 2.17a). All of the measured displacements in this work are significantly larger than the measurement accuracy.

The displacement vectors of these pillars plotted over time. All of the vectors were showing jittering movements with no specific direction (Fig. 2.17b).

Dimeter (D) (μm)	Height (H) (μm)	Stiffness (k) (nN/μm)	Effective Modulus (E_{eff}) (kPa)
2	12.5	2.4	1.72
	10	4.7	3.4
	6	21.8	15.6
1	5	2.3	3.3
	4	4.6	6.6
	2.6	16.7	24
0.5	1.88	2.7	7.7
	1.1	13.9	40
	0.95	21.5	61.6

Table 2.1: Library of pillars used in this work. The stiffness k corresponds to the bending stiffness of an individual pillar, whereas the effective modulus E_{eff} corresponds to the rigidity of an equivalent continuous substrate.

2.4 Main results

PDMS elastomer pillar arrays were prepared with diameters of 0.5, 1, and 2 μm. For each diameter, three different heights were also prepared to produce about the same range of bending stiffness. The height of pillars has been varied according to their diameter so that we ensure the deflection of pillars caused by cells stay in linear regime of deformation. Pillar spring constants were calculated by Euler-Bernouli beam theory [57]. Since the stiffness of the pillars are proportional to the 4th power of the diameter and inverse cube of the height, we can vary the stiffness ranging roughly from 2 to 22 nN/μm. The equivalent Young's modulus of a pillar substrate compared to a semi-infinite continuous elastic substrate, E_{eff}, was calculated by $E_{eff} = 9k/2\pi D$ [58]. Table 2.1 shows pillar dimensions and resulting stiffness.

For each pillar array, we studied the force scaling and dynamics of pillar movement, cellular force distribution on pillar arrays and the focal adhesion distribution on pillars. All

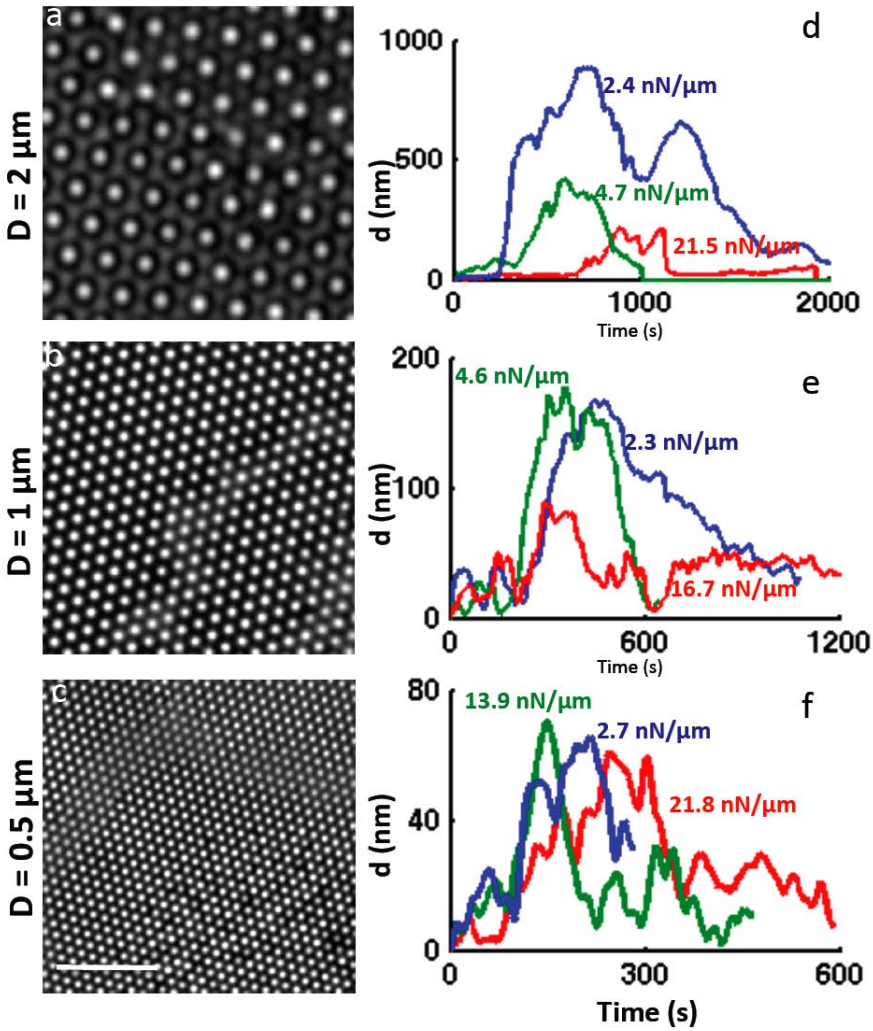

Figure 2.18: (a-c) Transmission image of MEF cells grown on pillars a few minutes after plating. The diameters of the pillars are 2 μm (a,d), 1 μm (b,e) and (c,f) 0.5 μm; the center-center distance is twice the diameter in each substrate. Scale bar 10 μm. (d-f) Deflection of representative pillars with three different stiffnesses for each diameter as a function of time.

the results were compared and analyzed with each other. A dramatic difference in cellular response on the micron and sub-micron pillars was observed.

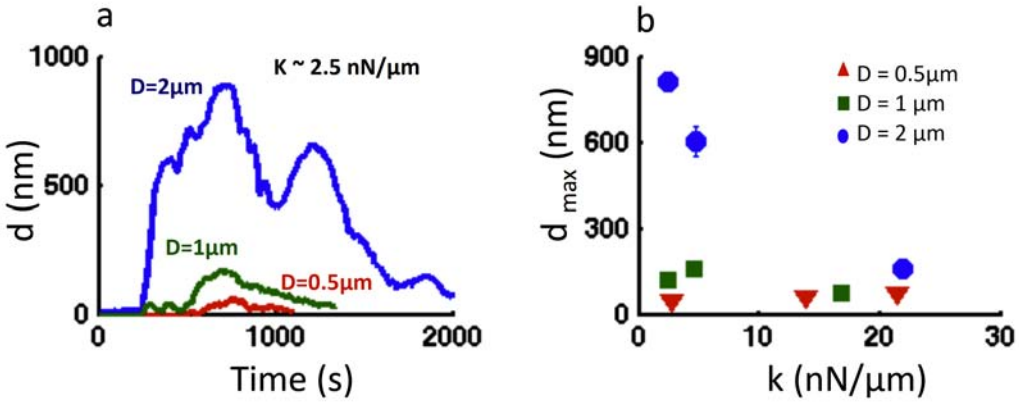

Figure 2.19: (a) Deflection of pillars with equal stiffness (∼2.5 nN/μm) but different diameter as a function of time. Pillar diameters are 2, 1 and 0.5 μm. (b) Averaged maximum deflection of individual pillars as a function of substrate rigidity. Blue, green and red points represent pillars with diameters of 2, 1 and 0.5 μm, respectively. More than 60 pillars, from 2-4 cells, were analyzed per shown value.

2.4.1 Force scaling and dynamics

Figure 2.18 shows displacement vs. time traces for representative pillars from the nine arrays, starting just before the time of first contact to each pillar. For each substrate, the statistics involved about 60 pillars. Pillar deflection patterns were markedly affected by pillar stiffness and diameter. For micron-scale ($D = 1, 2$ μm) pillars, displacement decreased with increasing stiffness (Fig. 2.18d-e). In contrast, the traces for sub-micron pillars ($D = 0.5$ μm) were largely independent of stiffness (Fig. 2.18f), showing peak displacements of 60 ± 18 nm ($\pm$SD) independent of rigidity. The kinetics of pillar pulling was also a function of pillar size: micron-scale pillars showed an inverse correlation between pillar stiffness and displacement period whereas sub-micron pillars had a constant time of displacement.

There was a dramatic effect of changing diameter on the displacements of the softest pillars (Fig. 2.19a). To quantify the variation in pillar deflection with diameter and stiffness,

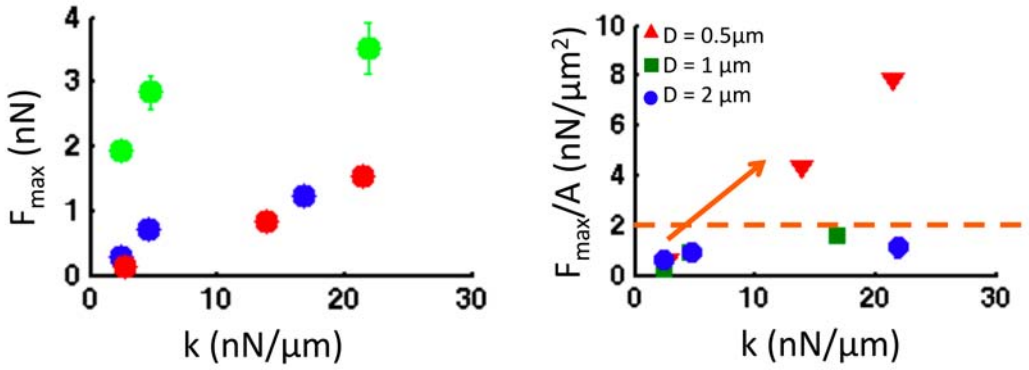

Figure 2.20: Averaged magnitude of traction force (a) and stress (b) on single pillars as a function of substrate rigidity. Blue, green and red points represent pillars with diameters of 2, 1 and 0.5 μm, respectively.

we calculated the average maximum deflection, d_{max}, for all of the pillars examined on each substrate (Fig. 2.19b). Confirming the trend seen in Fig. 2.18f, d_{max} decreased with pillar stiffness for micron-scale pillars, while it was constant for sub-micron pillars.

Figure 2.20a shows the corresponding maximal forces (F_{max}) that deflected the pillars, plotted versus k. It shows strong correlation with the stiffness of pillars. The magnitude of the force exerted by cells to the pillars increases as pillars become stiffer for all three different areas. These results are in agreement with pervious studies that show that softer substrates induce an enhancement of fluctuations at the cell boundaries and a decrease in force magnitude. In case of pillars with diameter of 0.5 μm, we observe a linear increase of the force with respect to the stiffness of the pillars that is not seen in pillars with diameters of 1 and 2 μm. This linear behavior implies that the pillar deflection keeps a constant value. To account for the effect of adhesive area, we then normalized the force corresponding to maximal deflection by pillar area (F_{max}/A), (Fig. 2.20b). For micron-scale pillars, this value stayed roughly constant under 2 nN/μm^2 for all stiffness, indicating that pillar force scaled with adhesive area as previously suggested [29; 43]. For sub-micron pillars, F_{max}/A

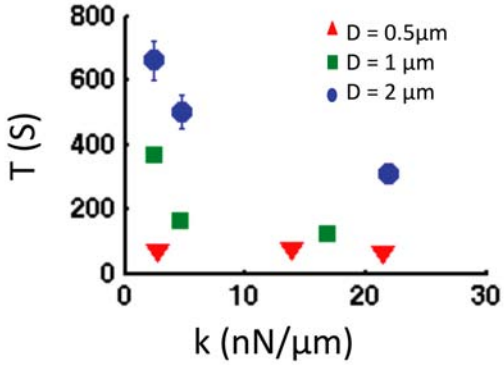

Figure 2.21: Average period of single pillar deflection peaks. Blue, green and red points represent pillars with diameters of 2, 1 and 0.5 μm, respectively.

increased linearly with pillar stiffness (reaching a maximum value of about 8 nN/μm^2), indicating a constant displacement.

To quantify the kinetic component, the average value of the period of the force peaks was also calculated (Fig. 2.21). The period of pulling decreased with decreasing pillar diameter and decreased with increasing stiffness for larger pillars but not for sub-micron pillars, confirming the qualitative change in behavior.

2.4.2 Force distribution

These data suggest that the displacement mechanism may be different for micron-scale and sub-micron pillars. Previous observations have shown that cells can assemble adhesions at the edges of micron-scale beads [2] and the larger pillars may be treated similarly. The lack of similar adhesions on single sub-micron beads suggests that sub-micron pillars may be locally pulled as part of a local rigidity sensing mechanism. This model suggests that the spatial force distribution should be different for micron-scale and sub-micron pillars. When the displacement vectors of the micron-scale pillars near the cell edge were plotted over time, all of the vectors were oriented inward, toward the center of the cell (Fig. 2.22a). This

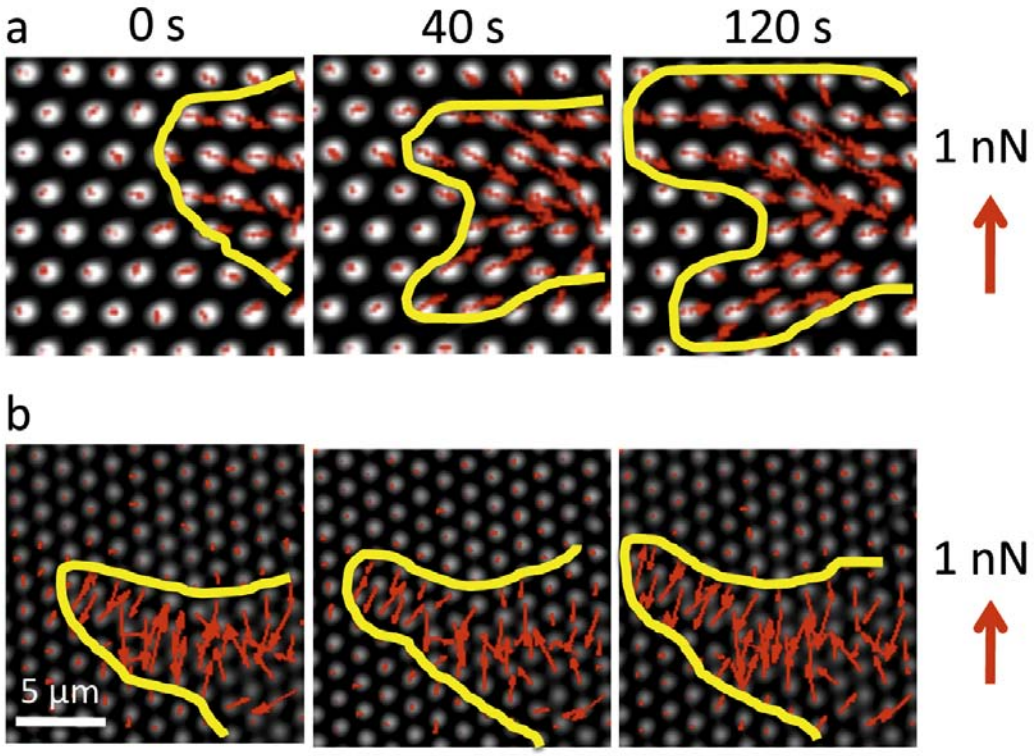

Figure 2.22: Spatial distribution of the force field (red arrows) near the edge of a single cell on pillars with diameters of 1 μm (a) and 0.5 μm (b), captured at the three times shown. The yellow line represents the approximate cell boundary. Scale bar 5 μm. The arrow lengths corresponding to 1 nN are shown to the right of each sequence.

behavior is consistent with previous observations [2; 51; 3] and indicates that the balancing forces were generated on the opposite side of the cell. In contrast, the 0.5 μm pillars showed heretofore unobserved local opposing forces, indicating that a local contraction unit was formed (Fig. 2.22b). Thus, it seems that the larger pillars are pulled centripetally as are all adhesions to rigid matrices, whereas small pillars are pulled locally (Fig. 2.23).

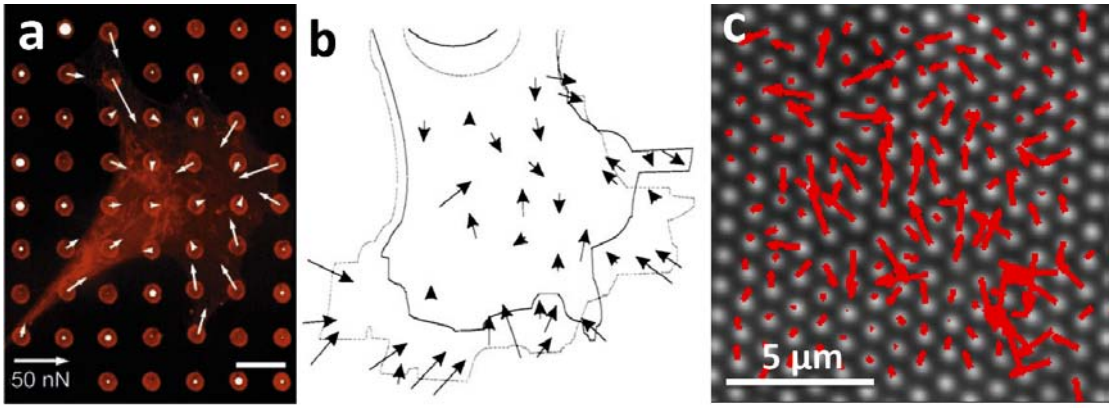

Figure 2.23: Spatial distribution of the force field on micron scale pillars (a-b) and submicron pillars (c). Larger pillars are pulled centripetally whereas small pillars are pulled locally.

2.4.3 Focal adhesion distribution

The distribution of focal adhesions on the pillars further illuminates the interaction of the cell with the substrate. To determine the pattern of focal adhesions, we visualized the distribution of paxillin on pillars with the same stiffness but different diameters. Paxillin was found around the micron-scale pillars and was relatively depleted over the pillars at these early times (Fig. 2.24a-b). In contrast, cells lying on sub-micron pillars formed well defined elongated focal adhesions across multiple pillars similar to those formed on flat substrates (Fig. 2.24c-d), indicating that the interaction with the smaller pillars was more like that with a continuous substrate.

2.5 Discussion

The dramatic differences in the cellular responses on the large and small pillars indicate that these substrates constitute two fundamentally different regimes. We suggest that when the diameter of the pillar is $\sim 1\mu$m or larger, a local contractile complex can form across an individual pillar and sense the very high rigidity of the PDMS (2 MPa). The contractile complex produces the largest forces at the edges of the pillars where the adhesion proteins

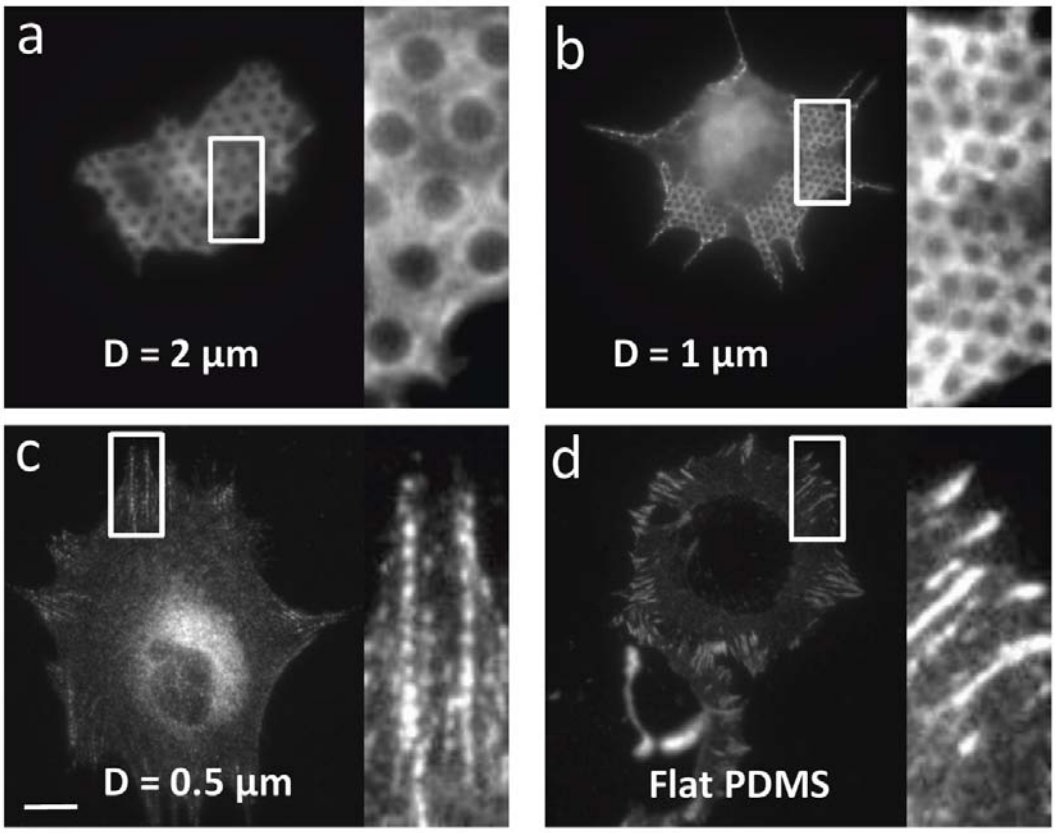

Figure 2.24: Images of immunofluorescence staining of the focal adhesion protein paxillin for pillars of different diameter but equal stiffness (∼2.5 nN/μm), and on a flat substrate (d). The scale bar shown in (c) is 10 μm.

are assembled as was previously observed with matrix-coated beads that had contact areas larger than one micron [62]. Once adhesions are formed, they can couple to the cohesive flow of the actin cytoskeleton and move in the direction of the actin flow. It is interesting that the maximum displacement for the larger pillars scales roughly with the stiffness, giving a constant force per unit area of about 1 nN/μm^2. We note that, in contrast to previous studies [62; 46], this is at an early time when there are no stress fibers and only early adhesions are formed. Thus, the maximal force per unit area is less than observed later

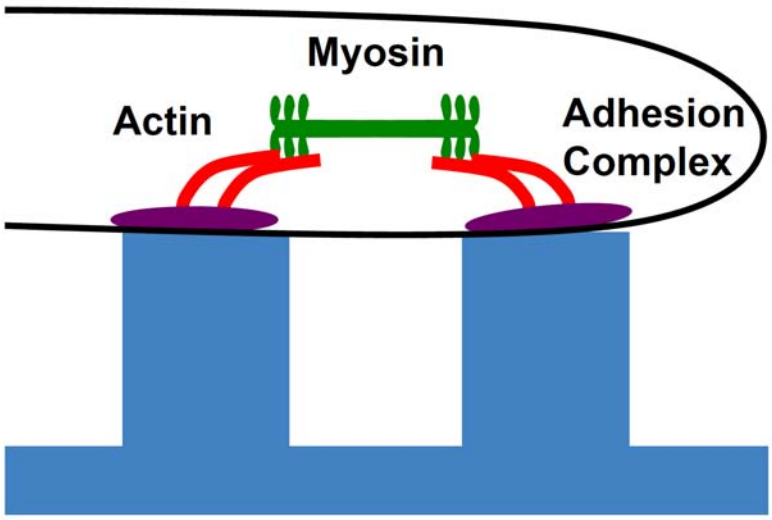

Figure 2.25: (a) Schematic representation of local contractile unit spanning sub-micron pillars

when stress fibers and mature adhesions are formed. The different behavior observed for sub-micron pillars suggests that the local contractile complex is larger than the sub-micron pillars and thus unable to test the rigidity of the PDMS. Instead, a local contractile complex forms between neighboring pillars and tests their bending stiffness (Fig. 2.29). Thus, the pillars are displaced toward each other, and paxillin is distributed evenly across the pillar tops. We suggest that rigidity sensing is accomplished by measuring the force required to displace neighboring pillars by ~ 60 nm each. Because a ten-fold greater number of myosin molecules are needed to displace the ten-fold stiffer pillars by the observed amount, the level of myosin contraction should increase until the pillars are displaced by 60 nm. In such a case, the parallel activation of myosin and a diffusive signaling molecule until the substrate was displaced by 60 nm could produce a response proportional to substrate rigidity [12]. In terms of the mechanism by which the cell can limit the displacement of the pillars to 60 nm, single proteins can easily span such distances and mechanical displacements of over 100 nm have

been reported for adhesion proteins [34; 64]. Further, an average displacement of 130 nm has been found for micron-scale pillars after several hours irrespective of pillar rigidity [58; 60]. Thus, we suggest that localized (1-2 micrometer) contractions recruit active myosin until the matrix is displaced by a defined amount (very rigid surfaces would exceed the range of the system).

2.6 Future work

These studies show that the rigidity sensing system can be localized to matrix contacts separated by 1-2 micrometers and that cells will adjust the force needed to produce a constant displacement of the matrix. This greatly constrains molecular models of the rigidity sensing system and provides ways to test for proteins that might alter the process of early rigidity sensing [5]. These experiments also demonstrate the qualitative and quantitative difference between micron-scale and sub-micron pillar arrays, and suggest that sub-micron pillars should be used to accurately mimic continuous substrates with specified rigidity. These results can be extended to many future studies. A few examples of such studies are listed below:

- An immediate set of experiments is to repeat the same study for other cell lines. This study helps us to see if our findings of constant 60 nm displacement on sub-micron pillars can be extended to other cell lines.

- The same line of force measurement experiments can be done using cells with modified protein expression levels. This study can test the specific proteins that might alter the process of rigidity sensing by measuring the force and its distribution on sub-micron pillar substrates over time. The results will enable us to address the molecular base of cellular response. This study is in progress. Cells with knock down proteins such as α-actinin, filamin, FAK, RPTP, etc. were cultured on sub-micron pillar substrates and temporal variation of the position of the pillars was recorded.

- As it has been suggested in previous sections, the sub-micron pillar substrates should be used to accurately mimic continuous substrates with specified rigidity. The inter-

action of the cell with these substrates can be determined by visualizing the process of distribution of focal adhesion proteins on sub-micron pillars in real time. The pattern of formation of focal adhesion proteins on sub-micron pillar substrates with different stiffness over time can help us to understand the dynamic evolution of cellmatrix adhesions as a function of the stiffness of the matrix. Such experiments could help us understand the interaction of cells with their environment and the mechanisms of rigidity sensing in greater detail.

- Recent experiments have shown that cells can generate periodic waves on sub-micron pillar substrate. Measuring the spatial force distribution of a cell during the generation of periodic waves could help us understand the underlying mechanisms behind protrusion-retraction cycles. This study is important for understanding the mechanical mechanism of rigidity sensing by cells and its time and spatial relation with retraction of the edge with generating force on the substrate. To this end, long time-scale studies on deflection of sub-micron pillars, myosin II, and the focal adhesion protein paxillin, simultaneously with GFP-actin imaging of the cell, enable us to visualize the cellular force map within the evolving cell edge. This could introduce a hypothesis on how periodic protrusion-retraction cycles can function as a mechanism for rigidity sensing at the cell leading edge.

- Recent studies have shown that the rigidity of the extracellular matrix plays a role in stem cell differentiation, by examining differentiation on substrates whose stiffness range from that of brain tissue to that of bone [65; 66]. Chen *et al.* used micron scale pillar substrate to locally change the mechanical properties of the substrate. They have shown that the by changing the rigidity of the pillar substrate, cell differentiation can be modified [66]. Our findings indicate that sub-micron pillars are deflected in fundamentally different regime than micron-scale pillars. It is then expected that using sub-micron pillars will have a different impact on cell differentiation. These substrates can be used to study the mechanics of cell differentiation and investigate the forces associated with differentiation. This might help to engineer artificial tissues and induce and control cell differentiation.

- A challenge in manipulation of immune cells for adoptive immunotherapy applications has been to generate cells with effective self-renewal in vivo to maintain host protection from infection and cancer over weeks to years. Recent evidence suggests that mechanical properties of the ECM have an impact on T cell differentiation. Milone *et al.* have found that softer substrates induce T cells with a memory surface phenotype. These preliminary data support the hypothesis that changing the rigidity of the substrate can have an impact on T cell differentiation. To this end, submicron pillar substrates with different rigidities can be used to study the mechanism of rigidity sensing by T cells and the effect of different rigidity on their differentiation. This study will help to identify mechanical parameters that will be useful in memory T cell expansion.

- Fabricating pillars with diameters smaller than 500 nm as well as changing the density of the pillars can be an addition challenge for future work. This work is in progress. Pillars with diameters of $200 \sim 700$ nm have been fabricated using Silicon substrate. Having such substrates will help us to discover characteristic sizes at the nano-scale regime, study the effect of such substrates on mechanisms of rigidity sensing, and get closer to the molecular level.

2.7 Conclusion

We demonstrated the fabrication process of a flexible PDMS pillar substrate with different diameters and stiffness to study the process of rigidity sensing by cells. We can measure the pattern of traction force generation on matrices. This study showed that cells treat larger pillars fundamentally differently than sub-micron pillars during initial contact formation. In the case of larger pillars, mouse embryo fibroblasts generated a constant force per unit area of about 1 nN/μm^2 on pillars of different stiffness by different displacements; whereas, the sub-micrometer pillars were displaced by about 60 nm irrespective of stiffness. Further, the focal adhesion protein, paxillin, was concentrated at the edges of large pillars but it was focused on the tops of small pillars in a pattern analogous to the pattern on continuous substrates. Thus, we suggest that submicron pillars provide a better substrate for measuring

the basic aspects of rigidity sensing during initial cell spreading.

Chapter 3

Double-height pillars

3.1 Abstract

The mechanical properties of a cell's environment can alter behavior such as migration and spreading, and control the differentiation path of stem cells. Here we describe a technique for fabricating substrates whose rigidity can be controlled locally without altering the contact area for cell spreading. The substrates consist of elastomeric pillar arrays in which the top surface is uniform but the pillar height is changed across a sharp step. Preliminary results demonstrate the effects on cell migration and morphology at the step boundary.

3.2 Introduction

As explained previously in chapter 1, cells generate traction forces in the nanonewton range during adhesion and migration. They respond to many environmental cues including substrate physical attributes such as geometry, density and stiffness[1]. In order to quantify the mechanical interaction of cells with their environment, it is important to control the mechanical properties of the cell's environment, and measure the forces exerted by the cell.

The complex interplay between the rigidity of the substrate and the cells' force response is still poorly understood, as seen previously in chapter 2. In order to explore how cells can detect their environments and study the effect of rigidity, a system is needed that can mimic biological stiffness. To this end, high-density microfabricated arrays of vertical elastomeric

posts have been used to both control the rigidity of the substrate and to measure cellular forces.

A question of primary importance is the behavior of cells at the boundary between regions of substrate with different rigidities. Measurements of cells behavior and force generation in this peculiar state will shed new light on the mechanisms at play in cellular rigidity response. In order to isolate the effect of rigidity, the top surface of the substrate should be uniform (both geometrically and chemically) across the boundary, while the underlying stiffness changes. To accomplish such a goal, we use arrays of posts with the same diameter and spacing, but different heights.

In this work, we describe fabrication and initial testing of structures that provide multiple stiffness surfaces in a single substrate. The structures are hexagonal arrays of posts in which the post diameter is kept constant and the top surface of the posts lies in one plane but the height of the posts in selected areas is varied, resulting in a change in stiffness. These arrays are designed to probe the effect of a sharp rigidity change on the mechanical interaction of cells with their underlying substrate.

3.3 Experimental

3.3.1 Fabrication of arrays of deep holes

The central part of the work described below involves fabrication of a Si structure, which is then used as a mold for fabrication of the elastomer posts. The mold is made by first etching a uniform array of holes into a wafer, then performing a second etch that reduces the height of the Si substrate over half of the array while leaving the hole bottoms at the same level. Molding silicone elastomer into the structure yields the reverse structure, namely an array of posts with a uniform top surface but with a step in the underlying substrate (Fig. 3.1j).

The fabrication process is illustrated in Fig. 3.1. fig. Uniform array of holes in silicon wafer was made by photolithography as described previously in chapter 2. Briefly, RCA-cleaned Si wafers were oxidized at 1100 C for 2 h to form a 950 nm-thick SiO_2 film. The wafers were coated with 1.2 μm-thick photoresist (Shipley SPR 7000) using Hexamethyldisilazane (HMDS) as an adhesion promoter. The resist was then soft-baked on a hot

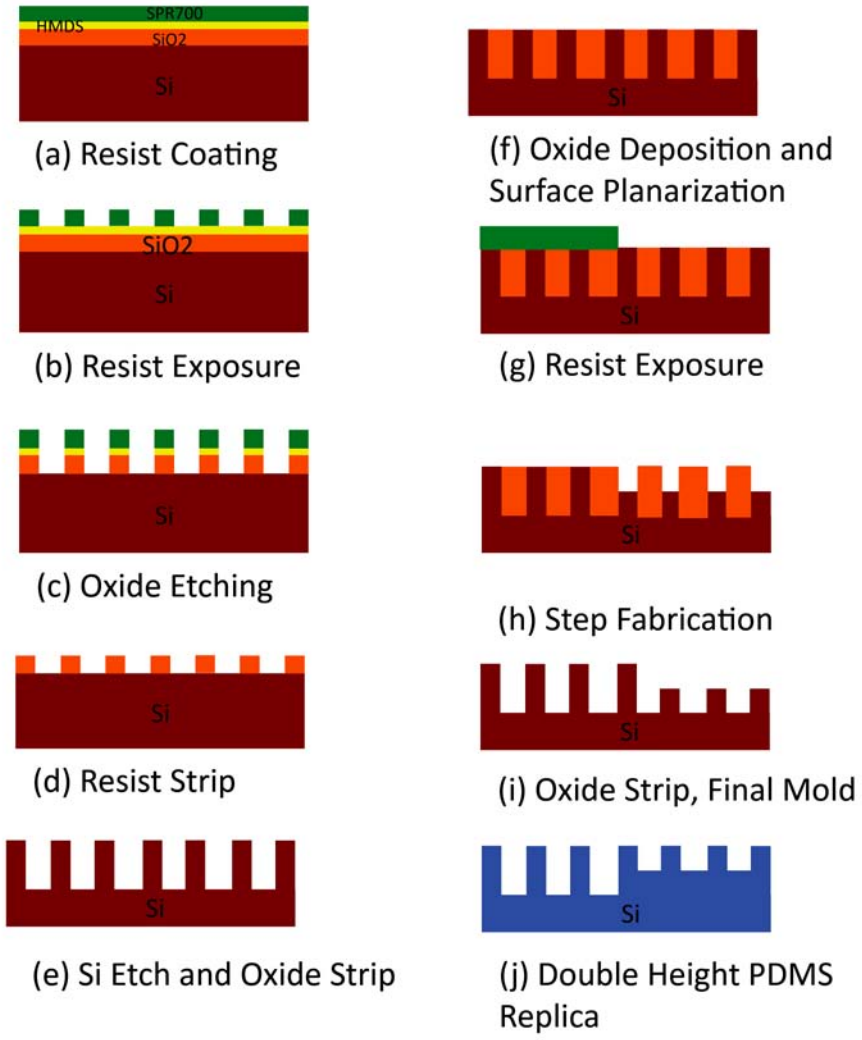

Figure 3.1: Schematic process flow for drawing fabrication of arrays of PDMS posts with variable height and constant top surface topology.

plate at 90 °C for 60 s, followed by another bake at 115 °C for 60 s to remove residual solvent and mechanical stress in the film. The hexagonal array of holes was replicated in positive photoresist by UV photolithography (Fig. 3.1b). After developing, it was treated with a post-development bake at 90 °C for one hour in order to smooth the sidewalls then

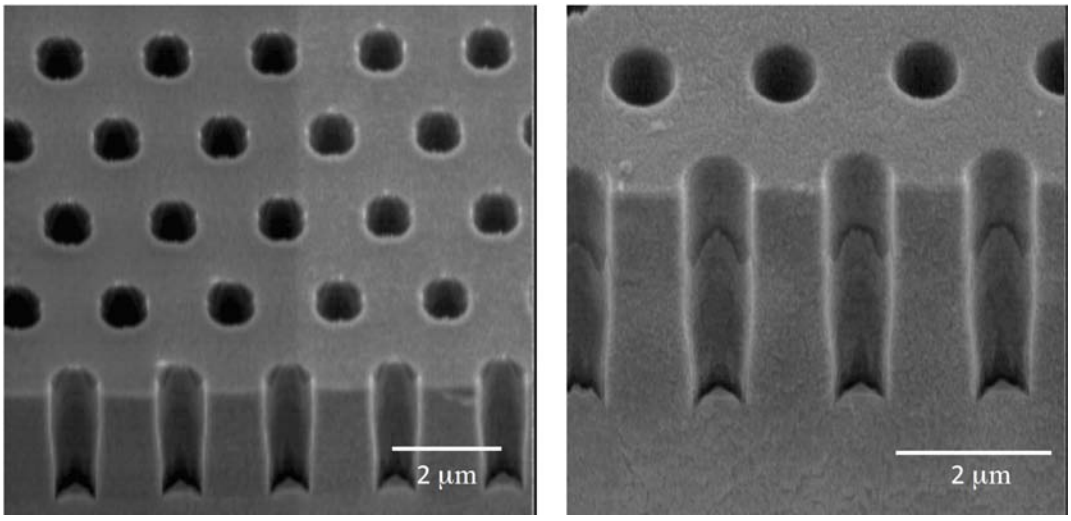

Figure 3.2: SEM image of deep holes in silicon substrate. The diameter of the holes is 1 μm and the pitch size is 2 μm. The height of hole is 6.6 μm.

descummed in O_2 plasma for one minute. The oxide layer was etched, using the resist as a mask, in fluorine based system (Fig. 3.1c). The Si holes were etched to the desired depth in a Cl-based reactive ion etching including inductively coupled plasma (ICP-RIE) system using the SiO_2 as a hard mask (Fig. 3.1d-e). The resulting wafer was then immersed in buffered oxide etch (BOE), leaving the Si mold shown in figure 3.1e. Figure 3.2 shows the SEM image of Si holes.

3.3.2 Fabrication of the multi-height step

The next step involved the step fabrication, which consists of etching the Si in selected areas. In order to protect areas that were not to be etched, SiO_2 with a thickness of 2 μm was deposited conformally over the entire wafer by plasma enhanced chemical vapor deposition (PECVD) (Fig. 3.1f). The deposition thickness was chosen so that the resulting film would protect the holes from subsequent etching. The surface of the wafer was then planarized using a chemical-mechanical polishing (CMP) process.

After planarization, the wafer was coated with photoresist (Shipley 1813) and soft-baked

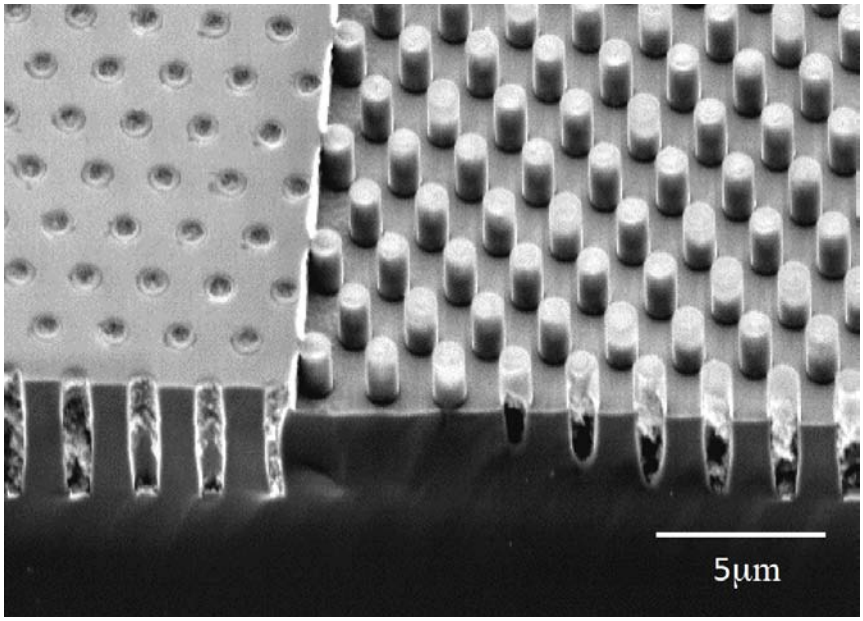

Figure 3.3: SEM image of double height holes in silicon substrate after fabrication of the step height and before removing of the oxide. The thickness of the deposited oxide is 2 μm. The deposition thickness is chosen such that the resulting film protects the holes from further fabrication process.

on a hot plate at 110 °C for 60 s. The photoresist was then exposed in a HTG System III-HR Contact Aligner for 85 s using a mask that defined large areas in which the Si would undergo further etching (Fig. 3.1g). The photoresist was developed with AZ 300 MIF developer. The exposed Si was then etched in a fluorine based Bosch process to the desired height step (Fig. 3.1h).

Figure 3.3 shows a sample that underwent all the processing steps described above. The fabricated step height and subsequent change in depth of the holes can be observed. The holes are still filled with the oxide, which protects them from the second Si etch. This oxide is subsequently removed in BOE. Figure 3.4 shows the final Si mold. The etch process results in a smooth and vertical sidewall profile that is critical for the release of PDMS, from the mold as well as determining the profile of PDMS posts.

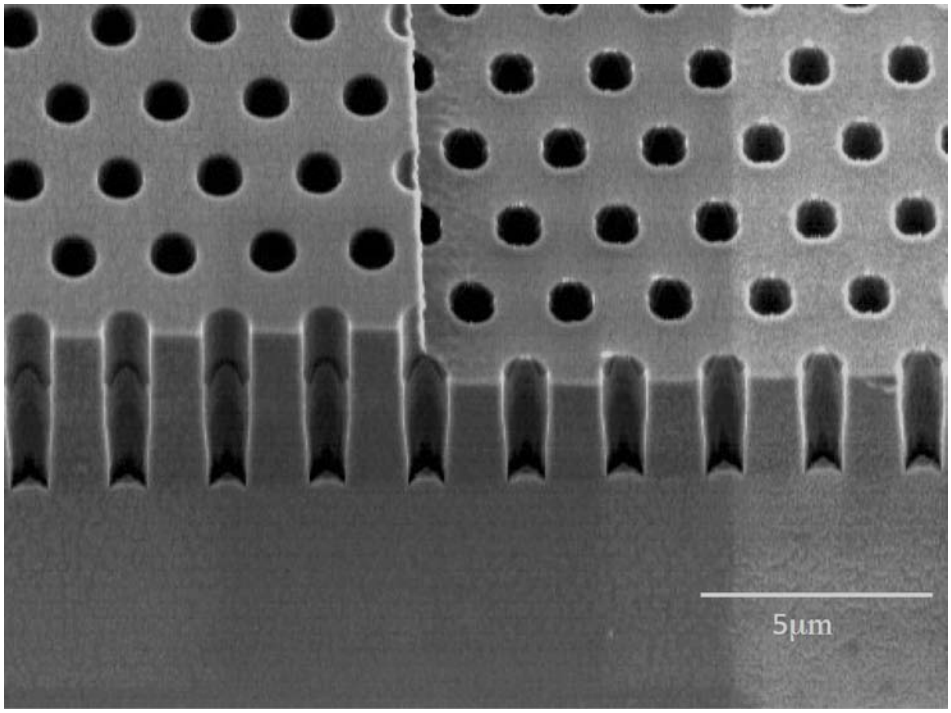

Figure 3.4: SEM image of double height holes in silicon substrate. The diameter of the holes is 1 μm and the pitch size is 2 μm. The height of the deeper hole is 6.6 μm and the height of the shallower hole is 3.9 μm

Using the process described above, samples were fabricated with a range of hole diameters as well as different heights. The diameter of the holes can vary. We made samples with diameters from 1 to 3 μm, although the diameter was kept constant for each substrate. The pillar height was varied from 2 - 8 μm. Since the stiffness varies inversely with the cube of the height (Eq. 1), this height range results in a modulation of the pillar stiffness by a factor of 64, thereby covering a wide range of rigidities on a single substrate.

3.3.3 Elastomer pillars, surface chemistry, and cell culture

The Si structures were used as molds for fabrication of post arrays using PDMS. Prior to PDMS molding, the patterned wafers were piranha cleaned for 6 h at room tempera-

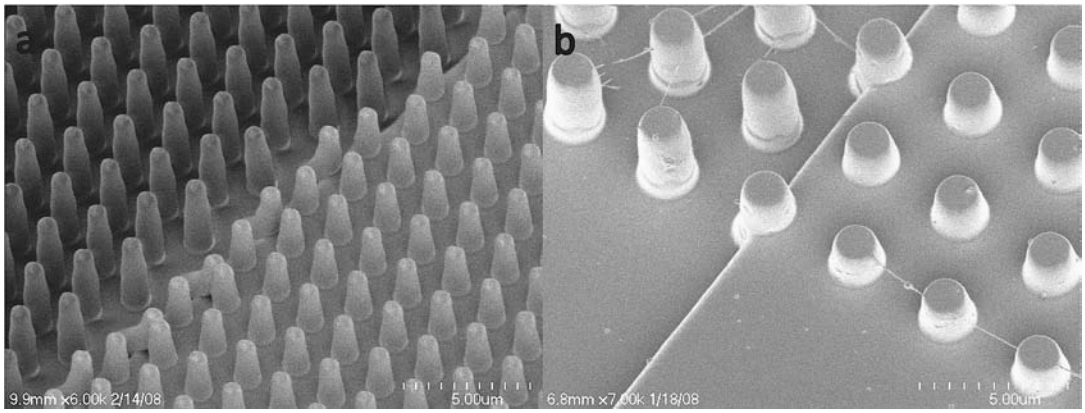

Figure 3.5: SEM image of double height PDMS posts. The diameter of posts is constant but the height is different such that the top contact area of the posts lies in one plane. This will generate controlled step increase in substrate stiffness. The diameter of the posts is 1 μm and the pitch is 2 μm. The shorter posts are about 13 times stiffer than the taller posts.

ture, followed by a one minute O_2 plasma clean and overnight silanization in vapor phase tridecafluoro-trichlorosilane in vacuum (100 μL in a glass vial inside the vacuum jar). The PDMS was mixed with its curing agent, was then poured over the silicon mold and cured at 70 °C for 12 h, in order to achieve a Young's modulus of 2 $\pm$ 0.1 MPa. The PDMS was then peeled off of the mold while immersed in ethanol. Figure 3.5 shows a scanning electron micrograph of a uniform array of PDMS posts with two different heights (3 μm and 7 μm). Using Eq. 1.1, we estimate the stiffness of the short posts to be $\sim$ 10.7 nN / μm, as compared to $\sim$ 0.9 nN / μm for the tall posts respectively, assuming a perfectly cylindrical geometry. Since our posts are slightly tapered, the actual stiffness is numerically calculated to be approximately 8.2 nN / μm and 0.6 nN / μm, respectively. For applications requiring more precise determination of the pillar stiffness, independent calibration using microplates is possible [2].

To promote cellular adhesion, the substrates were immersed in 50 μg/ml fibronectin in PBS (Phosphate Buffered Saline) for one hour prior to plating. NIH 3T3 mouse fibroblast cells were cultured in DMEM (Dulbecco's Modified Eagle Medium) supplemented with 10%

FBS (Fetal Bovine Serum), 1% PSN (penicillin-streptomycin-neomycin) antibiotic, 7.5 mL of HEPES buffering agent and 5 mL of L-glutamine. The substrates were washed three times with PBS and the cells were plated on the substrate overnight. Images of 3T3 cells were collected using an inverted microscope with a 20X objective with a rate of one image every 10 seconds.

3.3.4 Results

In order to investigate the effect of rigidity on the migration of cells, 3T3 cells were plated on elastomer pillars with diameters of 1 and 2 μm and two different heights of 6.6 and 3.9 μm, and therefore a range of stiffness from 0.85 to 170 nN / μm. In order to avoid the effect of cell-to-cell interaction, cells were plated at sub-confluent density. The cells were left to spread overnight and then were imaged for about two hours. Bright field microscopy was used to follow the cell movement on the substrate. Ten different cells were observed to spread across the boundary between areas of different rigidity. In nine of these cases, the cells migrated towards the stiffer area and never returned to the soft part. Figure 3.6 shows a time series of images of one 3T3 cell plated on the boundary between posts of heights 3.9 and 6.6 μm. The cell initially spread across the boundary and then migrated toward the stiffer area. This behavior is typical for 3T3 cells responding to different rigidity of the substrate [1]. These preliminary results demonstrate that these substrates can be used to probe the rigidity sensing response of individual cells.

3.4 Mesenchymal stem cells: their phenotype, differentiation

Mesenchymal stem cells (MSCs) are non-hematopoietic stormal cells that are capable of renewing themselves and potential of multi lineage differentiation. They can differentiate into bone, cartilage, muscle, ligament, tendon and adipose as well as fibroblast [67; 68]. They can be found in several tissues such as in bone and bone marrow [69]. They are able to migrate and adhere to the site of injury. The properties of these cells make them potentially an ideal candidate for regenerative medicine and tissue engineering in particular for applications in skeletal and hard tissue repair [70; 71]. MSCs, which are isolated form

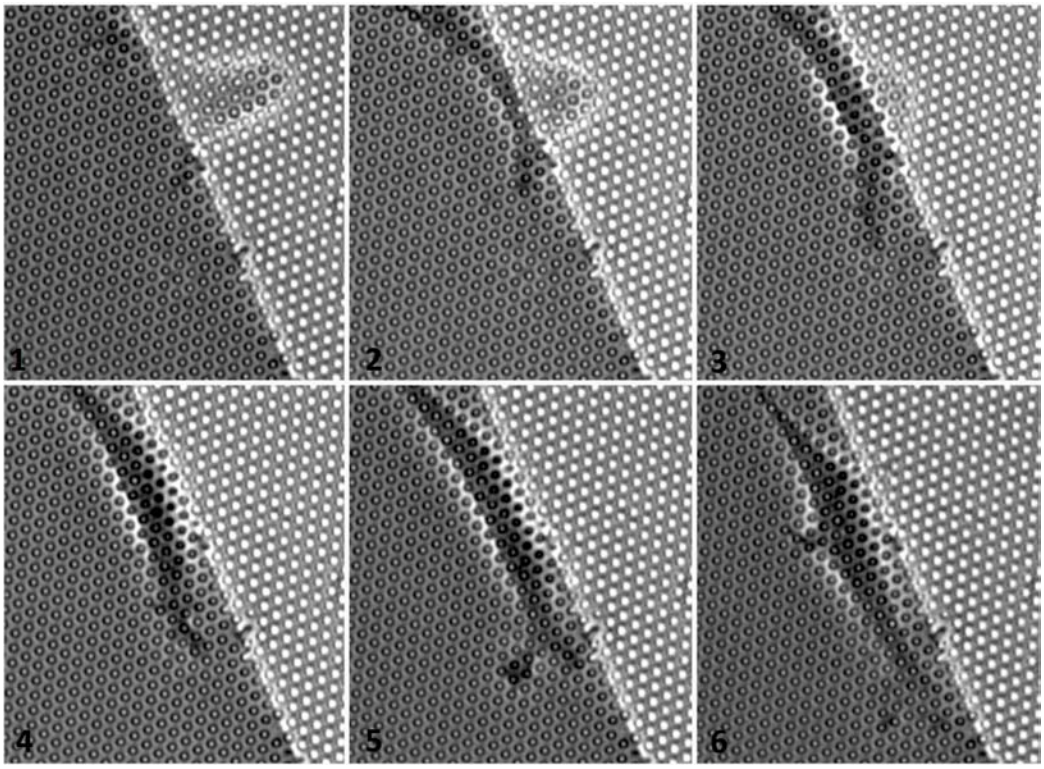

Figure 3.6: Time-lapse optical micrograph of migration of 3T3 cells on a double rigidity substrate. The stiff part (left side) is about five times stiffer than the soft part. The cell on the boundary migrates toward the rigid part. The time interval is 10 s between frames.

bone marrow, can differentiate into an osteogenic lineage when cultured in the presence of growth factors and other stimuli [72]. Osteogenic differentiation is characterized by the time dependent synthesis of a variety of bone specific proteins (e. g. collagen or osteocalcin) along with major changes in cell morphology (Fig. 3.7) [73; 74]. Osteogenic differentiation in vitro is characterized by initiation of the synthesis of extracellular matrix (ECM) that consists primarily of collagen type I (Col I). Subsequently cells produce alkaline phosphatase (ALP) and a variety of non-collagenous proteins, such as osteopontin (OPN), osteonectin (ON), bone sialo protein-II (BSP) and osteocalcin (OC), followed by induction of ECM calcification (Fig. 3.8) [75]. Expression of these markers can be localized by immunohistochemistry

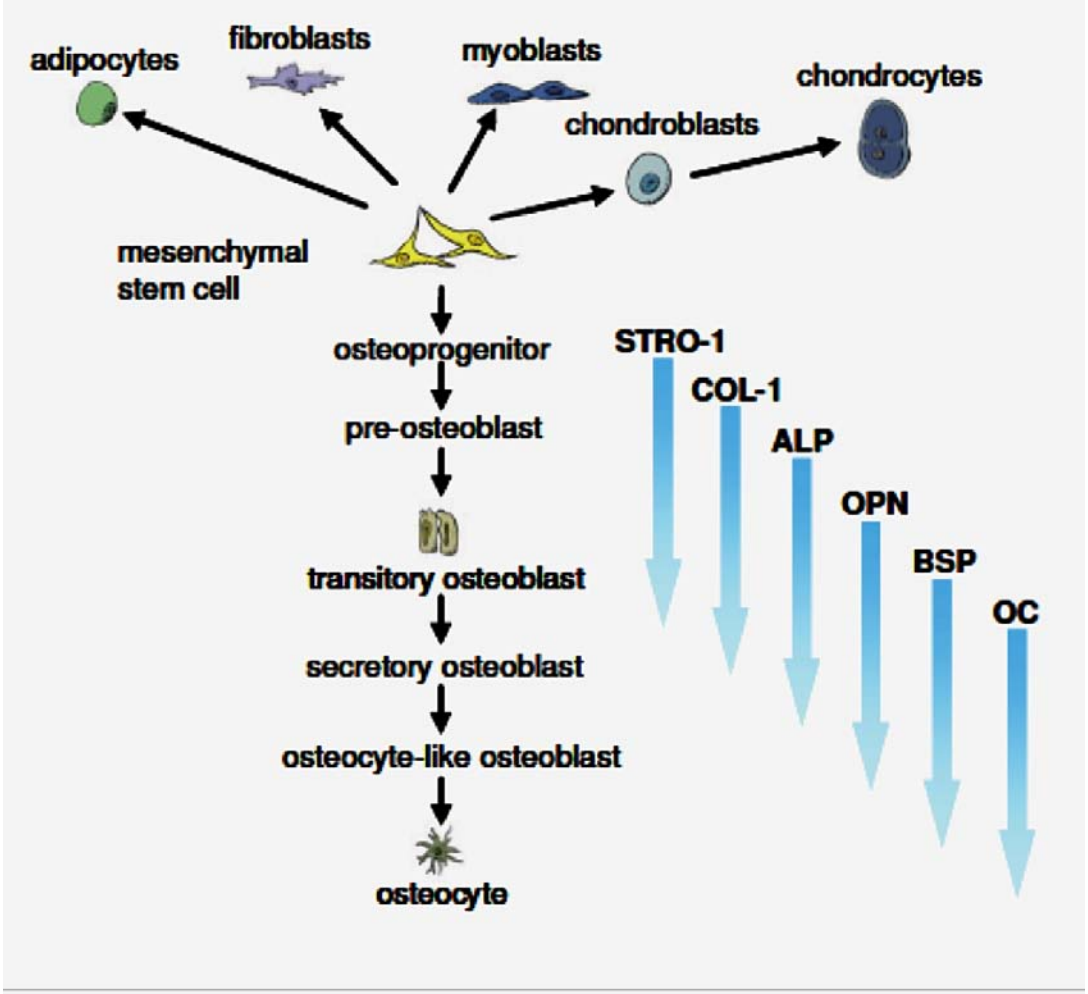

Figure 3.7: Mesenchymal stem cells are multipotent stem cells. Their osteogenic differentiation is characterized by the time dependent synthesis of a variety of bone specific proteins depicted on right.

staining of specific protein of interest exploiting the principle of antibodies, which is tagged to a fluorophore, binding specifically to antigens.

MSCs can also be identified based on their morphologic or phenotype characteristic. When these cells are cultured in medium with 10% FCS, they will adhere to the tissue culture plastic. Other cells may adhere as well but over time in culture they are washed

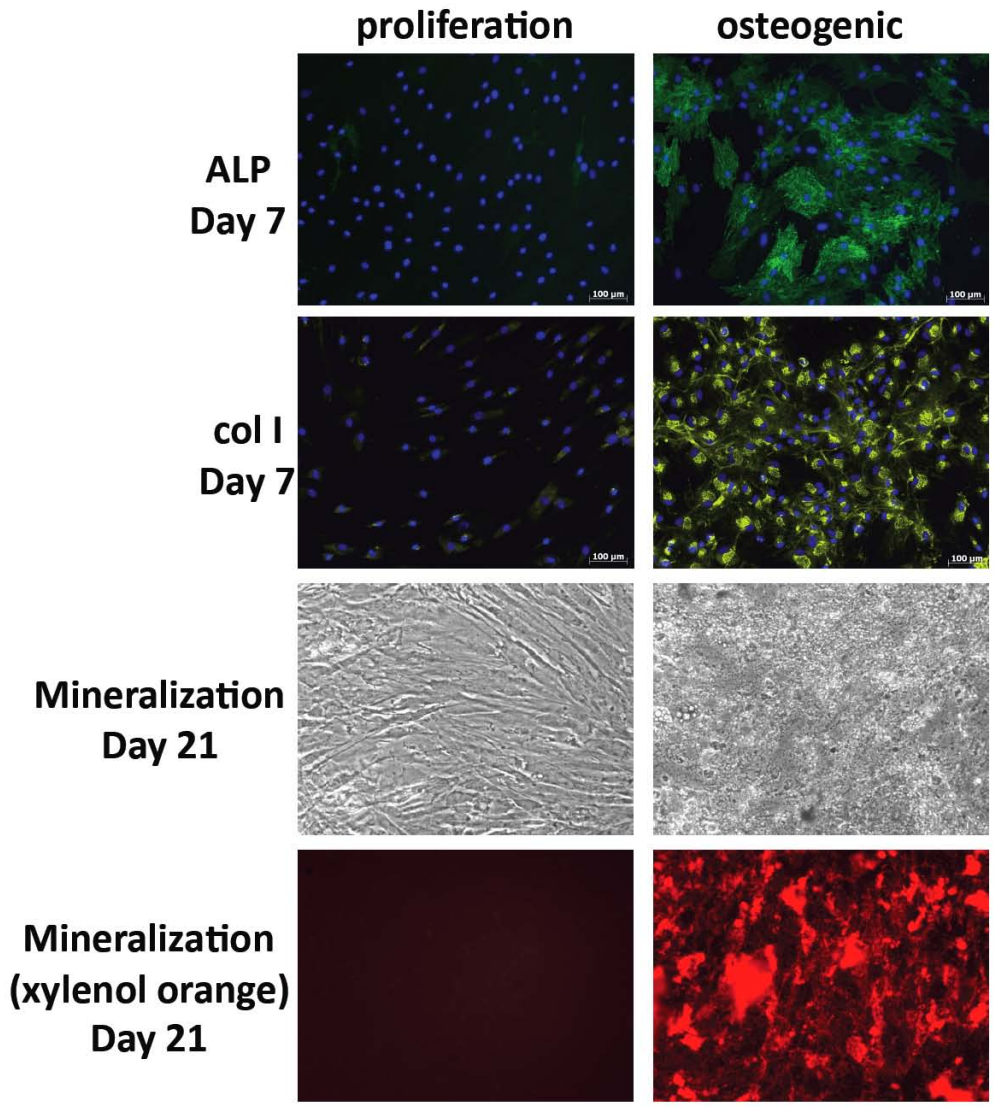

Figure 3.8: Images of immunofluorescence staining of the bone specific protein in MSCs in proliferation (left column) and osteogenic (right column) medium. They express several markers in osteogenic medium while no markers appear in proliferation medium.

away. In the beginning, adherent cells look heterogeneous but the tightly adhered ones have a spindle shape and form foci of two or more cells. In the beginning, they remain inactive but after two to four days, they begin to multiply rapidly depending on the initial plating density.

Culturing cells on substrates made of Polyacrylamide or polyethylene glycol gels, which their rigidity can be modulated by the amount of cross-linker, has revealed that substrate rigidity alone can modulate many cellular functions, including stem cell differentiation [15; 65]. MSCs have previously been shown to respond to environmental cues [65; 76]. We examined if hMSCs cultured on pillar arrays would respond to changes in pillars rigidity. We used different substrates with double height pillars, which result in a change in stiffness. Using such substrate, we could probe the effect of a sharp rigidity change on the mechanical interaction of cells with their underlying substrate.

3.4.1 Cell culture and osteogenic differentiation

Human bone marrow stromal cells (HBMC) and human bone cells (HBC) were obtained form bone marrow specimens of patients during surgical hip replacement procedures of otherwise healthy patients. Since these cells were directly from bone out growth, therefore mainly restricted to osteogenic lineage. HBMCs represent a heterogenic cell group that contains a subpopulation of MSCs with ability to differentiate into osteoblasts, chondrocytes or muscle cells, etc. HBCs are cells derived from trabecular bone explants with only a limited number of multipotent cells [72].

HBMC and HBC cells were cultured on were plated on elastomer pillars with diameters of 1 and 2 μm and two different heights of 6.6 and 3.9 μm, and under proliferative and osteogenic medium conditions in parallel to verify the ability to differentiate on pillar substrate (Fig. 3.9). The difference between proliferation and osteogenic differentiation was verified by immunohistochemical staining.

Different seeding density was tested. In order to have single cell for the force measurement and also enough cells on the substrate, MSCs were seeded 10000 cells per 60 mm non-adhesive tissue culture plastic dish. Each dish, contains 4 to 6 substrate, which the area was ~ 1 cm^2. To promote cellular adhesion, the substrates were immersed in 50 μg/ml

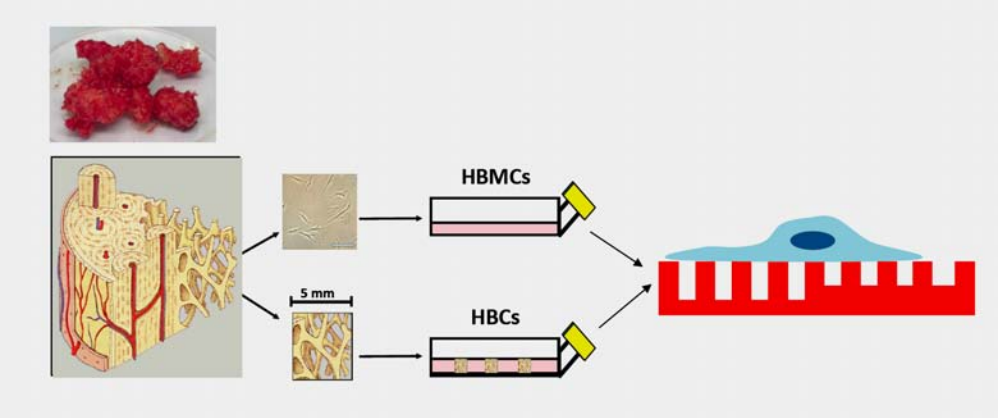

Figure 3.9: Schematic process flow of culturing HBCs and HMBCs on double height PDMS pillars with variable height and constant top surface topology.

fibronectin in PBS for one h prior to plating.

At first, cells were cultured in proliferation medium- α-MEM supplemented 10% FBS (Fetal Bovine Serum), 1% PSN (penicillin-streptomycin-neomycin) antibiotic and 20 μl FGF (fibroblast growth factor (FGF)- was used so that MSCs can adhere to the pillars. After a few hours incubating at 37 C, providing the cell adhesion, the medium is change to osteogenic differentiation- Alpha MEM supplemented 10% FBS (Fetal Bovine Serum), 1% PSN (penicillin-streptomycin-neomycin) and 50 μl Dexamethason, 6.4 mg Ascorbic Acid Phosphat, 216 mg -Glycerophosphat and 21 μl Vitamin D3 per 100 ml medium. The medium was changed every 3 $\sim$ 4 days. The pillar substrates were maintained wet in all the processes in order to avoid pillars to collapse. Cells were plated on substrate for several days. After 7 days of culture, cells were washed three times with PBS without glucose, fixed with 4% paraformaldehyde in PBS for 15 minutes at room temperature and were then rinsed with PBS without glucose. Cells were stained for bone specific ALP. For total cell counts, cell nuclei were stained with 4,6-diamidino-2-phenylindole (DAPI; Invitrogen).

Cells cultured under osteogenic medium conditions express high level of ALP as a differentiation marker compared to cells in proliferation medium (Fig. 3.10). The marked difference in cell shape was observed on substrate with different rigidity. Cells on soft

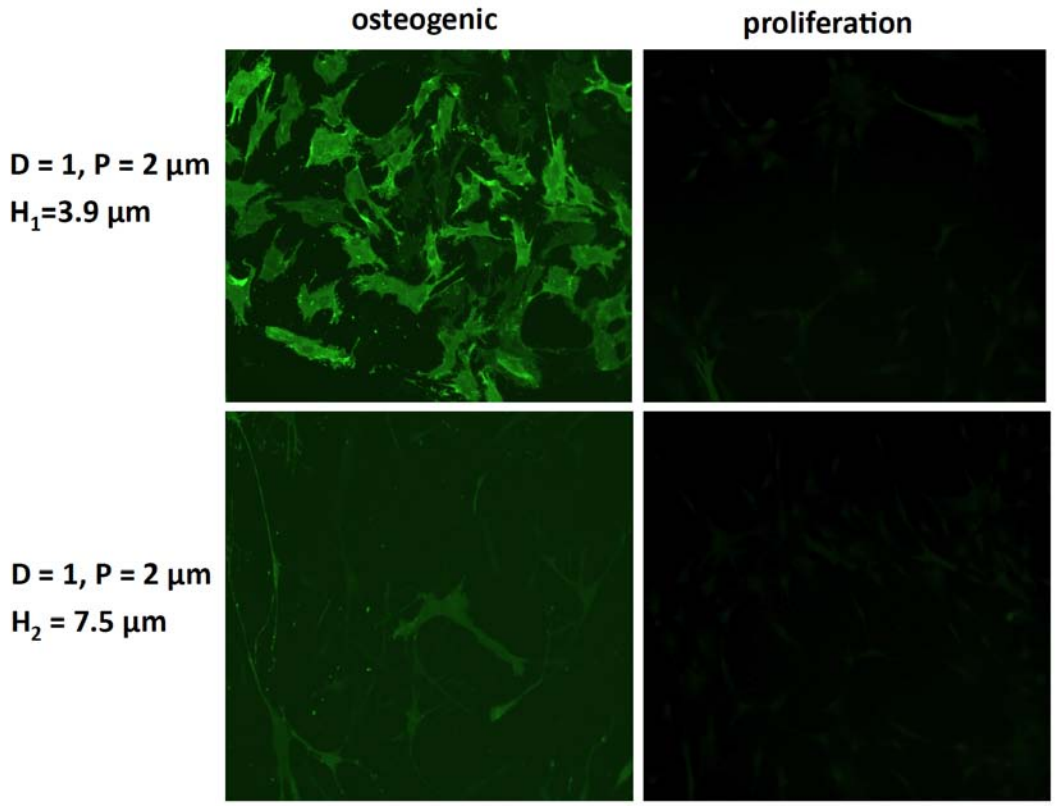

Figure 3.10: Images of immunofluorescence staining of ALP for HBMCs on a double rigidity substrate. They express high level of ALP in osteogenic medium (left side) compared to proliferation medium (right part) after seven days. The stiff pillars (top images) are about six times stiffer than the soft part (bottom images). The level of ALP expression as well as cell shape is different on soft and stiff pillars.

substrates showed elongated shape whereas on stiff substrate, they were more round (Fig. 3.10). The unique design of the double height PDMS pillars was used to compare directly the effect of rigidity on shape of cells at the boundary between regions of substrate with different rigidities (Fig. 3.11).

Another observation was made with ImMSCs [77] plated on elastomer pillars with different heights and therefore different rigidity. They were cultured in DMEM supplemented

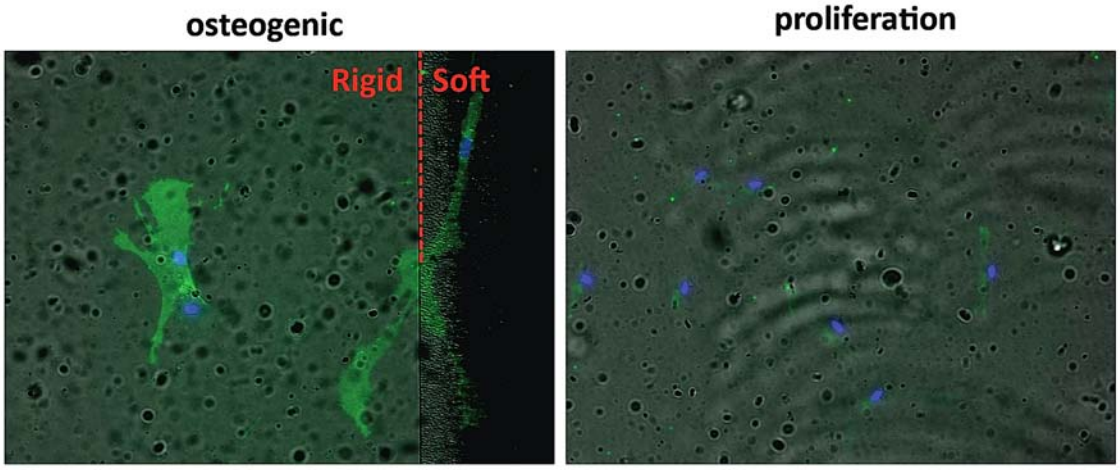

Figure 3.11: Images of immunofluorescence staining of ALP for HBCs on a double rigidity substrate after 7 days. They express high level of ALP in osteogenic medium (left side) compared to proliferation medium (right part). The cell is more spread on the rigid part than the softer part.

with 5% FBS and fixed in paraformaldehyde, dried using a critical point dryer, and then observed by scanning electron microscopy. A marked difference in phenotype can be observed on either side: they look more round on the soft part and more spread out on the stiff part (Fig. 3.12).

The direct effect of rigidity on differentiation remained unclear but the difference in cell shape and architecture suggests that rigidity of the substrate could lead to different differentiation paths in the two areas, as indicated by the work of Engler *et al.* [65].

The unique design of the double height PDMS pillars can be used to track traction force of individual cells on substrate with two different rigidity and those measurements can be compared with the endpoint point respond of the cells under differentiation.

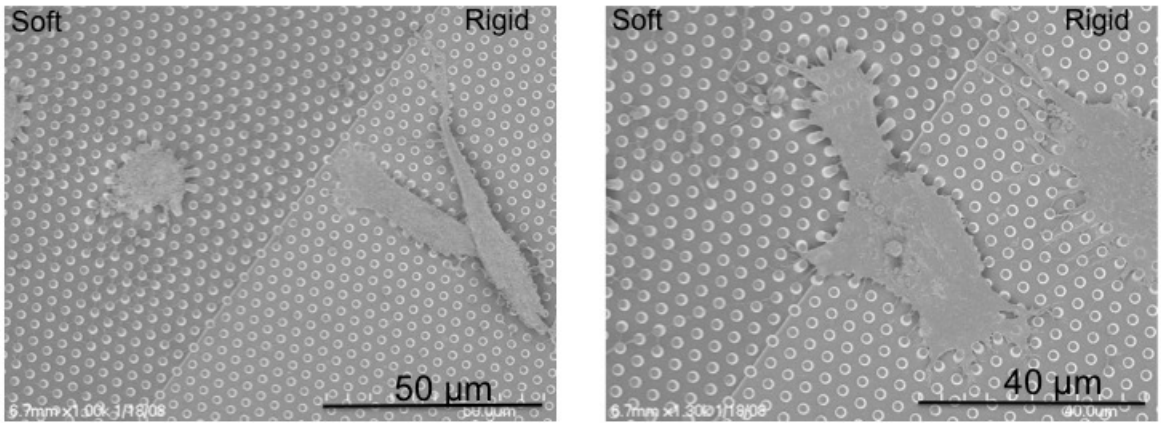

Figure 3.12: SEM image of an immortalized mesenchymal stem cell attached to a hexagonal array of pillars with a constant diameter of 1 μm, pitch of 2 μm, and two different heights of 6.6 and 3.9 μm, which causes a change in rigidity of the substrate. The cell is more spread on the rigid part (right side) than the softer part (left side). Also, on the softer area, the posts are bent to a greater extent compared to the rigid posts. The arrows indicate the direction of pillar deflection.

3.5 Conclusion

We demonstrate the fabrication process of a flexible substrate with a uniform top surface but with a modulated stiffness to study the effect of rigidity on the cellular behavior. The PDMS substrates used have the advantage that their stiffness can be easily modified by changing their geometry and can precisely detect the cellular activities. Surface rigidity modifies cell migration and adhesion, and is also likely to modify the force exerted by cells on the substrate [60]. Our future goal is to quantify these forces and study the relationship between the change in the motility behavior and the forces applied by the cells. In the longer term, it will be straightforward to modify the fabrication procedure to yield multiple pillar heights on a single array, and to modulate the pillar heights locally. More complex patterns of pillar rigidity will help us to study the physical and topographical effect of the substrate on cellular behavior in a more versatile manner.

Chapter 4

Metal-Tipped Pillars

4.1 Abstract

We describe a technique for the fabrication of arrays of elastomeric pillars whose top surfaces are treated with selective chemical functionalization to promote cellular adhesion in cellular force transduction experiments. The technique involves the creation of a rigid mold consisting of arrays of circular holes into which a thin layer of Au is deposited, while the top surface of the mold and the sidewalls of the holes are protected by a sacrificial layer of Cr. When an elastomer is formed in the mold, Au adheres to the tops of the molded pillars. This can then be selectively functionalized with a protein that induces cell adhesion, while the rest of the surface is treated with a repellent substance. An additional benefit is that the tops of the pillars can be fluorescently labeled for improved accuracy in force transduction measurements.

4.2 Introduction

As explained previously, the physical properties and topography of the cellular environment are key factors in determining cellular function and behavior. In order to study the mechanical interaction of cells with their environment, we culture cells on microfabricated arrays of elastomeric pillars. The pillar geometry and material can be easily modified to control the bending stiffness and hence the mechanical properties of the cellular environment. Figure

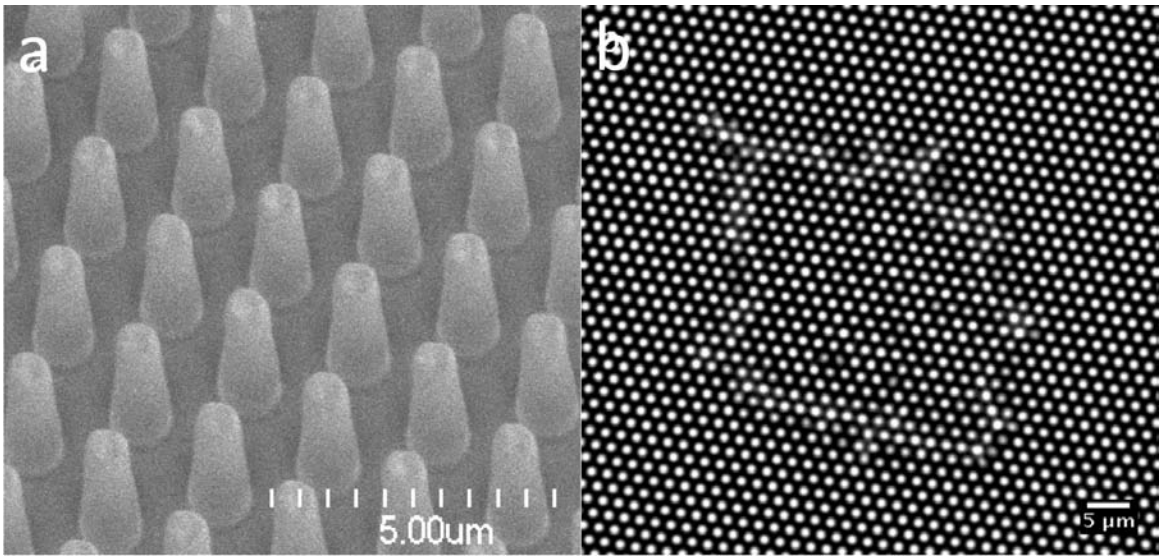

Figure 4.1: (a) SEM image of the PDMS posts. The diameter of the posts is 1 μm and the pitch is 2 μm. The height of the posts is 6.6 μm. The stiffness of the post is about 1 nN/μm. (b) Bright-field micrograph of the spreading of mouse embryonic fibroblast cell on the pillar substrate.

4.1a shows a scanning electron micrograph of a uniform array of elastomeric pillars, and figure 4.1b shows an optical micrograph of a fibroblast cell on this array.

For many such experiments, it is advantageous to selectively functionalize the tops of the pillars for two purposes. First, application of proteins that promote cellular adhesion (such as fibronectin) encourages cell spreading and help to restrict the adhesion points to the tops of the pillars, making the force measurements much more straightforward to interpret. Second, fluorescent labeling of the tops of the pillars can facilitate detection of the pillar displacements. The most common technique for selective functionalization of the pillar tops is microcontact printing, *i.e.*, stamping [2; 3; 51; 60]. However, this technique can only be used for relatively rigid pillars; flexible pillars tend to adhere to one another or collapse as a result of the stamping process.

We have developed an alternative method for selective chemical functionalization of the

top surface of elastomer pillars. We coat the tops of the pillars with a thin gold film that can then be functionalized using thiol chemistry, facilitating both cellular adhesion and fluorescence. This functionalization can be performed while the sample is kept in liquid to prevent adhesion of the pillars to one another. In addition, the rest of the surface (*i.e.*, the sidewalls of the pillars and the interstitial spaces) can then be functionalized with an anti-adhesion coating to further discourage spreading on these surfaces. In this work, we describe fabrication and initial testing of substrates with arrays of gold-tipped pillars.

4.3 Au-tipped pillars

4.3.1 Fabrication of arrays of holes

The central part of the work described below involves fabrication of a Si structure, which is used as a mold for the fabrication of the gold-tipped elastomer pillars. The mold is made by first etching a uniform array of holes in a Si wafer. A silicone elastomer is poured into the mold to yield the reverse structure, namely an array of micron-scale pillars whose mechanical properties are a function of their dimensions and the Young's modulus of the elastomer material. The latter can be tuned by adjusting the degree of crosslinking of the elastomer. The new feature introduced in this work is the deposition of a thin layer of Au at the bottom of the etched holes in the Si mold prior to the curing of the elastomer. When the elastomer is thermally crosslinked, the Au adheres to the tops of the pillars, resulting in an array of gold-tipped elastomeric pillars (Fig. 2i).

The fabrication process is illustrated in figure 4.2. Uniform array of holes in silicon wafer was made by photolithography as described in chapter 2. Briefly, RCA-cleaned Si wafers were oxidized at 1100 °C for 2 h to form a 950 nm-thick SiO_2 film. The wafers were coated with 1.2 μm-thick photoresist (Shipley SPR 7000) using Hexamethyldisilazane (HMDS) as an adhesion promoter. The resist was then soft-baked on a hot plate at 90 °C for 60 s, followed by another bake at 115 °C for 60 s to remove residual solvent and mechanical stress in the film. The hexagonal array of holes was replicated in positive photoresist by UV photolithography (Fig. 4.2b). After developing, it was treated with a post-development bake at 90 °C for one hour in order to smooth the sidewalls then descummed in O_2 plasma

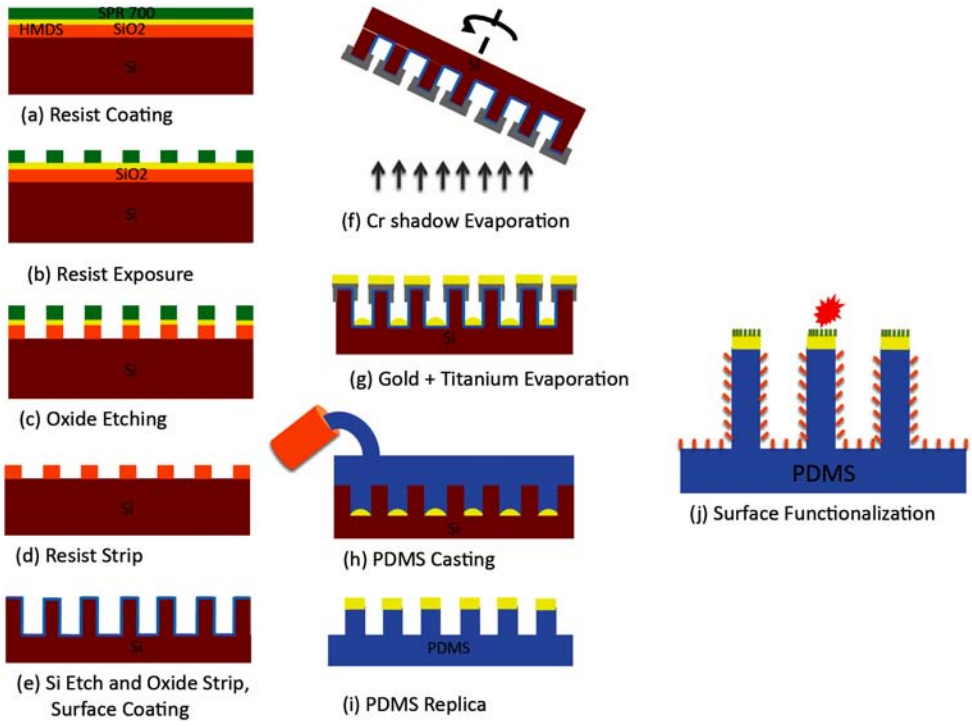

Figure 4.2: Schematic of the process flow for fabricating arrays of the PDMS pillars with functionalized Au on the top surface.

for one minute. The oxide layer was etched, using the resist as a mask, in fluorine based system (Fig. 4.2c). The Si holes were etched to the desired depth in a Cl-based reactive ion etching including inductively coupled plasma (ICP-RIE) system using the SiO_2 as a hard mask (Fig. 4.2d-e). The resulting wafer was then immersed in buffered oxide etch (BOE), leaving the Si mold shown in figure 4.2e. Figure 4.3a shows the SEM image of holes in Si.

The mold was then cleaned in piranha solution for 6h at room temperature, followed by a one minute O_2 plasma clean and overnight silanization in vapor phase tridecafluoro-trichlorosilane in vacuum (100 μL in a glass vial inside a vacuum jar). This facilitates the subsequent release of elastomer and gold from the wafer after curing.

Following formation of the Si mold structure, a layer of Cr was deposited onto the mold

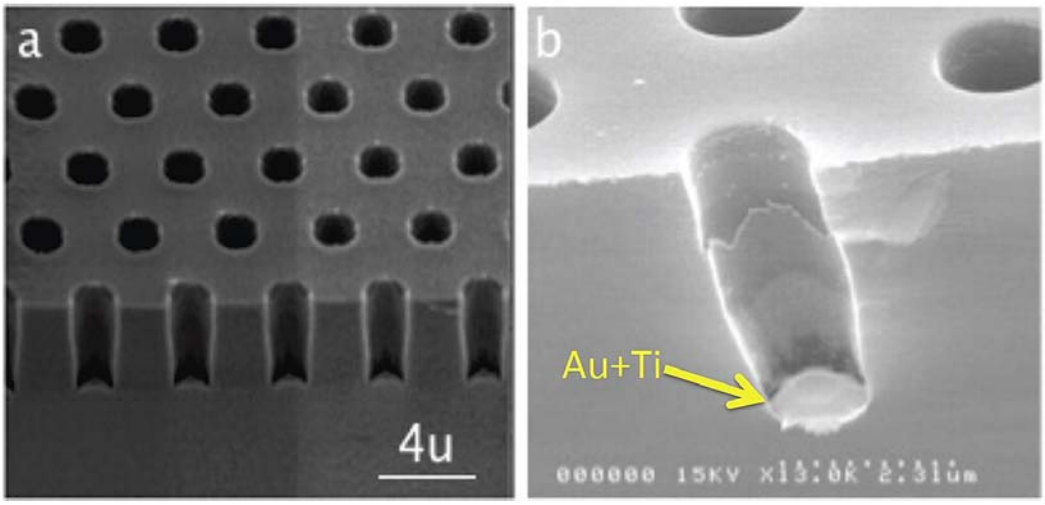

Figure 4.3: (a) SEM image of holes in the silicon substrate. The diameter of the holes is 1 μm and the pitch size is 2 μm. The height of the hole is 6.6 μm. (b) SEM image of final Si mold with a thin layer of Au and Ti at the bottom of the holes.

at a 30° angle, using a rotary sample holder in an electron beam evaporator. Rotating the substrate is necessary for achieving a homogeneous deposition of Cr around the holes. This shadow evaporation results in Cr deposition on the top surface and upper portion of the sidewalls of the etched holes but not on the bottoms, as in figure 4.2f. A 20 nm layer of Au followed by 5 nm of Ti was then deposited normal to the mold surface, using electron beam evaporation. Because the sidewalls are not perfectly vertical, the thin layer of Cr on the top lip of each hole is used to prevent deposition of the Au/Ti onto the sidewalls; the thickness of the layer was adjusted depending on the depth of the hole. Removal of the Cr sacrificial layer results in a Si mold with Au+Ti at the bottoms of the etched holes (Fig. 4.2g). Figure 4.3b shows the final Si mold with a thin layer of Au and Ti on the bottom of the holes.

The Si structures were used as molds for fabrication of gold tipped pillar arrays using PDMS. The PDMS was mixed with its curing agent, poured over the mold and cured at 70 °C for 12 hours, in order to achieve a Young's modulus of 2 ± 0.1 MPa. The PDMS was

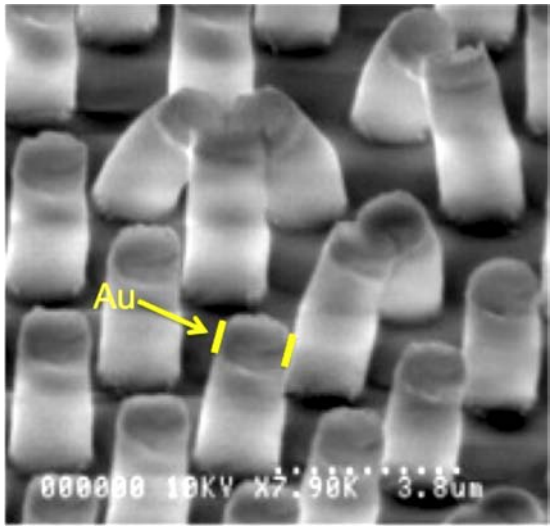

Figure 4.4: SEM of Au-tipped PDMS pillars. The tops of the pillars can be selectively chemical functionalized.

then peeled off in ethanol. The silane treatment previously applied to the Si allows both the PDMS and the gold to be removed easily. In addition, the titanium on top of the gold acts promotes adhesion of the metal to the PDMS. Therefore, the gold at the bottom of each hole is removed by the PDMS, resulting in gold-tipped pillars (Fig. 4.2i). Figure 4.4 shows a scanning electron micrograph of the PDMS pillars with the gold on their tips.

Using the process described above, samples were fabricated with a range of pillar diameters and pitches as well as different heights. The diameter of the holes varied from 1 to 5 μm to achieve different pillar stiffness range of the substrate.

4.3.2 Surface chemistry: self assembled monolayers of thiols on gold

Having gold on the tips of the pillars allows the use of thiol-based chemistry, which permits a quasi-covalent bond between a variety of molecules (*e.g.* fibronectin) and the gold-coated pillars [78]. Long chain alkanethiol, $HS(CH_2)_nX$, adsorb from solution onto gold surfaces and form a densely packed self assembly monolayer (SAMs). The specific interaction of the sulfur atom in the thiol binds strongly to the gold substrate, while a wide range of chemi-

cal functionalities can be designed into the other end of alkanethiol molecule by attaching different functional end-groups. Thus a surface can be engineered where the chemical properties of the surface will be defined by the terminal functional group [79]. In this work, we control the chemical functionality of the surface using a methyl group (CH_3) tail. This group confers hydrophobicity to the substrate, which is used to adsorb fibronectin on the substrate. To this end, the Au-tipped PDMS pillar substrates were immersed in 2 mM ethanolic solution of HS-C18 thiol overnight at room temperature. The substrates were washed extensively with ethanol followed by PBS washes. Substrates were incubated in a solution of 0.1% Pluronics F127, a block copolymer of ethylene oxide and propylene oxide, in PBS (2h at room temperature) to passivate the rest of the areas against fibronectin and non-specific protein binding. Under these conditions, we obtained an array of gold-tipped PDMS pillars offering a surface prone to adsorb fibronectin on the top of the pillars, while the remaining areas were rendered non-adhesive by the Pluronic treatment. The substrates were immersed in 50 μg/ml fluorescently labeled fibronectin in PBS for one hour. As a control experiment, we incubated non-functionalized pillars with fluorescently labeled fibronectin under the same conditions.

4.3.3 Results

In order to examine adsorption of fibronectin to the tops of the pillars, immunofluorescence microscopy was used to image the pillars. Figure 4.5 shows an image of the tops of pillars. The pillar diameters were 5 μm with a center-to-center distance of 10 μm. To determine whether the fluorescence signal was indeed restricted to the top of the pillars, we used confocal laser scanning microscopy (CLSM). Figure 4.6 shows confocal microscopy images of the bottom of the pillars in a functionalized substrate as well as a control sample that were not treated with the gold at the tops of the pillars. The fluorescence signal in Fig. 4.6a is seen to decrease as the focus is moved downward along the length of the pillar, indicating that the signal originates at the top of pillars. Rings of fluorescence signal in control experiments were observed along the sidewalls of pillars, indicating the complete coating of the sidewall. These images confirm that the fibronectin coating was restricted to the tops of the gold-coated pillars.

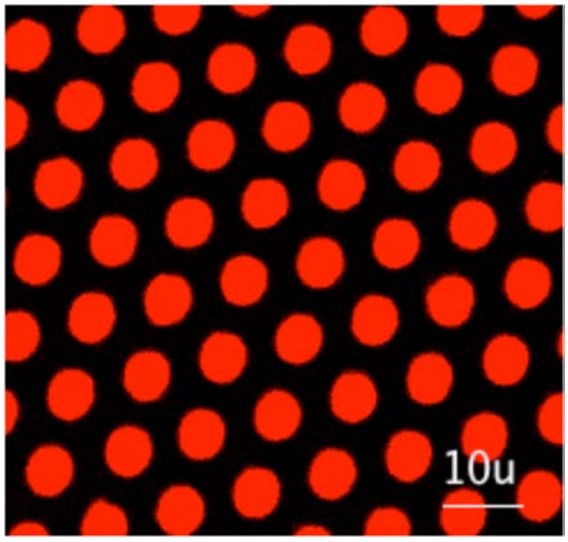

Figure 4.5: Epifluorescence image of the tip of the functionalized pillars with diameter of 5 μm and center-to-center distance of 10 μm. The tops of the pillars are coated homogeneously with fluorescently labeled fibronectin and there is no signal from the bottom of the pillars.

4.4 Magnetically actuated pillars

Cells sense and generate traction forces via the cytoskeleton during adhesion and migration. The response of the cell to the force controls cell shape, growth and differentiation [19; 35; 38; 76]. Much effort is currently being applied to understand the biomolecular interactions involved in these force generating processes. The pillar substrate works as independent force sensors and provide direct measurement of the traction force at specific locations [2; 58; 51; 3]. The forces are inferred from the deflection of the pillars and can be as large as several nN [38].

Cells are also responsive to externally applied force. It is important to understand the dynamic of cellular force response in order to understand cellular behavior. However few studies have been done to date in this area because of the difficulty in engineering biocompatible, micron-scale mechanical actuators that can be integrated into a cell assay system [80].

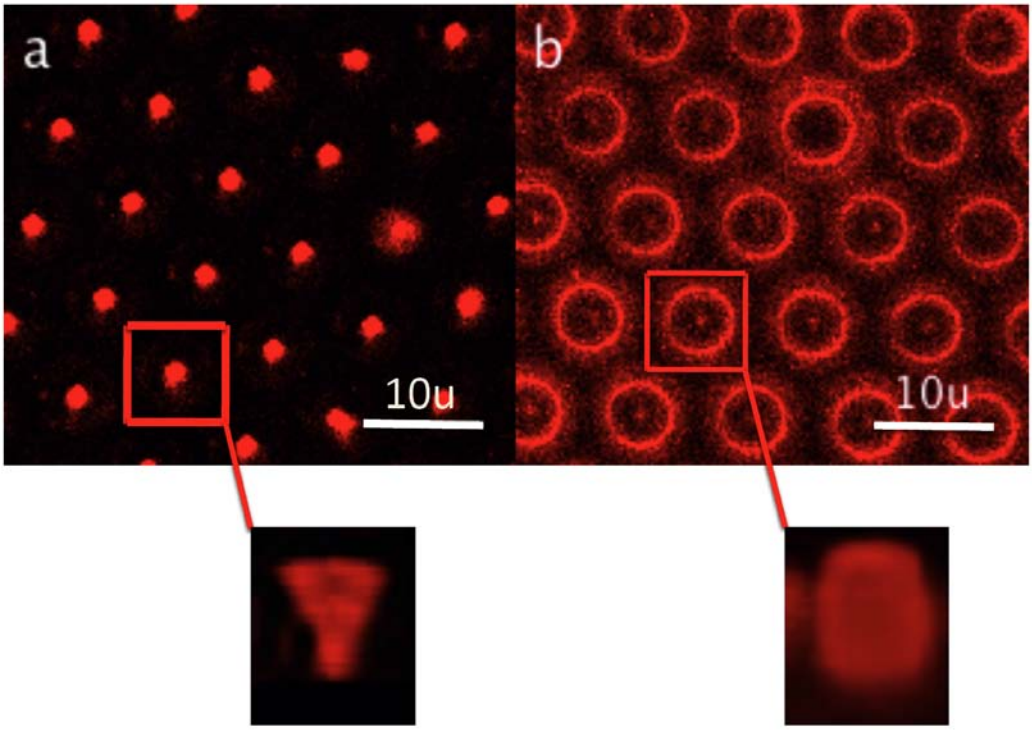

Figure 4.6: Image of the bottom of the pillars using confocal laser scanning microscopy. (a) The fluorescence signal of functionalized pillars decreases as along the length of the pillar, indicating that signal is coming from the top of pillars. (b) Rings of fluorescence signal around the sidewall of pillars in a nonfunctionalized substrate, indicating the complete coating of the sidewall.

In this work, we have developed a simple system in which mechanical force can be applied to cells as they migrate and spread on a surface. Using the same platform consisting of arrays of elastomeric pillars mentioned above, we embed a microscale magnet within each pillar, so that groups of pillars in a given region can be deflected by an external magnetic field. Cells adhering to the tops of the pillars will experience a force as the pillars are deflected. In this way, we can quantitatively study the response of cells to externally applied force.

4.4.1 Fabrication process

A Si structure is fabricated and used as a mold for the fabrication of the magnetic elastomer pillars. The mold is made by first etching a uniform array of holes in a Si wafer. A silicone elastomer is poured into the mold to yield the reverse structure, namely an array of micron-scale pillars. A thin layer of permalloy is deposited at the bottom of the etched holes in the Si mold prior to the curing of the elastomer. When the elastomer is thermally crosslinked, the permalloy adheres to the tops of the pillars, resulting in an array of magnetically actuated elastomeric pillars.

The fabrication process is similar to the fabrication process of gold-tipped pillar that was illustrated at figure 4.1. Uniform array of holes in silicon wafer was made by photolithography as described in chapter 2.

Following formation of the Si mold structure, a layer of Cr was deposited onto the mold at a 30° angle, using a rotary sample holder in an electron beam evaporator. Rotating the substrate is necessary for achieving a homogeneous deposition of Cr around the holes. A 10 nm layer of Au is then deposited normal to the template surface followed by a 200 nm layer of Permalloy. 5 nm of Ti is then deposited to aid adhesion of the material to the elastomer using electron beam evaporation. Gold is deposited so that permalloy would stay deeper in the PDMS and also for biological compatibility. Removal of the Cr sacrificial layer results in a Si mold with Au+Permalloy+Ti at the bottoms of the etched holes (Fig. 4.2h).

We used PDMS and Polyacrylamide as elastomer material here. In case of PDMS, it was prepared as explained in chapter previously. It then poured over the mold, cured at 70 °C for 12 h and peeled off in ethanol. In order to use Polyacrylamide elastomer pillars, mixture of acrylamyde and bis in distilled water was prepared according to the desired concentration. 1/100 of the volume of 10 % ammonium persulfate and 1/1000 of the volume of TEMED was added to the mixture. A drop of the mixture was added on the top of Si molds which was O_2 plasma treated in advance. The mixture was left for about 15 minutes. Once the mixture is hardened, it was peeled off in ethanol.

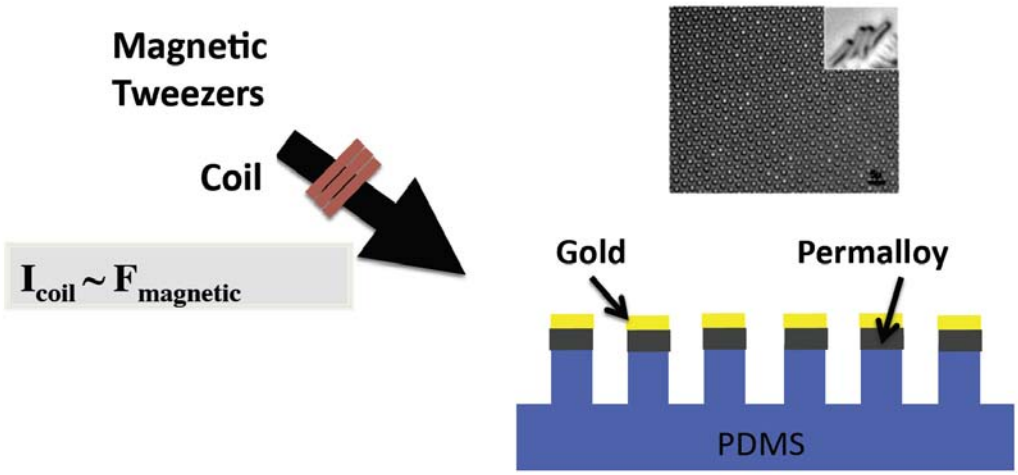

Figure 4.7: Schematic of the process flow for applying force to arrays of the PDMS pillars with a plug of permalloy and gold layer on the top surface.

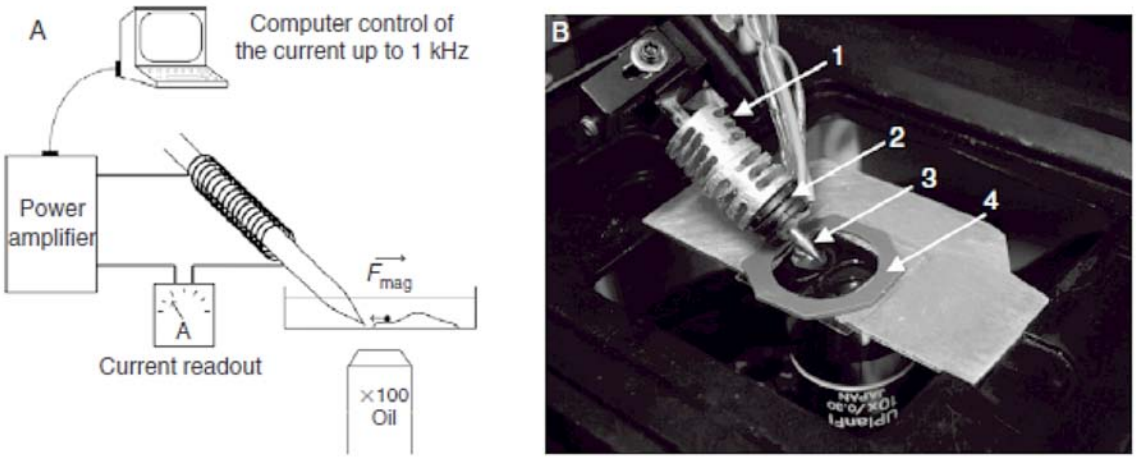

Figure 4.8: (a) Schematic representation of the magnetic tweezers and imaging system. (b) Electromagnetic system used in our laboratory (from [81]).

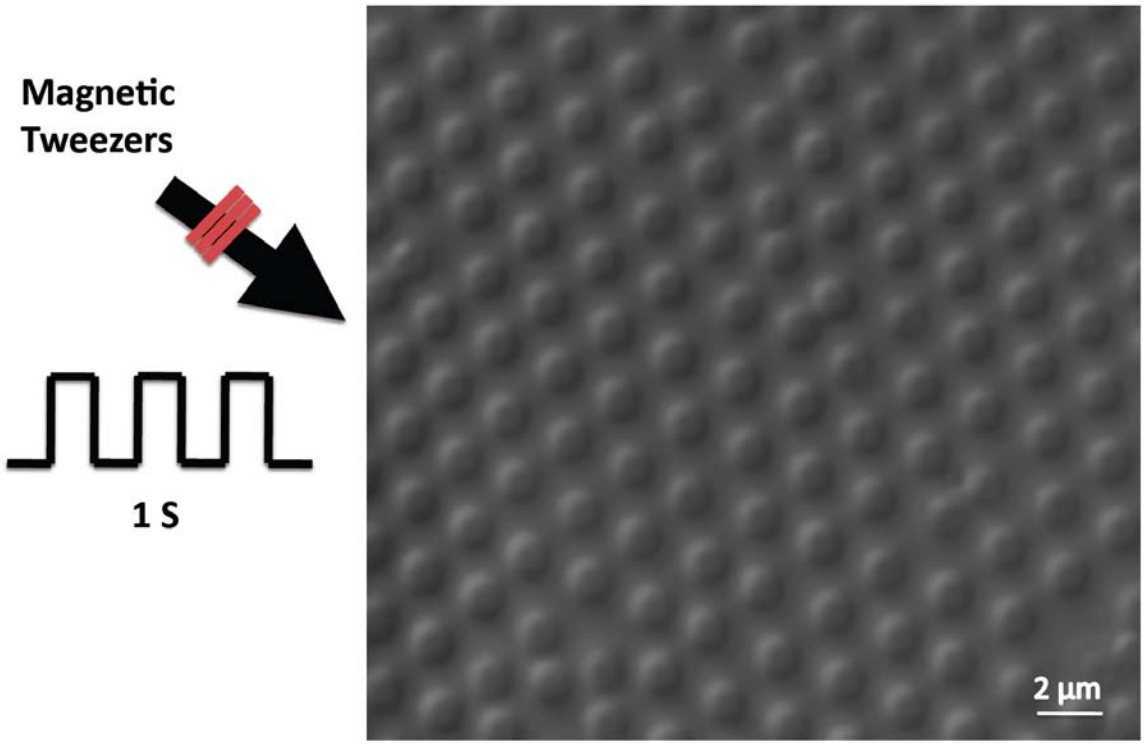

Figure 4.9: Bright-field micrograph of magnetically actuated Polyacrylamide pillars. Application of an oscillatory force results in actuating pillars toward the direction of magnetic tweezer.

4.4.2 Results

In order to examine the magnetic characteristic of pillars, magnetic tweezer was used to image the pillars [81]. Force was applied on the magnetic plug of the top of elastomeric pillars by running current in magnetic tweezer (Fig. 4.7). Figure 4.8 shows the construction of a magnetic tweezer used in Sheetz lab. The hexagonal array of polyacrylamide pillars array with a magnetic head is depicted in figure 4.9. With the application of an oscillatory force with frequency of 1 Hz, pillars were moved toward the direction of magnetic tweezer. These pillars behaved like an individual magnetically actuated spring.

4.5 Conclusions

We have described a fabrication process of elastomeric pillar substrates with a thin layer of metal on the top of the pillars.

The Au-tipped PDMS pillar substrates have the advantage that the chemistry of the top of the pillars can be specifically controlled by selective chemical functionalization. This approach facilitates cell spreading exclusively on the top of the force sensing pillars. Fluorescent labeling improves detection of the tops of the pillars, enabling and precise monitoring of cellular force generation during motile processes.

The magnetic pillars can be use as a new cell platform, which is compatible with existing elastomeric pillar technology. Application of force on magnetic pillars can mimic the was ECM forces are applied to the cells. It is a well-controlled system. The gold layer on the top of magnetic PDMS pillar substrates enable us to specifically control the chemistry of the top of the magnetic pillars as well. This approach enables the application of external forces on pillars in a precise manner and helps us to measure the localized stress and study the cellular response to localized mechanostimulation.

Part III

Bibliography

Bibliography

[1] C. M. Lo, H. B. Wang, M. Dembo, and Y. L. Wang, "Cell movement is guided by the rigidity of the substrate," *Biophys J*, vol. 79, no. 1, pp. 144–52, 2000.

[2] O. du Roure, A. Saez, A. Buguin, R. H. Austin, P. Chavrier, P. Silberzan, and B. Ladoux, "Force mapping in epithelial cell migration," *Proc Natl Acad Sci U S A*, vol. 102, no. 7, pp. 2390–5, 2005.

[3] J. L. Tan, J. Tien, D. M. Pirone, D. S. Gray, K. Bhadriraju, and C. S. Chen, "Cells lying on a bed of microneedles: an approach to isolate mechanical force," *Proc Natl Acad Sci U S A*, vol. 100, no. 4, pp. 1484–9, 2003.

[4] N. Tymchenko, J. Wallentin, S. Petronis, L. M. Bjursten, B. Kasemo, and J. Gold, "A novel cell force sensor for quantification of traction during cell spreading and contact guidance," *Biophys J*, vol. 93, no. 1, pp. 335–45, 2007.

[5] N. Xia, C. K. Thodeti, T. P. Hunt, Q. Xu, M. Ho, G. M. Whitesides, R. Westervelt, and D. E. Ingber, "Directional control of cell motility through focal adhesion positioning and spatial control of rac activation," *FASEB J*, vol. 22, no. 6, pp. 1649–59, 2008.

[6] F. Grinnell, "Fibroblasts, myofibroblasts, and wound contraction," *Journal of Cell Biology*, vol. 124, no. 4, pp. 401–404, 1994.

[7] A. Subramanian and H. Y. Lin, "Crosslinked chitosan: Its physical properties and the effects of matrix stiffness on chondrocyte cell morphology and proliferation," *Journal of Biomedical Materials Research Part A*, vol. 75A, no. 3, pp. 742–753, 2005.

[8] A. Kostic, C. D. Lynch, and M. P. Sheetz, "Differential matrix rigidity response in breast cancer cell lines correlates with the tissue tropism," *Plos One*, vol. 4, no. 7, pp. –, 2009.

[9] S. C. Wang, K. Makino, W. Y. Xia, J. S. Kim, S. A. Im, H. Peng, S. C. Mok, S. E. Singletary, and M. C. Hung, "Doc-2/hdab-2 inhibits ilk activity and induces anoikis in breast cancer cells through an akt-independent pathway," *Oncogene*, vol. 20, no. 47, pp. 6960–6964, 2001.

[10] E. Ruoslahti, "Fibronectin and its integrin receptors in cancer," *Adv Cancer Res*, vol. 76, pp. 1–20, 1999.

[11] D. E. Discher, P. Janmey, and Y. L. Wang, "Tissue cells feel and respond to the stiffness of their substrate," *Science*, vol. 310, no. 5751, pp. 1139–43, 2005.

[12] S. W. Moore, P. Roca-Cusachs, and M. P. Sheetz, "Stretchy proteins on stretchy substrates: the important elements of integrin-mediated rigidity sensing," *Dev Cell*, vol. 19, no. 2, pp. 194–206, 2010.

[13] A. P. Balgude, X. Yu, A. Szymanski, and R. V. Bellamkonda, "Agarose gel stiffness determines rate of drg neurite extension in 3d cultures," *Biomaterials*, vol. 22, no. 10, pp. 1077–1084, 2001.

[14] L. A. Flanagan, Y. E. Ju, B. Marg, M. Osterfield, and P. A. Janmey, "Neurite branching on deformable substrates," *Neuroreport*, vol. 13, no. 18, pp. 2411–2415, 2002.

[15] R. J. Pelham and Y. L. Wang, "Cell locomotion and focal adhesions are regulated by substrate flexibility (vol 94, pg 13661, 1997)," *Proceedings of the National Academy of Sciences of the United States of America*, vol. 95, no. 20, pp. 12070–12070, 1998.

[16] T. Yeung, P. C. Georges, L. A. Flanagan, B. Marg, M. Ortiz, M. Funaki, N. Zahir, W. Y. Ming, V. Weaver, and P. A. Janmey, "Effects of substrate stiffness on cell morphology, cytoskeletal structure, and adhesion," *Cell Motility and the Cytoskeleton*, vol. 60, no. 1, pp. 24–34, 2005.

[17] S. Ghassemi, N. Biais, K. Maniura, S. J. Wind, M. P. Sheetz, and J. Hone, "Fabrication of elastomer pillar arrays with modulated stiffness for cellular force measurements," *Journal of Vacuum Science Technology B*, vol. 26, no. 6, pp. 2549–2553, 2008.

[18] A. J. Engler, H. L. Sweeney, D. E. Discher, and J. E. Schwarzbauer, "Extracellular matrix elasticity directs stem cell differentiation," *J Musculoskelet Neuronal Interact*, vol. 7, no. 4, p. 335, 2007.

[19] V. Vogel and M. Sheetz, "Local force and geometry sensing regulate cell functions," *Nature Reviews Molecular Cell Biology*, vol. 7, no. 4, pp. 265–275, 2006.

[20] M. Barczyk, S. Carracedo, and D. Gullberg, "Integrins," *Cell Tissue Res*, vol. 339, no. 1, pp. 269–80.

[21] V. Vogel, "Mechanotransduction involving multimodular proteins: converting force into biochemical signals," *Annu Rev Biophys Biomol Struct*, vol. 35, pp. 459–88, 2006.

[22] E. P. Gee, D. E. Ingber, and C. M. Stultz, "Fibronectin unfolding revisited: modeling cell traction-mediated unfolding of the tenth type-iii repeat," *PLoS One*, vol. 3, no. 6, p. e2373, 2008.

[23] M. D. Pierschbacher and E. Ruoslahti, "Cell attachment activity of fibronectin can be duplicated by small synthetic fragments of the molecule," *Nature*, vol. 309, no. 5963, pp. 30–3, 1984.

[24] Y. Takada, X. Ye, and S. Simon, "The integrins," *Genome Biol*, vol. 8, no. 5, p. 215, 2007.

[25] C. K. Miranti and J. S. Brugge, "Sensing the environment: a historical perspective on integrin signal transduction," *Nat Cell Biol*, vol. 4, no. 4, pp. E83–90, 2002.

[26] J. D. Humphries, A. Byron, and M. J. Humphries, "Integrin ligands at a glance," *J Cell Sci*, vol. 119, no. Pt 19, pp. 3901–3, 2006.

[27] D. S. Harburger and D. A. Calderwood, "Integrin signalling at a glance," *J Cell Sci*, vol. 122, no. Pt 2, pp. 159–63, 2009.

[28] C. D. Nobes and A. Hall, "Rho, rac, and cdc42 gtpases regulate the assembly of multimolecular focal complexes associated with actin stress fibers, lamellipodia, and filopodia," *Cell*, vol. 81, no. 1, pp. 53–62, 1995.

[29] N. Q. Balaban, U. S. Schwarz, D. Riveline, P. Goichberg, G. Tzur, I. Sabanay, D. Mahalu, S. Safran, A. Bershadsky, L. Addadi, and B. Geiger, "Force and focal adhesion assembly: a close relationship studied using elastic micropatterned substrates," *Nat Cell Biol*, vol. 3, no. 5, pp. 466–72, 2001.

[30] D. Riveline, E. Zamir, N. Q. Balaban, U. S. Schwarz, T. Ishizaki, S. Narumiya, Z. Kam, B. Geiger, and A. D. Bershadsky, "Focal contacts as mechanosensors: Externally applied local mechanical force induces growth of focal contacts by an mdia1-dependent and rock-independent mechanism," *Journal of Cell Biology*, vol. 153, no. 6, pp. 1175–1185, 2001.

[31] R. Zaidel-Bar, S. Itzkovitz, A. Ma'ayan, R. Iyengar, and B. Geiger, "Functional atlas of the integrin adhesome," *Nat Cell Biol*, vol. 9, no. 8, pp. 858–67, 2007.

[32] S. K. Mitra, D. A. Hanson, and D. D. Schlaepfer, "Focal adhesion kinase: in command and control of cell motility," *Nat Rev Mol Cell Biol*, vol. 6, no. 1, pp. 56–68, 2005.

[33] N. O. Deakin and C. E. Turner, "Paxillin comes of age," *J Cell Sci*, vol. 121, no. Pt 15, pp. 2435–44, 2008.

[34] Y. Sawada, M. Tamada, B. J. Dubin-Thaler, O. Cherniavskaya, R. Sakai, S. Tanaka, and M. P. Sheetz, "Force sensing by mechanical extension of the src family kinase substrate p130cas," *Cell*, vol. 127, no. 5, pp. 1015–26, 2006.

[35] M. Tamada, M. P. Sheetz, and Y. Sawada, "Activation of a signaling cascade by cytoskeleton stretch," *Dev Cell*, vol. 7, no. 5, pp. 709–18, 2004.

[36] C. Zhong, M. Chrzanowska-Wodnicka, J. Brown, A. Shaub, A. M. Belkin, and K. Burridge, "Rho-mediated contractility exposes a cryptic site in fibronectin and induces fibronectin matrix assembly," *J Cell Biol*, vol. 141, no. 2, pp. 539–51, 1998.

[37] D. Ingber, "Integrins as mechanochemical transducers," *Curr Opin Cell Biol*, vol. 3, no. 5, pp. 841–8, 1991.

[38] D. Choquet, D. P. Felsenfeld, and M. P. Sheetz, "Extracellular matrix rigidity causes strengthening of integrin-cytoskeleton linkages," *Cell*, vol. 88, no. 1, pp. 39–48, 1997.

[39] S. Sukharev and D. P. Corey, "Mechanosensitive channels: multiplicity of families and gating paradigms," *Sci STKE*, vol. 2004, no. 219, p. re4, 2004.

[40] S. Munevar, Y. L. Wang, and M. Dembo, "Regulation of mechanical interactions between fibroblasts and the substratum by stretch-activated ca2+ entry," *J Cell Sci*, vol. 117, no. Pt 1, pp. 85–92, 2004.

[41] A. K. Harris, P. Wild, and D. Stopak, "Silicone rubber substrata: a new wrinkle in the study of cell locomotion," *Science*, vol. 208, no. 4440, pp. 177–9, 1980.

[42] M. Chrzanowska-Wodnicka and K. Burridge, "Rho-stimulated contractility drives the formation of stress fibers and focal adhesions," *J Cell Biol*, vol. 133, no. 6, pp. 1403–15, 1996.

[43] J. Lee, M. Leonard, T. Oliver, A. Ishihara, and K. Jacobson, "Traction forces generated by locomoting keratocytes," *J Cell Biol*, vol. 127, no. 6 Pt 2, pp. 1957–64, 1994.

[44] M. Dembo, T. Oliver, A. Ishihara, and K. Jacobson, "Imaging the traction stresses exerted by locomoting cells with the elastic substratum method," *Biophys J*, vol. 70, no. 4, pp. 2008–22, 1996.

[45] I. M. Tolic-Norrelykke, J. P. Butler, J. Chen, and N. Wang, "Spatial and temporal traction response in human airway smooth muscle cells," *Am J Physiol Cell Physiol*, vol. 283, no. 4, pp. C1254–66, 2002.

[46] M. Dembo and Y. L. Wang, "Stresses at the cell-to-substrate interface during locomotion of fibroblasts," *Biophys J*, vol. 76, no. 4, pp. 2307–16, 1999.

[47] N. Wang, K. Naruse, D. Stamenovic, J. J. Fredberg, S. M. Mijailovich, I. M. Tolic-Norrelykke, T. Polte, R. Mannix, and D. E. Ingber, "Mechanical behavior in living

cells consistent with the tensegrity model," *Proc Natl Acad Sci U S A*, vol. 98, no. 14, pp. 7765–70, 2001.

[48] U. S. Schwarz, N. Q. Balaban, D. Riveline, A. Bershadsky, B. Geiger, and S. A. Safran, "Calculation of forces at focal adhesions from elastic substrate data: the effect of localized force and the need for regularization," *Biophys J*, vol. 83, no. 3, pp. 1380–94, 2002.

[49] J. Pelham, R. J. and Y. Wang, "High resolution detection of mechanical forces exerted by locomoting fibroblasts on the substrate," *Mol Biol Cell*, vol. 10, no. 4, pp. 935–45, 1999.

[50] C. G. Galbraith and M. P. Sheetz, "A micromachined device provides a new bend on fibroblast traction forces," *Proc Natl Acad Sci U S A*, vol. 94, no. 17, pp. 9114–8, 1997.

[51] A. Saez, M. Ghibaudo, A. Buguin, P. Silberzan, and B. Ladoux, "Rigidity-driven growth and migration of epithelial cells on microstructured anisotropic substrates," *Proc Natl Acad Sci U S A*, vol. 104, no. 20, pp. 8281–6, 2007.

[52] S. R. Peyton and A. J. Putnam, "Extracellular matrix rigidity governs smooth muscle cell motility in a biphasic fashion," *J Cell Physiol*, vol. 204, no. 1, pp. 198–209, 2005.

[53] G. Jiang, A. H. Huang, Y. Cai, M. Tanase, and M. P. Sheetz, "Rigidity sensing at the leading edge through alphavbeta3 integrins and rptpalpha," *Biophys J*, vol. 90, no. 5, pp. 1804–9, 2006.

[54] G. Giannone, B. J. Dubin-Thaler, H. G. Dobereiner, N. Kieffer, A. R. Bresnick, and M. P. Sheetz, "Periodic lamellipodial contractions correlate with rearward actin waves," *Cell*, vol. 116, no. 3, pp. 431–443, 2004.

[55] B. Geiger, A. Bershadsky, R. Pankov, and K. M. Yamada, "Transmembrane crosstalk between the extracellular matrix–cytoskeleton crosstalk," *Nat Rev Mol Cell Biol*, vol. 2, no. 11, pp. 793–805, 2001.

[56] A. J. Engler, M. A. Griffin, S. Sen, C. G. Bonnemann, H. L. Sweeney, and D. E. Discher, "Myotubes differentiate optimally on substrates with tissue-like stiffness: pathological

implications for soft or stiff microenvironments," *J Cell Biol*, vol. 166, no. 6, pp. 877–87, 2004.

[57] L. Landau and E. Lifschitz, *Theorie de l'Elasticite*. M.I.R., 2nd ed., 1990.

[58] M. Ghibaudo, A. Saez, L. Trichet, A. Xayaphoummine, J. Browaeys, P. Silberzan, A. Buguin, and B. Ladoux, "Traction forces and rigidity sensing regulate cell functions," *Soft Matter*, vol. 4, no. 9, pp. 1836–1843, 2008.

[59] C.-W. Wang, W.-R. Chen, C.-C. Wu, and H.-C. Chang, "Study on the cell mechanics of mdck cells by elastic micro-pillars arrays," 2007.

[60] A. Saez, A. Buguin, P. Silberzan, and B. Ladoux, "Is the mechanical activity of epithelial cells controlled by deformations or forces?," *Biophys J*, vol. 89, no. 6, pp. L52–4, 2005.

[61] R. Keller, L. A. Davidson, and D. R. Shook, "How we are shaped: the biomechanics of gastrulation," *Differentiation*, vol. 71, no. 3, pp. 171–205, 2003.

[62] C. G. Galbraith, K. M. Yamada, and M. P. Sheetz, "The relationship between force and focal complex development," *J Cell Biol*, vol. 159, no. 4, pp. 695–705, 2002.

[63] G. Giannone, B. J. Dubin-Thaler, O. Rossier, Y. Cai, O. Chaga, G. Jiang, W. Beaver, H. G. Dobereiner, Y. Freund, G. Borisy, and M. P. Sheetz, "Lamellipodial actin mechanically links myosin activity with adhesion-site formation," *Cell*, vol. 128, no. 3, pp. 561–75, 2007.

[64] A. del Rio, R. Perez-Jimenez, R. Liu, P. Roca-Cusachs, J. M. Fernandez, and M. P. Sheetz, "Stretching single talin rod molecules activates vinculin binding," *Science*, vol. 323, no. 5914, pp. 638–41, 2009.

[65] A. J. Engler, S. Sen, H. L. Sweeney, and D. E. Discher, "Matrix elasticity directs stem cell lineage specification," *Cell*, vol. 126, no. 4, pp. 677–89, 2006.

[66] J. Fu, Y. K. Wang, M. T. Yang, R. A. Desai, X. Yu, Z. Liu, and C. S. Chen, "Mechanical regulation of cell function with geometrically modulated elastomeric substrates," *Nat Methods*, vol. 7, no. 9, pp. 733–6.

[67] G. Chamberlain, J. Fox, B. Ashton, and J. Middleton, "Concise review: mesenchymal stem cells: their phenotype, differentiation capacity, immunological features, and potential for homing," *Stem Cells*, vol. 25, no. 11, pp. 2739–49, 2007.

[68] A. J. Friedenstein, "Osteogenetic activity of transplanted transitional epithelium," *Acta Anat (Basel)*, vol. 45, pp. 31–59, 1961.

[69] J. E. Aubin, "Bone stem cells," *J Cell Biochem Suppl*, vol. 30-31, pp. 73–82, 1998.

[70] F. P. Barry, "Biology and clinical applications of mesenchymal stem cells," *Birth Defects Res C Embryo Today*, vol. 69, no. 3, pp. 250–6, 2003.

[71] D. Shirley, D. Marsh, G. Jordan, S. McQuaid, and G. Li, "Systemic recruitment of osteoblastic cells in fracture healing," *J Orthop Res*, vol. 23, no. 5, pp. 1013–21, 2005.

[72] U. Noth, A. M. Osyczka, R. Tuli, N. J. Hickok, K. G. Danielson, and R. S. Tuan, "Multilineage mesenchymal differentiation potential of human trabecular bone-derived cells," *J Orthop Res*, vol. 20, no. 5, pp. 1060–9, 2002.

[73] B. Kulterer, G. Friedl, A. Jandrositz, F. Sanchez-Cabo, A. Prokesch, C. Paar, M. Scheideler, R. Windhager, K. H. Preisegger, and Z. Trajanoski, "Gene expression profiling of human mesenchymal stem cells derived from bone marrow during expansion and osteoblast differentiation," *BMC Genomics*, vol. 8, p. 70, 2007.

[74] T. Komori, "Regulation of osteoblast differentiation by transcription factors," *J Cell Biochem*, vol. 99, no. 5, pp. 1233–9, 2006.

[75] N. Jaiswal, S. E. Haynesworth, A. I. Caplan, and S. P. Bruder, "Osteogenic differentiation of purified, culture-expanded human mesenchymal stem cells in vitro," *J Cell Biochem*, vol. 64, no. 2, pp. 295–312, 1997.

[76] R. McBeath, D. M. Pirone, C. M. Nelson, K. Bhadriraju, and C. S. Chen, "Cell shape, cytoskeletal tension, and rhoa regulate stem cell lineage commitment," *Dev Cell*, vol. 6, no. 4, pp. 483–95, 2004.

[77] T. Okamoto, T. Aoyama, T. Nakayama, T. Nakamata, T. Hosaka, K. Nishijo, T. Nakamura, T. Kiyono, and J. Toguchida, "Clonal heterogeneity in differentiation potential of immortalized human mesenchymal stem cells," *Biochem Biophys Res Commun*, vol. 295, no. 2, pp. 354–61, 2002.

[78] C. D. Bain, E. B. Troughton, Y. T. Tao, J. Evall, G. M. Whitesides, and R. G. Nuzzo, "Formation of monolayer films by the spontaneous assembly of organic thiols from solution onto gold," *Journal of the American Chemical Society*, vol. 111, no. 1, pp. 321–335, 1989.

[79] A. Ulman, "Formation and structure of self-assembled monolayers," *Chem Rev*, vol. 96, no. 4, pp. 1533–1554, 1996.

[80] N. J. Sniadecki, A. Anguelouch, M. T. Yang, C. M. Lamb, Z. Liu, S. B. Kirschner, Y. Liu, D. H. Reich, and C. S. Chen, "Magnetic microposts as an approach to apply forces to living cells," *Proceedings of the National Academy of Sciences of the United States of America*, vol. 104, no. 37, pp. 14553–14558, 2007.

[81] M. Tanase, N. Biais, and M. Sheetz, "Magnetic tweezers in cell biology," *Methods Cell Biol*, vol. 83, pp. 473–93, 2007.

Part IV

Appendices

Appendix A

Matlab source code for peak finder

```
clear;
Dia = 1; % um diameter
L = 2.6; % um height
E = 2000; % Young's modulus in nN/um^2
rad = Dia/2;
spring = (3/4)*pi*E*((rad^4)/(L^3)); % spring constant in nN/um^2
Threshold=10; % threshold to distinguish peaks. It is set to 15% of dmax
Global_results=[];
meanf=[]; % mean force
stdf=[];  % standard deviation of force
fmax=[];  % maximum force
meanv=[]; % mean velocity
stdv=[]; % standard deviation of velocity
dmax=[]; % maximum displacement
tmax=[]; % period of highest peak
NewTime=[]; % time starting at the first manually picked minimum
d_filterednew=[]; % displacement starting after picked minimum
pxx_r=[]; % power spectrum of single trace
fr_r=[]; % frequency of single trace
pxx_norm=[]; % normalized power spectrum single trace
fr_norm=[]; % normalized frequency of single trace

r1=load('Data1.csv'); % load filtered delta r in columns for n pillar
```

```
24 r2=load('Data2.csv'); % load delta r in columns with different time scale than
       r1 for n pillar
25 raw(1).disp = r1; % data with different total time in a structure
26 raw(2).disp = r2;
27
28 b=1;
29 for n=1:2
30     nm_pillar = size(raw(n).disp,2); % number of pillars
31 for k=1:nm_pillar
32     d_filtered=raw(n).disp(:,k);
33     ntime = size(d_filtered,1);
34     time = zeros(ntime,1);
35     j=1;
36     for i=1:ntime % creating time for 1 sec intervals
37       time(i)=j;
38       j=j+1;
39     end
40     figure;
41     plot(time, d_filtered);
42     [x y] = ginput(1) % picking the initial point as first minimum
43     x = round(x);
44     timezero=x;
45     timenew=zeros(ntime-timezero,1);
46     d_filterednew=zeros(ntime-timezero,1);
47     ntimenew=size(d_filterednew,1); % creating new time based on initial point
48     h=1;
49     for i=1:(ntime-timezero)
50         timenew(i)=h;
51         d_filterednew(i) = d_filtered(timezero+i); % in nm
52         fnew(i) = d_filterednew(i).*spring*10^-3; % Force nN
53         h=h+1;
54     end
55
56    New(b).disp = d_filterednew;  % structure made of new displacement and
          force
57    New(b).force = fnew;
58    New(b).time = size(d_filterednew,1);
```

```
59
60      Min_list=zeros(ntime,1);
61      Max_list=zeros(ntime,1);
62
63      % finding global maximum
64
65      Global_max=1;
66      for i=x:ntime,
67          if d_filtered(i)>d_filtered(Global_max),
68              Global_max=i;
69          end
70      end
71      disp_max=d_filtered(Global_max);
72      F_max = spring*d_filtered(Global_max)*10^-3; % maximum force nN
73      Max_list(Global_max)=1; % global max is marked on the list
74
75      % finding peaks; the picked initial point is the first minimum
76
77      Runing_min=1;
78      Runing_max=1;
79      Target_type='Max';
80      Min_list(x)=1;
81      for i=x:ntime,
82          if Target_type=='Max'
83              if d_filtered(i)>d_filtered(Runing_max)
84                  Runing_max=i;
85              elseif (d_filtered(Runing_max)-d_filtered(i)) > Threshold % we are
                    back down more than 'Threshold' from the Runing_min
86                  Max_list(Runing_max)=1; % thus the Runing_max is validated
87                  Runing_min=i;
88                  Target_type='Min'; % and we start to look for a new minimum
89              end
90          end
91          if Target_type=='Min'
92              if d_filtered(i)<d_filtered(Runing_min)
93                  Runing_min=i;
```

```
94            elseif (d_filtered(i)-d_filtered(Runing_min)) > Threshold % we are
                  back up more than 'Threshold' from the Runing_min
95                Min_list(Runing_min)=1; % thus the Runing_min is validated
96                Runing_max=i;
97                Target_type='Max'; % and we start to look for a new maximum
98            end
99        end
100   end
101
102   if Target_type=='Min'
103       if d_filtered(Runing_min)<0.2*d_filtered(Runing_max) % if the last
              point is close enough to zero (smaller than 0.2 of the running
              maximum, it will be picked a minimum
104           Min_list(Runing_min)=1;
105       end
106   end
107
108   Nb_max=sum(Max_list);
109   Time_max_list=1:Nb_max;
110   Value_max_list=1:Nb_max;
111   j=1;
112   for i=1:ntime,
113       if Max_list(i)==1
114           Time_max_list(j)=i;
115           Value_max_list(j)=d_filtered(i);
116           j=j+1;
117       end
118   end
119
120   Nb_min=sum(Min_list);
121   Time_min_list=1:Nb_min;
122   Value_min_list=1:Nb_min;
123   j=1;
124   for i=1:ntime,
125       if Min_list(i)==1
126           Time_min_list(j)=i;
127           Value_min_list(j)=d_filtered(i);
```

```
128             j=j+1;
129         end
130     end
131     figure;
132     stem(Time_max_list,Value_max_list,'r');
133     hold on
134     stem(Time_min_list,Value_min_list,'g')
135
136     plot(time, d_filtered);
137     xlabel ('Time (s)','FontSize',15);
138     ylabel ('Displacement (nm)','FontSize',15);
139     title ('D=1um, H=4um','FontSize',15);
140     legend ('K=16.7572 nN/um');
141     hold off
142     pause;
143     close all;
144     % for each peak, we will output
145     % 1- pillar number
146     % 2- number of the peaks found for one pillar
147     % 3- height from min to max
148     % 4- height from max to min
149     % 5- time from min to max
150     % 6- time from max to min
151     % 7- total time
152     % 8- average slope up
153     % 9- average slope down
154     % 10- r (displacement of a pillar)
155     Mlen=length(Time_max_list);
156     mlen=length(Time_min_list);
157     nPics=Mlen;
158     Results=zeros(nPics+1,10);
159
160     i=1;
161       if mlen>Mlen % if number of minimums are more than maximum (we have
              complete peaks)
162           for j=i:nPics
163               Results(j,1)=k; % 1
```

```
164             Results(j,2)=j; % 2
165             Results(j,3)=(Value_max_list(j)-Value_min_list(j)); % 3
166             Results(j,4)=(Value_max_list(j)-Value_min_list(j+1)); % 4
167             Results(j,5)=Time_max_list(j)-Time_min_list(j); % 5
168             Results(j,6)=Time_min_list(j+1)-Time_max_list(j); % 6
169             Results(j,7)=Results(j,5)+Results(j,6); % 7
170             Results(j,8)=Results(j,3)/Results(j,5); % 8
171             Results(j,9)=Results(j,4)/Results(j,6); % 9
172             Results(j,10)=Value_max_list(j); % 10
173         end
174     else  % The last peak is incomplete. NaN in non relevant properties
175         for j=i:nPics
176             if j == nPics
177                 Results(j,1)=k;
178                 Results(j,2)=j;
179                 Results(j,3)=(Value_max_list(j)-Value_min_list(j));
180                 Results(j,4)=NaN;
181                 Results(j,5)=Time_max_list(j)-Time_min_list(j);
182                 Results(j,6)=NaN;
183                 Results(j,7)=NaN;
184                 Results(j,8)=Results(j,3)/Results(j,5);
185                 Results(j,9)=NaN;
186                 Results(j,10)=Value_max_list(j);
187             else
188                  Results(j,1)=k;
189                  Results(j,2)=j;
190                  Results(j,3)=(Value_max_list(j)-Value_min_list(j));
191                  Results(j,4)=(Value_max_list(j)-Value_min_list(j+1));
192                  Results(j,5)=Time_max_list(j)-Time_min_list(j);
193                  Results(j,6)=Time_min_list(j+1)-Time_max_list(j);
194                  Results(j,7)=Results(j,5)+Results(j,6);
195                  Results(j,8)=Results(j,3)/Results(j,5);
196                  Results(j,9)=Results(j,4)/Results(j,6);
197                  Results(j,10)=Value_max_list(j);
198             end
199         end
200     end
```

```
201      Global_results=[Global_results;Results];
202      NewTime =[NewTime;ntimenew];
203
204      [Y,I] = max(Results(:,10));
205      T_max = Results(:,7);
206      tmax=[tmax;T_max];
207
208      fmax=[fmax;F_max];
209      ave_f = mean(fnew);
210      dmax=[dmax;disp_max];
211      std_avef = std(fnew)./sqrt(ntimenew);
212
213      meanf=[meanf;ave_f];
214      stdf=[stdf;std_avef];
215      b=b+1;
216 end
217 end
218
219 rows_to_delete = [];   % delete rows with zero in it in global result
220 for i=1:length(results(:,1))
221   if results(i,:)==zeros(size(results(i,:)))
222       rows_to_delete = [rows_to_delete i];
223   end;
224 end;
225 results(rows_to_delete,:) = [];
226
227 mean_result = zeros(1,length(results(1,:)));
228 std_result = zeros(1,length(results(1,:)));
229 for i=1:length(mean_result)
230      temp = results(:,i);
231      temp(isnan(temp)) = [];
232      mean_result(i) = mean(temp);
233      AA = length(temp);
234      stderr_result(i) = std(temp)./sqrt(AA);
235 end;
```